Model Predictive Control based Haptic Shared Steering System: A Driver Modelling Approach for Symbiotic Driving

Master thesis

Andrea Michelle Rios Lazcano

Delft University of Technology

Mechanical, Maritime and Materials Engineering Faculty

DELFT UNIVERSITY OF TECHNOLOGY

Master thesis

MSc. Mechanical Engineering, Vehicle Engineering track

Model Predictive Control based Haptic Shared Steering System: A Driver Modelling Approach for Symbiotic Driving

---

Andrea Michelle Rios Lazcano

to obtain the degree of Master of Science in Mechanical Engineering

at the Technical University of Delft,

to be defended publicly on Monday 28th of September, 2020.

September 20, 2020

This thesis is confidential and cannot be made public until September 28, 2022.

TU Delft Delft University of Technology

The thesis committee consisted of the following members:

Dr. ir. R. Happee,	Chair	CoR, Delft University of Technology
Dr. ir. B. Shyrokau,	Supervisor	CoR-IV, Delft University of Technology
Dr. L. Ferranti,	Committee member	CoR-LAC, Delft University of Technology
Dr. W. Mugge,	Committee member	BMechE, Delft University of Technology
Dr. Ir. X. Carrera,	Guest member	VPE-MBD, Toyota Motor Europe NV/SA

The work in this master thesis was performed at Toyota Motor Europe, Belgium. The author is grateful for their cooperation and support throughout the internship.

An electronic version of this thesis is available at http://repository.tudelft.nl/.

Cognitive Robotics

TOYOTA

TU Delft Delft University of Technology

Acknowledgements

I would like to extend my sincere thanks to all the individuals who gave me support and help during this challenging project.

First of all, I am grateful to my thesis supervisors. At TU Delft, Barys Shyrokau has been one of the greatest sources of intellectual motivation during the whole project. I am grateful for his trust and guidance, and I will forever be thankful to him for always believing in my potential. He is the best, most hard-working, and most committed professor I have ever met. And I would also like to extend a sincere acknowledgement to my manager at Toyota, Xabier Carrera, who always had new, challenging ideas for my research. I would also like to thank him for giving me the opportunity to stay at TME and continue with this exciting project, along with great teammates.

To my friends, all over the world, thank you for all the happiness, support, and understanding, no matter the distance between us. To my friends in Logroño, with whom I always feel like home. To my friends in Madrid, with whom I discovered the joys of University life. To my friends in Delft, for the sports tournaments, trips around Europe, and outstanding business tours. And to my friends at Toyota, who are passionate and inspire me to dream big.

To all my family in Mexico, whom I can always rely on, no matter the distance. In particular, to my beloved aunts, that are like second mothers to me. And to my cousins, who are like the siblings I never had.

To my mother, Rosario, who taught me to never surrender and to be the best version of myself every moment. She taught me to be resilient, and to look at the bright side even in the darkest moments. And to my father, Esteban, who I wish could see the person that I have become and, above all, how much positive impact he had in my life with his eternal patience and love.

Last but not least, I would like to express my deepest and most sincere gratitude to the love of my life, Michael Atsma. This journey would not have been as joyful and worth it without his constant support and love every step of the way. He has taught me what true love looks like, and that we can always beat the odds, as long as we are together.

Andrea Lazcano
Brussels, September 2020

Abstract

The work in this thesis presents a case of Haptic Shared Control to provide continuous guidance to the driver during the steering task, in which the optimal torque control law is calculated in the Model Predictive Control Framework. The key milestones and results of the proposed MPC-controller are presented in the form of an IEEE journal paper, in Chapter 2.

For this purpose, this research focuses on the state-of-the-art trends to develop Advanced Driver Assistance Systems (ADAS) that can collaborate with the driver. Therefore, the three main elements of this work are Driver Modelling, Model Predictive Control (MPC), and Haptic Shared Control (HSC), of which an extensive literature review is presented in depth in Appendices A, B, and C. After a thorough investigation, a gap in the understanding of the closed-loop driver-vehicle interaction was identified.

An interesting finding is that, although ADAS can lead to increased safety and reduce driver effort, most systems do not take into account the driver in the loop, leading to driver-AI conflicts and unsatisfactory user-acceptance. In particular for this investigation, the selected case study is a Lane Keeping Assist (LKA) steering system, thus, the interaction takes place through the exchange of forces at the steering wheel. For this case, Haptic Shared Control is highlighted to be the most appropriate control approach.

The ultimate goal of this research was to design a novel MPC-based haptic shared controller and validate its applicability and user-acceptance in a driving simulator experiment. The proposed system integrates an advanced driver model within the prediction model. This driver model is composed of a preview-anticipatory LQR cognitive controller, sensory organs, and the neuromuscular dynamics of the arms, including the activation dynamics and the reflex loop. The results demonstrate a superior performance of the proposed MPC controller with respect to the state-of-the-art commercial benchmark, both subjectively and objectively. In Appendix D, the extended results of this study are presented.

Chapter 1 starts with an introduction and motivation for this research topic, followed by the journal paper in Chapter 2. Lastly, the submitted FISITA 2020 conference paper is presented in Appendix E, which contains the initial computer simulation results of this study.

Keywords: Haptic Shared Control, Model Predictive Control, Driving Simulator, Driver Modelling, Collaborative Driving.

We must design for the way people behave,
not for how we would wish them to behave.

Donald A. Norman

Contents in Brief

Contents

Nomenclature

Greek Symbols

Symbol	Description	Units
α	Motoneurone signal coming from the brain, as the *expected torque command*	Nm
α_f	Front slip angle	rad
α_{reflex}	Motoneurone signal coming from the muscle spindles reflex action	Nm
α_r	Rear slip angle	rad
δ	Road wheel angle	rad
$\dot{\theta}_c$	Steering column velocity	rad/s
$\dot{\theta}_{sw}$	Steering wheel velocity	rad/s
γ	Motoneurone signal coming from the brain, as the *expected muscle angle*	rad
ψ	Heading angle or yaw angle	rad
τ_1	Neural excitation lag time constant	s
τ_2	Neuro-Muscular (de-)activation transduction delay constant	s
τ_{θ_a}	Somatosensory time delay on the muscle angle	s
τ_{cog}	Cognitive time delay	s
τ_{gto}	Golgi tendon organs time delay	s
τ_r	Reflex dynamics time delay	s
$\tau_{vi,\psi}$	Visual time delay on vehicle heading orientation	s
$\tau_{vi,y}$	Visual time delay on vehicle lateral position	s
θ_a	Muscle angle	rad

θ_c	Steering column angle	rad
θ_{sw}	Steering wheel angle	rad

Roman Symbols

Symbol	Description	Units
$\hat{\mathbf{x}}_{KF}$	Estimated states of the Kalman Filter	
$\mathbf{A}_{int}$	State matrix of the internal mental model	
$\mathbf{B}_{int}$	Input matrix of the internal mental model	
$\mathbf{C}_{int}$	Output matrix of the internal mental model	
$\mathbf{K}_{LQR}$	LQR gain	
$\mathbf{L}_{KF}$	Gain matrix of the Kalman Filter	
$\mathbf{P}$	Solution matrix of the Riccati equation	
$\mathbf{Q}_{KF}$	Process noise covariance matrix	
$\mathbf{R}_{KF}$	Measurement noise covariance matrix	
$\mathbf{v}$	Measurement noise	
$\mathbf{W}_{x_N}$	MPC weight for the terminal cost function of the states	
$\mathbf{W}_x$	MPC weight for the stage cost function of the states	
$\mathbf{x}(k)$	MPC states	
$\mathbf{x}_{delay}$	Perceived states by the sensory organs, subject to time delay	
$\mathbf{z}$	Measurement signals of the Kalman Filter	
a_x	Longitudinal vehicle acceleration	m/s^2
a_y	Lateral vehicle acceleration	m/s^2
$C_{\alpha_f,f}$	Front cornering stiffness per axle	N/rad
$C_{\alpha_r,r}$	Rear cornering stiffness per axle	N/rad
c_a	Muscle active damping	Nms/rad
c_p	Intrinsic dynamics damping	Nms/rad
c_{sw}	Damping coefficient of the steering system and the steering system friction	Nms/rad

c_t	Torsion bar damping coefficient	Nms/rad
d	Trail distance, based on the pneumatic plus caster distance	m
e_ψ	Heading error	rad
e_y	Lateral deviation	m
$F_{y,f}$	Front lateral axle force	N
$F_{y,r}$	Rear lateral axle force	N
G	Steering gear ratio	$[-]$
H_{act}	Activation dynamics transfer function	
H_{gto}	Golgi tendon organs representation	
H_r	Reflex dynamics transfer function	
I_{arms}	Inertia of the arms	kgm^2
I_c	Inertia of the rack and the front wheels, with respect to the pinion	kgm^2
I_{sw}	Inertia of the steering handwheel	kgm^2
I_{zz}	Inertia of the vehicle with respect to the center of mass	kgm^2
k_a	Tendon stiffness	Nm/rad
k_{gto}	Golgi tendon organs stiffness gain	Nm/rad
k_p	Intrinsic dynamics stiffness	Nm/rad
k_r	Reflex dynamics position gain	Nm/rad
k_{sw}	Stiffness of the steering system, due to the kingpin axes	Nm/rad
k_t	Steering column stiffness	Nm/rad
l_f	Distance from the center of mass to the front vehicle axle	m
l_r	Distance from the center of mass to the rear vehicle axle	m
m	Vehicle mass	kg
N_c	MPC control horizon	
N_p	MPC prediction horizon	
q_α	LQR cost on the driver expected torque input	

q_y	LQR cost on the shifted lateral position deviation with respect to the reference	
r	Yaw rate	rad/s
T_{act}	Activation torque	Nm
T_{arm}	Torque exerted by the arms muscle	Nm
T_c	Controller's torque input to the steering-vehicle system	Nm
T_d	Driver's torque input to the steering-vehicle system	Nm
T_{fb}	Driver's feedback torque	Nm
T_{int}	Intrinsic dynamics muscle torque	Nm
T_p	Preview time	s
T_s	MPC sampling time	s
$T_{s,DM}$	Sampling time of the Driver Model	s
$T_{s,sim}$	Sampling time of the simulation	s
T_{sup}	Supraspinal muscle torque	Nm
T_{sw}	Steering wheel torque	Nm
T_t	Target shift time constant	s
T_w	Self-aligning moment	Nm
$u(k)$	MPC control input	Nm
V_x	Longitudinal velocity	m/s
V_y	Lateral velocity	m/s
w_α	Process noise	Nm
w_c	Gain crossover frequency	Hz
W_u	MPC weight for the stage cost function of the input	
X_p	Longitudinal position	m
Y_p	Lateral position	m
y_{ref}	Reference trajectory of the lateral position	m

Abbreviations

ADAS Advanced Driver Assistance Systems. v, 1, 43, 55, 58, 62, 66

ASME American Society of Mechanical Engineers. 5

CNS Central Nervous System. 18, 22, 29, 34, 36

HSC Haptic Shared Control. v, 46, 58–62, 65, 66

IEEE Institute of Electrical and Electronics Engineers. 5

KPI Key Performance Indicator. 73, 76

LKA Lane Keeping Assist. v, 1, 2, 53, 71

LOHA Level of Haptic Authority. 64

LQG Linear Quadratic Gaussian. 38, 39

LQR Linear-Quadratic-Regulator. v, 22, 26, 31, 39

LTV Linear Time-Varying. 53

MOSAIC Modular selection and identification for control model. 24

MPC Model Predictive Control. v, xx, 3, 4, 22, 26, 47–51, 53, 55, 63

NMS Neuromuscular System. 18, 20, 25, 26, 30, 33, 35, 38, 41, 46, 61–63

NN Neural Network. 23

OCP Optimal Control Problem. 51, 52

ODD Operational Design Domain. 58

QP Quadratic Programming. 51–54

RHC Receding Horizon Control. 48, 55

SQP Sequential Quadratic Programming. 52

List of Figures

List of Tables

1

Introduction and Motivation

Advanced Driver Assistance Systems have been one of the main focuses in the path towards full automation during the last decades. These systems are introduced to increase comfort and safety, as well as to reduce mental workload while driving [65, 107]. The principle behind these systems is to capture the vehicle response and, if needed, intervene to accomplish a task or to avoid dangerous situations. In the case of Lane Keeping Assist systems, a study performed on German roads revealed that unintentional lane departures represented more than $1/3$ of all accidents with severely injured passengers [10], which makes the positive safety benefits of LKAs clear, as discussed in [104]. However, if the ADAS overrule the driver when it is not critical, user-acceptance is typically decreased, which can lead to drivers turning off the driving assist systems [85]. Moroever, as described by Farah et al. [28], a mismatch in the driver's expected outcome can have a direct negative impact on safety and trust.

In particular for the steering task, current driving assist systems heavily rely on the path tracking error to generate the system's control approach, without taking into account the driver's behaviour. This often results in conflict with the driver and tends to unexpectedly overrule their actions, which leads to suboptimal acceptance and discomfort.

Therefore, until fully-automated vehicles become a reality, it is fundamental to include the interaction between the driver and the vehicle in order to develop safe, human-like, user-acceptable driving assist systems [35, 67]. For the scope of this thesis, which focuses on the steering task, the interaction between the steering-vehicle dynamics and the driver's arms is coupled at the steering wheel. Thereby, torques between the driver and controller can be exchanged to enhance the driving task, also known as haptic guidance.

The importance of considering this interaction in a closed-loop system has been widely recognised in previous studies [80], because it is representative of effective vehicle usage and includes the driver dependency. Furthermore, current research has shown that the understanding of the driver behaviour is essential to enhance driving assist systems [73]. In addition, driver models can be used to design new control alternatives that integrate the driver-in-the-loop dynamics and the cooperation or resistance with the driving assist systems.

However, the nature of the human behaviour is highly complex, nonlinear, and unpredictable. Thus, despite the huge impact that the driver has on the closed-loop system, its modelling has been ignored until recently and there has been uncertainty in the way the interaction takes place. On the other hand, the increased difficulty to objectivise the closed-loop dynamics motivates the need to use accurate driver models in the development of new steering control systems. In other words, driver models could help us explain the link between subjective evaluations and objective metrics.

Summarising, this thesis focuses on the design of a collaborative LKA with emphasis on the reduction of driver-assist conflicts in order to foster cooperation, tracking performance and safety. The problem with current assist systems is that the integration of the driver dynamics in the closed-loop driver-vehicle system is neglected, which often results in an intrusive, counter-intuitive guidance. However, this change of concept is key to guarantee effective shared control. In line with this requirement, the proposed SAE Level 2 system can cooperate with the driver by predicting the driver-vehicle behaviour. Hence, the design of this control based LKA, in combination with a standard ACC system, aims to provide an intuitive haptic torque guidance to drivers and reduce their workload through a collaborative behaviour.

1.1. Research objectives

Figure 1.1 presents a prospective timeline of the mobility sector. Automobiles with partial level of automation provide intermediate scenarios, from basic driving aids to effective shared control between man and machine. The work in this thesis presents a case of MPC-based Haptic Shared Control, predicting the driver-vehicle behaviour and, therefore, aiming to provide a pleasant driving experience by keeping smooth driver-in-the-loop dynamics, as well as intuitive levels of authority transitions. The proposed controller is implemented in a high fidelity model on IPG Carmaker [52], which includes a detailed characterisation of the tyre dynamics and a proprietary steering model [20]. The parametrisation of the steering model is based on a validated Toyota mass production model. The use of IPG Carmaker makes it possible to integrate vehicle sensors that can identify the lane marking, lane offset, and the yaw angle error with respect to the lane centerline, which serve as reference to the MPC-based assist system. The scenario is a highway road with straight and sinusoidal segments of different amplitudes, with a 5 m wide lane in order to allow for more driver variability. This feature makes it possible to assess the behaviour and adaptability of the proposed controller given different driver control strategies.

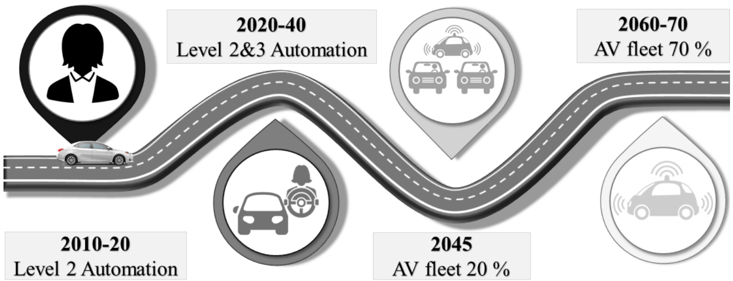

Figure 1.1: Timeline of the autonomous vehicles distribution.

In line with the aforementioned requirements and the gaps found in literature, as illustrated by the question mark in Fig 1.2, the main goal of this thesis is:

> "The design and assessment of a novel MPC-based shared steering control strategy using torque guidance and an extensive driver model to foster symbiotic driving."

This goal is broken down into the following research objectives:

I. Investigate driver models that can capture the driver's intention during the steering task, as well as the dynamics of the arms to tackle driver comfort at a neuromuscular level.

II. Perform a driving simulator pilot study in order to validate the applicability of the selected driver model. Appropriate models should include the predictive human cognitive capabilities, neuromuscular dynamics, and human limitations in the perception.

III. Design an MPC-based shared steering control that can integrate the driver model and the steering-vehicle dynamics to accurately model the driver-AI interaction, ensuring real-time applicability.

IV. Address the collaborative characteristics of the controller using the Haptic Shared Control framework as a strategy to keep the driver in the loop and continuously share the control authority of the steering task.

V. Implement a dynamic cost-function algorithm to adapt the MPC controller to the time-varying human behaviour and reduce conflicts between the driver and the driving assist system.

VI. Design a driver-in-the-loop experiment in a fixed-base driving simulator to validate the subjective acceptance of the proposed MPC controller. The selected scenario should allow for driver variability.

VII. Define a list of Key Performance Indicators to create a link between the subjective evaluations and objective metrics to assess the steering feel of the controller.

VIII. Compare the performance of the proposed MPC controller with respect to a state-of-the-art commercial benchmark. For this objective, the commercial benchmark should first be replicated and validated with real vehicle measurements.

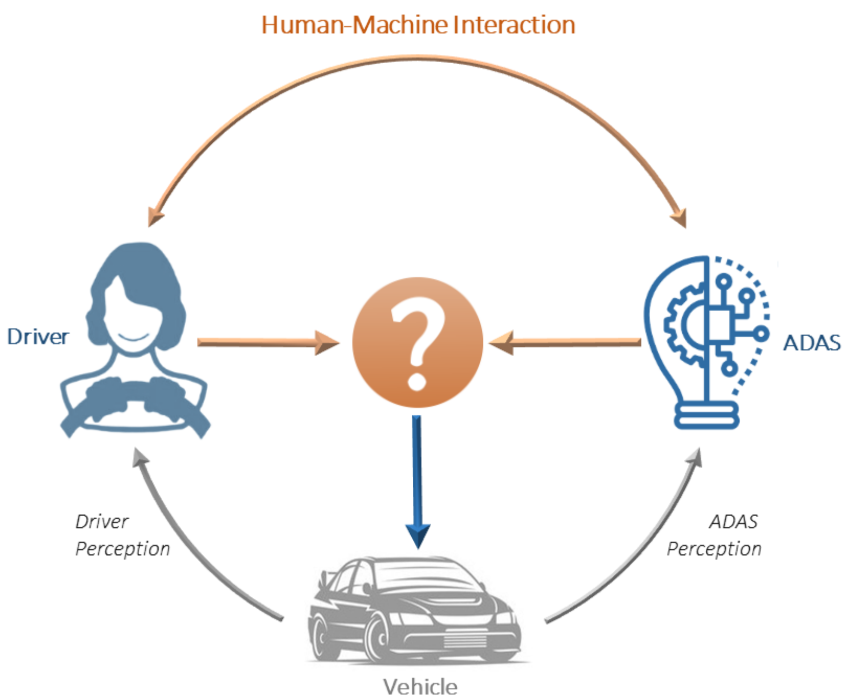

Figure 1.2: Representation of the uncertain human-machine interaction during the steering task.

2

Journal paper

The content of this chapter has been submitted to the IEEE-ASME Transactions on Mechatronics as part of the focused section on Mechatronics in Road Mobility Systems.

MPC-based Haptic Shared Steering System: A Driver Modelling Approach for Symbiotic Driving

Abstract—**Advanced Driver Assistance Systems (ADAS) aim to increase safety and reduce mental workload. However, the gap in the understanding of the closed-loop driver-vehicle interaction often leads to reduced user acceptance. In this research, an optimal torque control law is calculated online in the Model Predictive Control (MPC) framework to guarantee continuous guidance during the steering task. The novelty lies in the integration of an extensive driver-in-the-loop model within the MPC-based haptic controller to enhance collaboration. The driver model is composed of a preview cognitive strategy based on a Linear-Quadratic-Gaussian, sensory organs, and neuromuscular dynamics, including muscle co-activation and reflex action. Moreover, an adaptive cost-function algorithm enables dynamic allocation of the control authority. Experimental data was gathered from 19 participants in a fixed-base driving simulator at Toyota Motor Europe, evaluating an MPC controller with two different cost functions against a commercial Lane Keeping Assist (LKA) system as an industry benchmark. The results demonstrate that the proposed controller fosters symbiotic driving and reduces driver-vehicle conflicts with respect to a state-of-the-art commercial system, both subjectively and objectively, while still improving path-tracking performance. Summarising, this study tackles the need to blend human and ADAS control, demonstrating the validity of the proposed strategy.**

Index Terms—**Haptic Shared Control, Model Predictive Control, human–machine interaction, Driver Modelling, Collaborative Driving.**

I. Introduction

THE exponential growth of ADAS over the years has a direct impact on increased safety and reduction of mental workload while driving [1]. However, automation can also lead to unsatisfactory user acceptance when the driver's intention or expectation does not match the behaviour of the driving assist system [2].

Moreover, the different projections towards the deployment of fully Automated Vehicles (AV) predict several decades of progressive increase of automation before self-driving cars become widespread [3]. Vehicles with partial level of automation provide intermediate scenarios, from basic driving aids to effective shared control between human and AI.

The shared control approach is particularly suitable for the steering task as forces can be exchanged at the steering wheel to accomplish a common objective. Through Haptic Shared Control (HSC), detailed in Appendix C, the authority of the driving task is balanced between the driving assist system and the driver. However, although HSC can lead to less steering control activity and increased safety [4], drivers sometimes resist the assist system's guidance [5]. This can be due to, for example, a mismatch between the driver's cognitive intentions and the controller's objective, or, from a neuromuscular level, the reflex action of the muscle spindles [6].

Therefore, it is clear that the closed-loop driver-vehicle interaction needs to be carefully reviewed in order to design collaborative, user-accepted systems. On the one hand, there is an increasing interest in the study of driver models applicable to the driving task. However, human complexity and unpredictability have made it difficult to guarantee collaboration and seamless control. On the other hand, the difficulty to find objective metrics to analyse these closed-loop dynamics incentivises the use of driver models in the development of new driving assist systems to be able to determine which characteristics are the cause of certain subjective feelings. In the literature, the need to blend driver modelling and vehicle controller systems has been widely acknowledged [7], [8], but there has been limited implementation of detailed driver models in haptic shared controllers [9].

However, oversimplified models, representing the arms as a simple spring damper system, have been commonly used. In particular for the steering task, some research studies have tried to consider the driver-vehicle interaction, in which the MPC strategy is often recognised as the most attractive control approach. In a lane-keeping assist [10], this interaction is modelled by coupling the arm dynamics to the steering system, and this was also extended to a lane-changing scenario [11], both using MPC. Together with a simple arm model, an attempt to introduce an adaptive level of control authority within the MPC cost-function is presented in [12], but the results were constrained to a constant level of control authority for the shared driving case. A more extensive psycho-physiology-based driver model is implemented in [13] for an LKA case, where there was only one participant in the driving simulator experiment. The creation of important Key Performance Indicators (KPI) to assess the collaborative behaviour of the assistance is remarkable. From a more theoretical approach, the use of game theory models in [14]–[16] have also been designed using MPC to capture the driver-ADAS interaction. Furthermore, the model developed in [17] takes special care in tackling the human-machine conflicts, but the human-compatible reference used by the haptic shared controller is calculated offline. Thus, no modification during online simulations is possible. Finally, from the results of these studies, it can generally be seen that the conflicts in torque between driver and driving assist system are not successfully addressed and drivers either fight or correct the torque guidance instead of collaborating with it.

The work in this paper presents a case of Haptic Shared Control to provide continuous guidance during the steering task, in which the optimal torque control law is calculated in the Model Predictive Control Framework. The novelty of this approach is that the prediction model integrates both the vehicle-steering dynamics and an extensive driver-in-the-loop model. With this method, the MPC controller aims to foster collaboration and provide a pleasant driving experience by keeping smooth closed-loop dynamics.

The paper is an extension of the conference paper presented in Appendix E [18] and is structured as follows. Section II establishes the steering-vehicle dynamics. Section III describes the theory behind the driver model integrated within the MPC system, and Section IV presents the results of its validation in a driving simulator pilot experiment. Afterwards, in Section V, the MPC strategy is introduced. Section VI includes the details of the subsequent driving simulator experiments to evaluate the proposed driving assist system. In Section VII, the objective and subjective results of a benchmark comparison between a commercial LKA and two different collaborative modes of the MPC controller can be found. Lastly, in Section VIII and Section IX, the main conclusions of this research investigation and the future directions of work are outlined.

II. Steering-Vehicle Model

A. Vehicle dynamics

The vehicle dynamics presented in Fig. 1 are based on the linear single-track model. The model assumes a constant longitudinal velocity, linear tyre dynamics and small angle approximations. This model simplification can capture the vehicle handling characteristics within the scope of this investigation. Particularly, a range of lateral acceleration up to 4 m/s^2 for passenger cars, which includes path-following tasks in non-evasive manoeuvres. Moreover, the selected steering-vehicle parameters are derived from the complete nonlinear steering-vehicle plant to ensure its applicability for standard manoeuvres at 100 km/h.

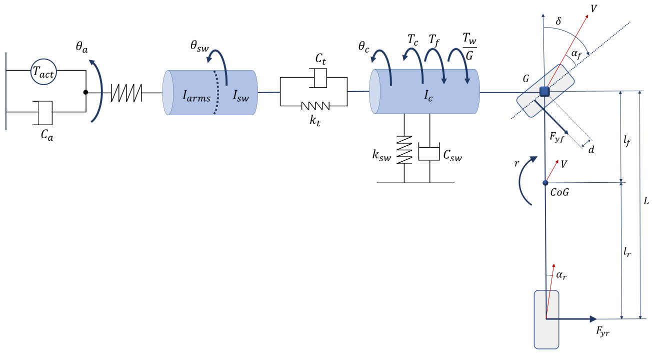

Fig. 1. Arms-steering-vehicle model

Equations (1)–(2) represent the linearised vehicle motion where m is the vehicle mass and I_{zz} the inertia with respect to the centre of mass. The vehicle front and rear distance from the centre of gravity are denoted by l_f and l_r, respectively. Moreover, the states of the vehicle are lateral acceleration, a_y, longitudinal vehicle velocity, V_x, lateral vehicle velocity, V_y, yaw rate, r, and heading angle, ψ.

$$ma_y = F_{y,f} + F_{y,r} \tag{1}$$

$$I_{zz}\ddot{\psi} = l_f F_{y,f} - l_r F_{y,r} \tag{2}$$

The lateral axle forces, $F_{y,i}$, have a linear relation with respect to the slip angles, α_i, with $i \in \{f, r\}$ to represent the front and rear axle, and are calculated as:

$$\alpha_f = -\delta + \frac{V_y + l_f r}{V_x} \tag{3}$$

$$\alpha_r = \frac{V_y - l_r r}{V_x} \tag{4}$$

$$F_{y,f} = -C_{\alpha_f,f} \cdot \alpha_f \tag{5}$$

$$F_{y,r} = -C_{\alpha_r,r} \cdot \alpha_r \tag{6}$$

B. Steering system dynamics

The introduction of the steering system dynamics is key to investigate the interaction between driver and driving assist system. The steering dynamics are rigidly coupled to the arms dynamics at the steering wheel, where torques are exchanged. Thereby resulting in a lumped inertia that is the sum of the inertia of the arms, I_{arms}, and the inertia of the steering wheel, I_{sw}. The neuromuscular dynamics of the arms are described in detail in Section III-B.

The linear steering dynamics [19] are represented in (7)–(8) with 2-Degrees-of-freedom (DoF), where the steering wheel angle, θ_{sw}, and steering column angle, θ_c, denote each DoF. The interaction of the driver is taken into account through the introduction of the muscle angle of the arms, θ_a, which also interacts with the steering wheel. In this paper, the difference of the angles at the steering column is defined as $\Delta\theta_{sc} = (\theta_{sw} - \theta_c)$, and the same notation follows for their derivatives with respect to time, $\Delta\dot{\theta_{sc}} = (\dot{\theta}_{sw} - \dot{\theta}_c)$.

$$(I_{sw} + I_{arms})\ddot{\theta}_{sw} = k_a(\theta_a - \theta_{sw}) - c_t\Delta\dot{\theta_{sc}} - k_t\Delta\theta_{sc} \tag{7}$$

$$I_c\ddot{\theta}_c + c_{sw}\dot{\theta}_c + k_{sw}\theta_c = c_t\Delta\dot{\theta_{sc}} + k_t\Delta\theta_{sc} - \frac{T_w}{G} + T_c \tag{8}$$

where I_c denotes the inertia of the rack and the front wheels with respect to the pinion, k_t and c_t are the steering column stiffness and the torsion bar damping, respectively, and c_{sw} and k_{sw} are the damping and self-centering stiffness with respect to the steering wheel axle.

Moreover, the road wheel angle is calculated proportionally to the steering angle column with the steering gear ratio, G,

$$\delta = \frac{\theta_c}{G} \tag{9}$$

The torques interacting at the steering wheel consist of the self-aligning moment, T_w, and the torque input from the driving assist system, T_c, calculated through the MPC strategy described in Section V. The torque generated about the king-pin axes is,

$$T_w = dF_{y,f} \tag{10}$$

where d is the pneumatic trail.

III. Driver Model

The integration of a realistic driver model is central to the design of the collaborative shared control strategy. A better accuracy of the torque predictions can directly improve the collaborative behaviour of the proposed driving assist system.

The driver model, as presented in Fig. 2, was developed by Niu and Cole [19], building upon earlier work by Nash and Cole [20]. The model is implemented in Simulink and the cognitive model is adapted to enhance its validity in realistic scenarios with real-time capability. It aims to represent the cognitive and physiological mechanisms of the human driver, and includes an internal model, neuromuscular dynamics, sensory dynamics, sensorimotor noise, state estimation, and cognitive and reflex control. In particular, the inclusion of neuromuscular dynamics makes the model appropriate for the development of a new driving assist system with torque feedback. A detailed description of the driver model can be found in Appendix A.5.

A. Cognitive behaviour

The cognitive model is used to predict the driver's steering intentions. For the cognitive control, a predictive approach based on a Linear-Quadratic Regulator (LQR) is chosen. Moreover, the states of the system are estimated with a Kalman Filter to reduce the effect of measurement noise of the sensory organs and process noise of the muscle activation. This combination of approaches is also known as the Linear-Quadratic-Gaussian and it requires an accurate internal mental representation of the plant in order to achieve optimal state estimation. In this regard, a forward internal mental model is assumed to be acquired a priori by the driver.

The cost function of the LQR, which calculates the expected driver torque input, is adapted and modified based on previous work [20], [21]. This function minimises the lateral deviation of the vehicle with respect to the upcoming reference trajectory of the road with a certain preview time, T_{prev}.

$$J_{LQR} = \sum_{0}^{\infty} \left[\begin{bmatrix} \mathbf{x}_{KF} & \mathbf{y}_p \end{bmatrix} \mathbf{C}^T \mathbf{Q} \mathbf{C} \begin{bmatrix} \mathbf{x}_{KF} \\ \mathbf{y}_p \end{bmatrix} \right] + \alpha R \alpha \quad (11)$$

where $\mathbf{C}$ is a matrix that selects the states on the lateral position, heading angle, and the road preview points. Finally, the expected driver torque input, α, is calculated as:

$$\alpha = -\mathbf{K}_{LQR} \cdot \begin{bmatrix} \mathbf{x}_{KF} \\ \mathbf{y}_p \end{bmatrix} \quad (12)$$

where $\mathbf{K}_{LQR}$ is the LQR gain, $\mathbf{x}_{KF}$ is a vector with the estimated states as derived from [19], and $\mathbf{y}_p$ a vector containing the upcoming preview lateral road coordinates of length $N_p = T_{prev}/T_{s,DM}$. The estimated states include the lateral reference target path, the arms-steering-vehicle states, the muscle activation states, and the delayed states perceived through the sensory organs. The rest of the cost function parameters can be found in Table I.

B. Neuromuscular dynamics

The muscle dynamics are described by a linearised Hill-muscle model [22]. The elasticity of the tendons is represented by the stiffness term, k_a. The contractile element, on the other hand, is described by the damping term, c_a, and the neural activation torque, T_{act}, which is a function of the desired driver torque and the reflex action.

The neuromuscular dynamics of the driver are thus composed of the reflex action of the muscle spindles, a linearised Hill-muscle model including the activation dynamics of the muscles, and the muscle dynamics of the arms, which are interacting with the steering system. These elements are necessary for the modelling of the co-activation mechanism of the muscles.

$$T_{act} = c_a \dot{\theta}_a + k_a(\theta_a - \theta_{sw}) \quad (13)$$

The activation dynamics, denoted by H_{act}, are subject to a lag time constant of the motor neurons excitation, τ_1, and a lumped neuro-muscular transduction delay, τ_2. The latter time constant represents the muscle activation and deactivation lag.

$$H_{act} = \frac{1}{(\tau_1 \cdot s + 1) \cdot (\tau_2 \cdot s + 1)} \quad (14)$$

The reflex loop, an essential element of the co-activation mechanism, is subject to a delay time constant, τ_r, and a gain

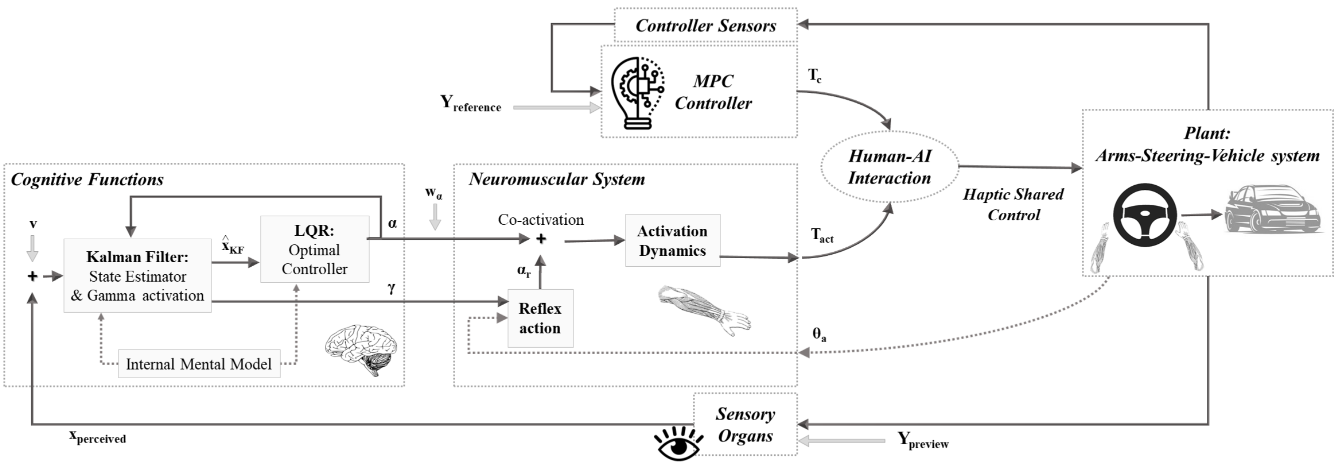

Fig. 2. Haptic Shared Control scheme with driver model representation.

factor, k_r. The expected muscle angle, γ, is calculated based on the internal mental model of the driver and the estimated states by the Kalman Filter.

$$\alpha_r = \frac{k_r}{\tau_r \cdot s + 1} \cdot (\gamma - \theta_a) \tag{15}$$

C. Sensory organs

The sensory organs modelled are the visual perception organs and the proprioceptors with the purpose of representing the human limitations in the perception. The modelling of the vestibular organs is considered out of the scope of this research because the validation is carried out in a fixed-base driving simulator [23]. The states perceived by the driver are the vehicle lateral deviation with respect to the desired path, e_y, the heading angle, ψ, and the muscle angle of the driver, θ_a. These states are subject to a visual delay, τ_{visual}, and a muscle sensory delay, τ_{muscle}.

The feedback sensed by these organs is then sent to the Central Nervous System, subject to additive measurement noise. These noisy signals are used to estimate the states of the plant with the Kalman Filter model, based on the assumption that the driver has a good internal mental representation of the vehicle and their own neuromuscular dynamics. In future work, the introduction of signal-dependent noise, as presented in [24], is of high interest. The parameters of the driver model are listed in Table I. Most values are extracted from [19], whereas T_{prev} and Q are selected based on the pilot experiment, described in Section IV.

TABLE I
DRIVER MODEL PARAMETERS

Parameter	Value	Parameter	Value
T_{prev}	1.4 s	I_{arms}	0.0718 kg m^2
k_a	30 Nmrad	c_a	3 Nms/rad
k_r	21 Nm/rad	τ_r	0.04 s
τ_1	0.03 s	τ_2	0.02 s
τ_{visual}	0.24 s	τ_{muscle}	0.19 s
Q	diag($3 \cdot 10^3$, $1 \cdot 10^2$)	R	1

IV. DRIVER MODEL VALIDATION

As a first step in the validation process of the driver model, the predictions of the torque are simulated offline in CarMaker. Here, the driver model is compared to the IPG CarMaker virtual driver. To represent the plant, we use nonlinear vehicle dynamics and a proprietary nonlinear steering system [25] with a Toyota production vehicle parametrisation. This allows for a high-fidelity simulation of real-world scenarios. Afterwards, a driver-in-the-loop pilot experiment was performed.

A. Pilot experiments with driving simulator

A pilot study was performed at Toyota Motor Europe, using the fixed-base driving simulator of Fig. 7. Three different drivers, listed in Table II in ascending order of driving experience, participated in the experiment to further validate the accuracy of the driver model. In order to test the driver model performance for different driving styles and behaviour, there is significant variability in the drivers' experience. Namely, the participants are a novice driver, a driver with 12-years of experience, and a driver with over 20 years of driving experience and expert knowledge in driving simulators.

B. Results and discussion

The driver model fits all three drivers well, as objectively shown in Table II, which further demonstrates the capabilities of the model to capture inter- and intra-driver variability.

The driver model parametrisation is found to match slightly better the novice and intermediate driver, which could be because the linear internal mental model captures better users with limited driving experience, whereas the mismatch between the linear model and the knowledge of expert drivers is more significant.

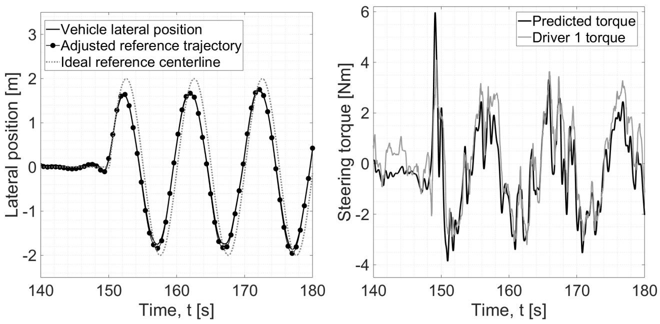

Fig. 3. Driver model predictions based on driver 1, novice

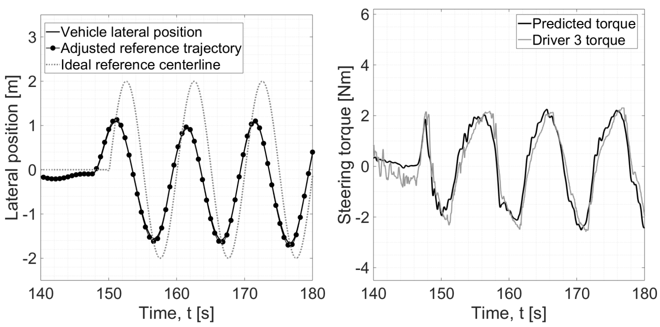

Fig. 4. Driver model predictions based on driver 3, expert level

The sensitivity of the different driver model parameters was studied preliminarily in order to obtain the best possible fit. From this analysis, the driver preview time of the road is highlighted and was tuned for each driver. This can be linked to the different cognitive strategies that each driver has in order to follow the road path. The novice driver, in Fig. 3, tends to have a shorter preview time, as well as a noisier torque input. On the other hand, for the most experienced driver, in Fig. 4, even though the perception of the ideal road trajectory was not correct, the torque input is smooth. This can be associated with the accuracy of internal knowledge that the experienced driver has concerning the vehicle dynamics, which influences the level of muscle spindles activation.

TABLE II
TORQUE PREDICTION ACCURACY OF THE DRIVER MODEL

Driver	RMSE [Nm]	% Accuracy
Driver 1: Novice	0.7344	89.96
Driver 2: Intermediate	0.6232	90.96
Driver 3: Expert	0.7355	87.30

Another relevant factor is that having the correct human road preview is key for the model to give an accurate torque prediction. A good fitting of the prediction was obtained for the three drivers under the assumption that the vehicle position corresponds to the desired vehicle trajectory. This assumption would not be valid in the presence of, for instance, external disturbances, in which case the muscle spindles torque would be activated.

V. MPC FRAMEWORK

The MPC approach can compute the optimisation online and in real-time, making it possible to integrate the driver's torque control behaviour in the loop, thereby capturing the haptic interaction.

In this section, an overview of the mathematical background of the proposed MPC-based LKA controller is presented. The complete investigations concerning MPC can be found in Appendix B. The general goal of the MPC is to iteratively calculate the trajectory of a future control input, $u(k)$, to optimise the performance of the plant being controlled by minimising a cost function subject to constraints. The optimisation takes into account the plant states' information, $x(k)$, at the start of the time window. The length of this finite-time window is called the prediction horizon, N_p. The control horizon of the control input sequence, N_c, can differ from the prediction horizon.

A. Structure of the MPC

The need for accurate precision in the steering task makes the MPC technique highly attractive for the development of ADAS systems. In this framework, we can introduce constraints on the control inputs and the states of the plant to guarantee safety, smooth control, and driver comfort. These additional benefits make the MPC ideal for the design of the proposed haptic controller.

The general structure of the prediction model is

$$\mathbf{x}(k+1) = f(\mathbf{x}(k), u(k)), \text{ with } \mathbf{x}(0) = \mathbf{x}_0 \tag{16}$$

where $\mathbf{x}$ is the vector of the system states, with $\mathbf{x} \in \mathbb{R}^{N_x}$. The variable $\mathbf{x}_0$ denotes the initial states, and f is the function describing the prediction model dynamic equations. Lastly, the variable $u \in \mathbb{R}^{N_u}$ is the control input, with $N_u = 1$ in this study.

The state solution is

$$\mathbf{x}(k) = \phi(k; \mathbf{x}_0, \mathbf{u}_k) \tag{17}$$

And the control input sequence is

$$\mathbf{u}_k := (u(0), u(1), ..., u(k-1)) \tag{18}$$

B. Cost function and system constraints

The constraints are essential to consider the driver-vehicle limitations, as well as guaranteeing smooth control inputs to foster driving comfort.

The cost function of this MPC-based haptic steering controller in (19) improves path tracking performance and reduces the driver-vehicle conflicts. Moreover, the settings are tuned to allow the assist system to provide a more intuitive torque guidance to the driver through the steering interface.

$$\begin{aligned} J(\mathbf{x}, u) = &\sum_{k=0}^{N_p-1} \|(h_x(\mathbf{x}_k) - \mathbf{y}_{r,k})\|^2_{\mathbf{W}_x} + \\ &+ \sum_{k=0}^{N_c-1} \|h_u(u_k)\|^2_{W_u} + \|h_N(\mathbf{x}_{N_p}) - \mathbf{y}_{r,N_p}\|^2_{\mathbf{W}_{x_N}} \end{aligned} \tag{19}$$

where $\mathbf{W}_x,\ \mathbf{W}_{x_N} \geq 0$, are the weighting matrices of the stage and terminal cost for the states. The parameter $W_u > 0$ corresponds to the stage cost for the input. The time-varying state reference vector is denoted as $\mathbf{y}_r$.

The selected costs for the MPC system can be seen in Table III. First of all, the tracking performance objective is implemented to minimise the lateral deviation with respect to the reference path, subject to a look-ahead distance factor depending on the vehicle velocity and the heading angle, ψ. Moreover, driving comfort can be enhanced through weights on the lateral velocity, V_y, and the yaw rate, r. Additional costs on the driver's effort or discomfort indicators can also be added to reduce the activation of the muscle spindles' torque or the total driver steering torque.

TABLE III
MPC SETTINGS AND WEIGHTS

Variable	Value	Variable	Value
$T_{s,cont}$	$1 \cdot 10^{-2}$ s	$T_{s,DM}$	$2 \cdot 10^{-2}$ s
$T_{s,sim}$	$1 \cdot 10^{-3}$ s	N_p	40
N_c	40	W_y	$1 \cdot 10^6$
W_{y_N}	$1 \cdot 10^2$	W_ψ	$V_x \cdot W_y$
W_{T_c}	600	$W_{T_{input}}$	40
W_{V_y}	$1 \cdot 10^2$	W_r	$1 \cdot 10^2$
$W_{spindles}$	$1 \cdot 10^2$	W_{driver}	$6 \cdot 10^2$
$\lvert V_{y,max}\rvert$	4 m/s	$\lvert r_{max}\rvert$	50 deg/s
$\lvert \theta_{sw,max}\rvert$	360 deg	$\lvert \dot{\theta}_{sw,max}\rvert$	800 deg
$\lvert T_{c,max}\rvert$	10 Nm	$\lvert \dot{T}_{c,max}\rvert$	20 Nm/s

Furthermore, the MPC model is subject to constraints, defined in Table III in absolute maximum value. These constraints are imposed on the lateral velocity and the yaw rate. Moreover, constraints on the steering wheel angle, θ_{sw}, and assist torque input, T_c, as well as their respective rates are also introduced to guarantee a smooth assist guidance. Hard constraints on the driver model states are avoided for stability and, instead, weights to penalise their magnitude are included.

The different sampling times and prediction horizons, as specified in Table III, are appropriately chosen to ensure that the controller can be run in real-time without compromising its performance, prediction capabilities, and stability. The nonlinear plant operates at a higher sampling frequency, $T_{s,sim}$, whereas the linear driver model can be accurately run at a lower sampling frequency, $T_{s,DM}$, which reduces the computational requirements. For the MPC, the maximum sampling frequency that allows the model to compute the optimal control input in real-time, $T_{s,cont}$, is selected to ensure stability and a long enough prediction time, $T_{s,cont} \cdot N_p$, which has a direct impact on its performance.

C. Adaptive MPC for conflict minimisation

Human behaviour is adaptive and time-varying. Therefore, one approach to deal with the competing behaviour between human and driving assist systems is to adapt the level of automation [26]. However, due to the increased complexity of the dynamic task allocation, most research studies implement binary switches of control authority.

In this research, the MPC optimisation problem is solved with the ACADO Toolbox [27]. This software allows us to implement an adaptive cost function algorithm through time-varying weights. These dynamic characteristics aim to minimise conflicts between the applied driver torque and the driving assist system torque, as well as dynamically share the control authority. Adaptive weights are applied to the MPC controller torque, its rate, and to the online difference with the driver torque. This feature further enhances collaboration. For instance, an increase in the control input torque cost results in higher driver control authority. On the other hand, if there are no torque conflicts, the cost is smoothly reduced, which results in less steering effort for the driver and a higher level of control authority for the collaborative automation system. An example of this behaviour is displayed in Fig. 5. In order to ensure smooth transitions, the dynamic objective has a parabolic shape, with fast increments to better tackle conflicts and slow reductions, reaching the minimum cost value in a longer time frame.

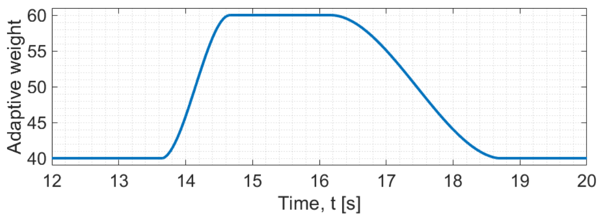

Fig. 5. Adaptive behaviour of the cost on the MPC input

VI. Driving Simulator Experiment: Collaborative Lane Keeping Assist

The aim of this fixed-base driving simulator experiment is to assess the performance and collaborative behaviour of the proposed MPC controller with two different cost-function settings, as well as to compare them against a commercial LKA used as a benchmark. All three controllers provide the drivers with haptic torque guidance to track the centre of the path.

A. Driving Scenario

The driving scenario designed was a route of 5 km long with four straight segments and four sinusoidal segments of different amplitudes. In every trial, the vehicle was driving at a constant vehicle speed of 100 km/h and the test subject's sole task was to control the lateral motion of the vehicle to drive in the centre of the lane. In order to allow for more driver variability, the lane width was set to 5 m and no lane markings were present. The importance of this variability is to better assess how the different LKA systems react and adapt to driver behaviours and diverse driving strategies. This is fundamental to obtain a meaningful comparison of the collaborative behaviour of the different assist systems proposed. An overview of the set-up for this driver-in-the-loop experiment can be seen in Fig. 6. The graphics were rendered with rFpro software based on an IPG CarMaker scenario in a 210 º projection screen, which can be seen in Fig. 7.

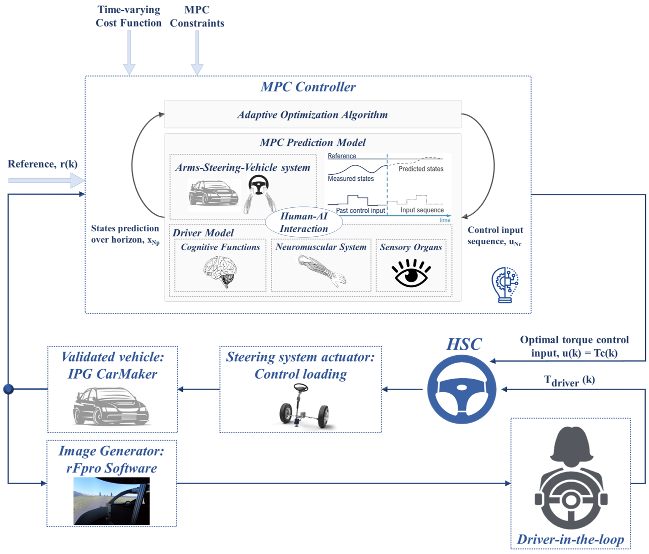

Fig. 6. Set-up for the driving simulator experiment at Toyota Motor Europe, Belgium

Fig. 7. Driving simulator at Toyota Motor Europe, Belgium

B. Experimental procedure

The experimental procedure was the same for all 19 participants, with drivers ranging from 22 to 41 years old. All participants are engineers at Toyota with comprehensive knowledge on vehicle dynamics, with an average age of 29.7 years (SD = 6.9) and 10.7 years (SD = 8.0) of driving experience. A relevant note is that three of the drivers have extensive professional experience assessing LKA systems. The experiment consisted of independent trials for each of the 3 driving assist systems evaluated. During each trial, the driving scenario and the task were the same, with the specific assist system used unknown to the driver. The consistency and statistical significance of the results strengthens the expectations that the number of participants was sufficient for this study.

At the start of the experiment, the participants were instructed of the task and the experimental conditions. The order of the trials was randomised to avoid human bias. During the driving experiment, the first minute of each trial was used as training. This initial data is discarded from the objective metrics and its purpose is to allow drivers to familiarise themselves with the assist system and the driving simulator set-up.

C. Lane Keeping Assist controllers

The controllers assessed during this experiment are described below.

1) Baseline Lane Keeping Assist: The MPC modes are evaluated against a commercial LKA system. The current systems available in the automotive industry are mainly focused on minimising a lateral offset and they do not integrate the driver interaction nor their impact on the closed-loop dynamics. This approach aims to improve path tracking performance, but it can result in a torque guidance with sub-optimal acceptance.

2) MPC Mode 1: The MPC framework makes it possible to change the behaviour of the controller through different cost-function parametrisations. The first MPC mode, which corresponds to a typical cost-function algorithm, has weights on the lateral error, yaw angle, and other vehicle states, as defined in Section V. The costs on the driver model states are not explicitly included in this cost-function. However, the driver behaviour is taken into account by having the extensive driver model from Section III within the prediction model of the controller, aiming a more human intuitive guidance.

3) MPC Mode 2: The second MPC parametrisation makes explicit use of the driver model in the cost-function through the introduction of additional weights on the driver torque and muscle spindles torque predicted by the driver model, which can be found in Table III. Specifically, the proposed MPC controller tries to minimise the muscle spindles activation, which is related to the rejection of disturbances and muscle discomfort at a neuromuscular level. Moreover, the adaptive behaviour of the MPC is further customised to reduce conflicts with the driver. For this purpose, the cost when the driving assist torque is opposing the real driver, as described in Section V-C, is increased.

VII. Results and Discussion

Statistical significance of the metrics was verified using a one-way ANOVA test comparing the three different LKA systems. Further box-plots of the presented metrics are presented in Appendix D. First of all, to ensure the robustness of the results, a Bartlett's test for equal variances between the three groups of controllers was executed. In the subjective evaluations, the null hypothesis of equal variances is rejected for the second criteria (tracking performance), thus, a non-parametric Kruskal-Wallis test was performed in this case. A similar approach is applied to the objective metrics.

A. Subjective evaluation

A questionnaire based on a 7-point scale with a total of 5 questions was designed to subjectively assess the behaviour of each LKA. At the end of the experiment, the participants were also asked to rank the three systems from best to worst. The outcomes of these evaluations show that the proposed MPC controllers outperform the baseline benchmark, with 84.21% of the subjective responses choosing the MPC mode 2 as the best LKA system, and the remaining 15.79% choosing MPC mode 1.

The assessed characteristics are listed below:

- Overall steering effort: Based on the torque applied by the driver, with the ideal range between 3-5 points.
- Performance and guidance level: Defined in terms of path tracking performance of the ideal centerline. A range of 6-7 corresponds to high tracking precision.
- Collaborative behaviour: An evaluation of 6-7 points means that torque conflicts between the driver and driving assist system are reduced.
- Feeling of being in control: Defined in terms of how easily the drivers feel that they can overrule the assist guidance if desired, with 6-7 points if it is easy.
- Smooth control: In terms of the presence of unnecessary corrections during authority transitions between the driver and assist system control. The lower range being abrupt (1-2) and the upper range smooth (6-7) control.

Fig. 8 presents the average grade of each subjective metric per controller. The ideal range is highlighted in light green. This is consistent with the preference of drivers to use the second mode of the proposed MPC.

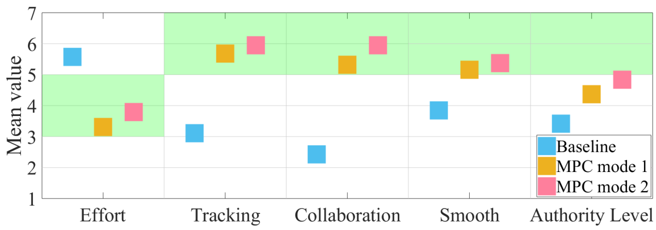

Fig. 8. Mean results of the subjective evaluation of 19 participants.

The participants consistently felt that proposed MPC controllers provide an even more natural feel than the state-of-the-art baseline system. In general, the presence of driver-assist conflicts creates a perception of the baseline controller being *heavier* than desired, as well as having a lower collaborative behaviour. Moreover, drivers do not perceive small path tracking errors that the baseline assist tries to minimise, which may explain a higher degree of conflict and, eventually, decreased tracking performance. The feeling of being in control, as expected, is lower because part of the control authority is *shared* with the assist system. However, the MPC modes are still graded higher than the baseline system for this last subjective quality, as well as providing an even more smooth guidance.

Statistical significance of the responses was positively verified, which can be seen in Table IV. For all five subjective metrics, MPC mode 2 is the best, closely followed by the fist

TABLE IV
ANALYSED DATA OF THE SUBJECTIVE EVALUATIONS

Criteria	Baseline	MPC 1	MPC 2	F	p
Overall effort	5.58 (0.90)	3.32 (1.25)	3.79 (1.18)	21.53	<0.001
Tracking performance	3.11 (1.73)	5.68 (1.11)	5.95 (0.91)	27.86	<0.001
Collaborative behaviour	2.42 (1.35)	5.32 (1.00)	5.95 (1.08)	50.60	<0.001
Feeling of control	3.42 (1.74)	4.37 (1.34)	4.84 (1.50)	4.21	0.02
Smooth control	3.84 (1.34)	5.16 (1.57)	5.37 (1.67)	5.51	0.007

MPC mode. The mean value of the responses for each metric, as well as their standard deviation (SD) are also included.

B. *Objective assessment*

The objective evaluation is based on an extensive list of Key Performance Indicators (KPI), which can be seen in Appendix A, based on a recompilation of both literature studies and industry standard metrics. These metrics were meticulously selected to impartially evaluate the responses to the subjective questions. Fig. 9 shows the box plot of two representative objective metrics. In the following paragraphs, the values of the numerical differences between the proposed MPC mode 2 and the baseline benchmark LKA are discussed.

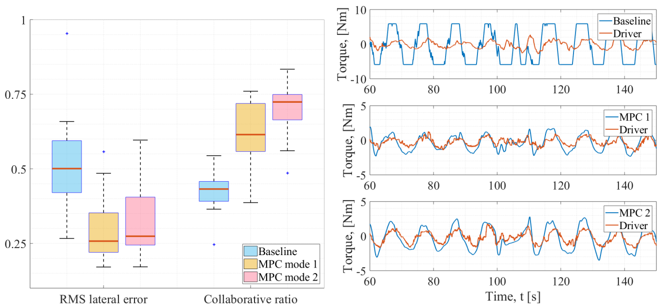

(a) (b)

Fig. 9. (a) Box plot of the objective KPIs of 19 participants (b) Torques over time for participant 1.

In Table V, the results of the one-way ANOVA test are presented, as well as the mean and SD values of each metric. From this, it is clear that the proposed MPC controllers significantly decreased the overall driver steering effort, in particular, with an average reduction of 55.47% with respect to the baseline system. This is in agreement with the subjective evaluation of the MPC modes, which were judged as *lighter* steering systems. The explanation lies in the behaviour of the MPC controllers, which actively cooperate with the driver and minimise the conflict, as can be seen in Fig. 9. In other words, the intuitive, continuous guidance of the MPC modes makes an efficient use of the torque feedback to achieve better symbiosis with the driver. Objectively, the collaborative ratio of the MPC controller in mode 2 increases by 62.86% with respect to the baseline benchmark.

TABLE V
ANALYSED DATA OF THE OBJECTIVE METRICS

Criteria	Baseline	MPC 1	MPC 2	F	p
Driver effort	177.01 (37.74)	51.32 (37.38)	78.83 (50.31)	46.49	< 0.001
Controller effort	2982.77 (170.05)	209.83 (92.90)	390.08 (193.23)	43.17	<0.001
Lateral RMSE	0.51 (0.15)	0.29 (0.11)	0.33 (0.12)	15.38	<0.001
Maximum e_y	1.14 (0.54)	0.66 (0.33)	0.75 (0.43)	6.17	0.004
Mean e_y	-0.06 (0.19)	0.03 (0.15)	0.03 (0.18)	1.81	0.173
SD e_y	0.47 (0.16)	0.25 (0.10)	0.28 (0.10)	17.53	<0.001
Collaborative ratio	0.43 (0.06)	0.62 (0.11)	0.70 (0.09)	45.70	<0.001
Intrusiveness ratio	0.57 (0.06)	0.38 (0.11)	0.30 (0.09)	45.70	<0.001
Resistance ratio	0.28 (0.04)	0.20 (0.13)	0.16 (0.11)	16.10	<0.001
Contradiction ratio	0.29 (0.04)	0.18 (0.13)	0.14 (0.11)	18.50	<0.001
Coherence	-0.17 (0.17)	0.15 (0.29)	0.36 (0.27)	21.88	<0.001
Level of control authority	17.56 (3.68)	7.73 (8.03)	8.22 (8.79)	20.91	<0.001
Steering reversal rate	31.84 (12.84)	23.76 (5.27)	22.68 (6.75)	8.38	0.015

Moreover, even though the baseline controller optimises almost solely the tracking performance, the results show that the proposed MPC mode 2 has an improvement of 35.93% in regards to the RMSE of lateral error. This can be explained because the closed-loop human-vehicle interaction is considered by the MPC controller. As previously mentioned, an accurate prediction of the driver's intention reduces conflicts. On the other hand, driver-assist conflicts can result in decreased tracking performance and user-acceptance.

Furthermore, the level of control authority is assessed in terms of the ratio between the torque effort of the controller and the driver. As expected, the authority is greatly shared with the LKA, which relieves the driver partially from the steering workload. Even though in all three controllers the level of control authority is dominated by the assist system, in the case of the MPC modes, the driver control is significantly higher than with the baseline system. This can lead to less driver opposition to regain control. Besides, from the subjective evaluations, most participants felt like they were still in full control with MPC mode 2. This further reassures the hypothesis that this novel LKA controller can provide a human-like, collaborative guidance. In other words, the assist system can make drivers feel in control while continuously guiding them to the correct path, decreasing driver workload, and significantly improving driver comfort. Lastly, the steering wheel reversal rate (SRR) is an indicator of the smoothness of both the control, as well as the driver workload. A lower SRR means that the driver requires less corrections to follow the target path. In this case, the proposed MPC mode 2 improves the smoothness of the control by 28.76% with respect to the baseline. In the case of the baseline controller, a higher SRR suggests that drivers tend to correct the guidance of the assist guidance.

VIII. Conclusion

This novel MPC control strategy tackles the need to blend driver and ADAS control through driver modelling in a Haptic Shared Control strategy. The controller is able to predict the human behaviour and, at the same time, it provides a smooth and intuitive guidance to the driver. The results show that the assist torque guidance matches the driver expectations and their perception of collaboration.

In this study, a comprehensive driver model has been integrated in the MPC controller, providing accurate torque predictions when the driver target trajectory is known, as shown by the pilot experiments performed in a fixed-base driving simulator.

The MPC controller handles the nonlinearities and system constraints, which enhances driving comfort. At the same time, it allows a dynamic control authority sharing between driver and assist system, which strengthens collaboration. The adaptability of the driving assist system is essential to positively cooperate with the time-varying human behaviour during the steering task. Moreover, the controller can be tuned to portray different behaviours, while maximising driver comfort and improving tracking performance.

The data acquired from the 19 participants in a fixed-base driving simulator consistently indicates that the proposed controller fosters symbiotic driving and reduces driver-vehicle conflicts. Moreover, it has been demonstrated that the proposed strategy significantly improves the performance of the currently available commercial system, both subjectively and objectively with extensive KPIs.

IX. Future work

As presented in this paper, while the users of the current system appreciate the support given, the study shows that the potential for further improvement towards top level comfort, considering the long term target of automated driving, is still high. This proposal suggests a significant step ahead in this aspect, and more extensive tests in the driving simulator for different scenarios are under investigation. Driving simulator experiments are appropriate for the initial stages of the development due to their reduced cost and their potential to help extrapolating subjective measurements into objective KPIs. Once validated, a wider scope of steering tasks, a higher degree of plant nonlinearities, and driver model suitability will be investigated in order to test the robustness of the proposed MPC.

In parallel to these experiments, a more realistic environment is needed to further assess the validity of this approach. For this purpose, the proposed MPC controller will be evaluated with a real-time control system on a physical test vehicle.

Appendix
List of Key Performance Indicators

A full list of all the Key Performance Indicators found both in literature and in the industry are listed below.

A. Overall steering effort

- Driver torque steering effort during the time of the manoeuver, se_{Td},

$$se_{Td} = \int_0^T \mathbf{T}_d^2 \; dt \tag{20}$$

- Driving assist system torque steering effort during the time of the manoeuver, se_{Tc},

$$se_{Tc} = \int_0^T \mathbf{T}_c^2 \; dt \tag{21}$$

B. Path tracking performance

- Root-mean-square error of the lateral position with respect to the ideal road centerline, $RMSE_y$, with N being the total number of data points.

$$RMSE_y = \sqrt{\frac{1}{N}\sum_{i=1}^{N} \mathbf{e}_{y,i}^2} \tag{22}$$

- Maximum lateral position error, $e_{y,max}$,

$$e_{y,max} = max(\mathbf{e}_y) \tag{23}$$

- Mean of the lateral position error, $\overline{e_y}$,

$$\overline{e_y} = \frac{1}{N}\sum_{i=1}^{N} e_{y,i} \tag{24}$$

- Standard deviation of the lateral position error, σ_{e_y},

$$\sigma_{e_y} = \sqrt{\frac{1}{N-1}\sum_{i=1}^{N} |e_{y,i} - \overline{e_y}|^2} \tag{25}$$

C. Collaborative behaviour

- Consistency ratio [13], r_{co}, calculated as the ratio between the time where the driver torque and the assist system have the same sign and the total time of the simulated manoeuvre.

$$r_{co} = \frac{1}{T}\int_0^T sign(\mathbf{T}_{dr} \cdot \mathbf{T}_c) \; dt \text{ if } \mathbf{T}_{dr} \cdot \mathbf{T}_c \geq 0 \tag{26}$$

- Intrusiveness ratio, r_{int}, calculated as the ratio of the time where the driver torque and the assist system have opposite sign and the total time of the simulated manoeuvre.

$$r_{int} = \frac{1}{T}\int_0^T sign(\mathbf{T}_{dr} \cdot \mathbf{T}_c) \; dt \text{ if } \mathbf{T}_{dr} \cdot \mathbf{T}_c < 0 \tag{27}$$

- Resistance ratio [13], r_{re}, calculated as the ratio of the time where the driver torque and the assist system have opposite sign and the total time of the simulated manoeuvre, as long as the driver torque is bigger than the driving assist torque.

$$r_{re} = \frac{1}{T}\int_0^T sign(\mathbf{T}_{dr}\cdot\mathbf{T}_c)\ dt \quad \text{if } \mathbf{T}_{dr}\cdot\mathbf{T}_c < 0 \ \&\ \mathbf{T}_{dr} > \mathbf{T}_c \tag{28}$$

- Contradiction ratio [13], r_{cont}, calculated as the ratio of the time where the driver torque and the assist system have opposite sign and the total time of the simulated manoeuvre, as long as the driver torque is smaller than the driving assist torque.

$$r_{cont} = \frac{1}{T}\int_0^T sign(\mathbf{T}_{dr}\cdot\mathbf{T}_c)\ dt \quad \text{if } \mathbf{T}_{dr}\cdot\mathbf{T}_c < 0 \text{ and } \mathbf{T}_{dr} < \mathbf{T}_c \tag{29}$$

- Coherence [28], γ, defined in terms of the cosine of the angles formed by the driver and driving assist torque. It should be positive if the assist system is mainly portraying a collaborative behaviour during the total time of the simulated manoeuvre.

$$\gamma = \frac{\int_0^T \mathbf{T}_{dr}\cdot\mathbf{T}_c\ dt}{\sqrt{\int_0^T \mathbf{T}_{dr}^2\ dt\cdot\int_0^T \mathbf{T}_c^2\ dt}} \tag{30}$$

D. Control authority level

- Level of sharing [28], T_{share}, is the ratio between the assist system steering effort and the driver steering effort.

$$T_{share} = \frac{se_{Tc}}{se_{Td}} \tag{31}$$

E. Smooth driving

- Steering reversal rate [29], SRR, is the number of steering wheel reversals, per minute, that are larger than a gap value, $\theta_{sw,min}$. To reduce high-frequency noise, the steering wheel angle and steering wheel velocity signals are filtered with a 2^{nd} order Butterworth filter with cut-off frequency, $f_{cut} = 0.6$ Hz. The SRR is calculated as the number of times where $|\theta_{sw}(t_1)-\theta_{sw}(t_2)| \geq \theta_{sw,min}$ for time-steps t_1, t_2 corresponding to consecutive steering wheel velocities equal to zero.

$$\theta_{sw,min} = 3\ deg, \tag{32}$$

$$SRR = \frac{n_{change}}{T}\cdot 60 \tag{33}$$

F. Driver model accuracy

- Root-mean-square error (RMSE) of the predicted driver torque, $T_{d,pred}$, with respect to the real driver, T_d ,

$$RMSE_{Tpred} = \sqrt{\frac{1}{N}\sum_{i=1}^{N}(T_{d,pred,i}-T_{d,i})^2} \tag{34}$$

- Accuracy of the driver model torque prediction in percentage, defined as:

$$A(\%) = \left[1 - \frac{1}{SD(T_d)}RMSE_{Tpred}\right]\cdot 100 \tag{35}$$

ACKNOWLEDGMENT

The authors would like to thank Dr. Riender Happee and Sarvesh Kolekar for their valuable scientific feedback.

REFERENCES

[1] D. I. Katzourakis, N. Lazic, C. Olsson, and M. R. Lidberg, "Driver steering override for lane-keeping aid using computer-aided engineering," *IEEE/ASME Transactions on Mechatronics*, vol. 20(4), pp. 1543–1552, 2015.

[2] M. Itoh, F. Flemisch, and D. Abbink, "A hierarchical framework to analyze shared control conflicts between human and machine," in *13th IFAC Symp. of Human-Machine Systems, Kyoto, Japan*, vol. 49(19), 2016, pp. 96–101.

[3] T. A. Litman, "Autonomous vehicle implementation predictions: Implications for transport planning," *Transportation Research Board 94th Annual Meeting*, 2015.

[4] M. Mulder, D. A. Abbink, and E. Boer, "Sharing control with haptics: Seamless driver support from manual to automatic control," *Human Factors*, vol. 54(5), pp. 786–798, 2012.

[5] R. Boink, M. M. van Paassen, M. Mulder, and D. A. Abbink, "Understanding and reducing conflicts between driver and haptic shared control," *IEEE International Conference on Systems, Man, and Cybernetics*, pp. 1510–1515, 2014.

[6] D. Franklin, R. Osu, E. Burdet, M. Kawato, and T. Milner, "Adaptation to stable and unstable dynamics achieved by combined impedance control and inverse dynamics model," *Journal of Neurophysiology*, vol. 90(5), pp. 3270–3282, 2003.

[7] D. A. Abbink and M. Mulder, "Neuromuscular analysis as a guideline in designing shared control," in *Advances in Haptics*. IntechOpen, 2010, ch. 27.

[8] C. Lv, H. Wang, D. Cao, Y. Zhao, D. J. Auger, M. Sullman, R. Matthias, L. Skrypchuk, and A. Mouzakitis, "Characterization of driver neuromuscular dynamics for human–automation collaboration design of automated vehicles," *IEEE/ASME Transactions on Mechatronics*, vol. 23(6), pp. 2558–2567, 2018.

[9] F. Mars, L. Saleh, P. Chevrel, F. Claveau, and J. Lafay, "Modeling the visual and motor control of steering with an eye to shared-control automation," in *Proceedings of the Human Factors and Ergonomics Society Annual Meeting*, vol. 55, 2011.

[10] Z. Ercan, A. Carvalho, M. Gokasan, and F. Borrelli, "Modeling, identification, and predictive control of a driver steering assistance system," *IEEE Transactions on human-machine systems*, vol. 47(5), pp. 1–11, 2017.

[11] Z. Ercan, A. Carvalho, H. E. Tseng, and F. Borrelli, "A predictive control framework for torque-based steering assistance to improve safety in highway driving," *Vehicle System Dynamics*, vol. 56(5), pp. 810–831, 2018.

[12] C. Guo, C. Sentouh, J.-B. Haué, and J. C. Popieul, "Driver–vehicle cooperation: A hierarchical cooperative control architecture for automated driving systems," *Cognition, Technology & Work*, vol. 21(4), p. 657–670, 2019.

[13] L. Saleh, P. Chevrel, F. Claveau, J. F. Lafay, and F. Mars, "Shared steering control between a driver and an automation: Stability in the presence of driver behavior uncertainty," *IEEE Transactions on Intelligent Transportation Systems*, vol. 14(2), pp. 974–983, 2013.

[14] X. Ji, K. Yang, X. Na, C. Lv, and Y. Liu, "Shared steering torque control for lane change assistance: A stochastic game-theoretic approach," *IEEE Transactions on Industrial Electronics*, vol. 66, pp. 3093–3105, 2018.

[15] X. Na and D. Cole, "Game theoretic modelling of the steering interaction between a human driver and a vehicle collision avoidance controller," *IEEE Transactions on Human-Machine Systems*, vol. 45(1), pp. 25–38, 2015.

[16] S. Ko and R. Langari, "Shared control between human driver and machine based on game theoretical model predictive control framework," *IEEE/ASME International Conference on Advanced Intelligent Mechatronics (AIM), Boston, MA, USA*, pp. 649–654, 2020.

[17] W. Scholtens, S. Barendswaard, D. M. Pool, M. van Paassen, and D. Abbink, "A new haptic shared controller reducing steering conflicts," *IEEE International Conference on Systems, Man, and Cybernetics*, pp. 2705–2710, 2018.

[18] A. M. Rios Lazcano, B. Shyrokau, T. Niu, D. J. Cole, and X. Carrera Akutain, "MPC-based shared steering system using torque control and driver modelling for collaborative driving," in *FISITA 2020 World Congress, Prague*, 2020.

[19] T. Niu and D. Cole, “A model of driver steering control incorporating steering torque feedback and state estimation,” Department of Engineering, University of Cambridge, Tech. Rep., 2020, (in preparation).
[20] C. J. Nash and D. J. Cole, “Identification and validation of a driver steering control model incorporating human sensory dynamics,” *Vehicle System Dynamics*, vol. 58, no. 4, pp. 495–517, 2020.
[21] R. S. Sharp and V. Valtetsiotis, “Optimal preview car steering control,” *Vehicle System Dynamics*, vol. 35, pp. 101–117, 2001.
[22] J. M. Winters and L. Stark, “Muscle models: What is gained and what is lost by varying model complexity,” *Biological Cybernetics*, vol. 55 (6), pp. 403–420, 1987.
[23] B. Shyrokau, J. De Winter, O. Stroosma, C. Dijksterhuis, J. Loof, R. van Paassen, and R. Happee, “The effect of steering-system linearity, simulator motion, and truck driving experience on steering of an articulated tractor-semitrailer combination,” *Applied ergonomics*, vol. 71, pp. 17–28, 2018.
[24] S. Kolekar, W. Mugge, and D. Abbink, “Modeling intradriver steering variability based on sensorimotor control theories,” *IEEE Transactions on Human-Machine Systems*, vol. 48(3), pp. 291–303, 2018.
[25] M. Damian, B. Shyrokau, A. Ocariz, and X. C. Akutain, “Torque control for more realistic hand-wheel haptics in a driving simulator,” in *Driving Simulation Conference Europe, Strasbourg, France*, 2019.
[26] T. Inagaki, “Adaptive automation: Sharing and trading of control,” *Handbook of cognitive task design*, p. 147–169, 2003.
[27] B. Houska, H. Ferreau, and M. Diehl, “ACADO toolkit—An open-source framework for automatic control and dynamic optimization,” *Optimal Control Applications and Methods*, vol. 32, no. 3, pp. 298–312, 2011.
[28] B. Pano, Y. Zhao, P. Chevrel, F. Claveau, and F. Mars, “Shared control based on an ecological feedforward and a driver model based feedback,” *9th IFAC International Symposium on Advances in Automotive Control, Orléans, France*, pp. 385–392, 2019.
[29] G. Markkula and J. Engström, “A steering wheel reversal rate metric for assessing effects of visual and cognitive secondary task load,” *13th ITS World Congress*, 2006.

A

Driver Models for the Steering Task

The modelling and understanding of the driver behaviour is key to create new control alternatives that can take into account the driver-in-the-loop dynamics to develop more collaborative driving assist systems.

A clear overview of the state-of-the-art driver models can be found in this section. The introduction of driver models is necessary to model the driver-vehicle interaction during the steering task and to provide more effective haptic torque guidance. It also allows for a subjective-objective interpretation of steering feel during closed-loop experiments with the driver. As demonstrated by Horiuchi and Yuhara [44], subjective perception of handling characteristics of actively controlled vehicles can be achieved by implementing driver models.

The main driver aspects to be modelled for a reliable representation can be divided into three categories, which are the cognitive behaviour, the neuromuscular dynamics, and the sensory organs, explained in Sections A.1, A.2 and A.3. Afterwards, the common range for the different parameter values is presented in Section A.4, followed by the extended description of the selected driver model in Section of A.5, with its validation in a pilot driving simulator experiment. Lastly, the main conclusions related to driver modelling are outlined in Section A.6.

A.1. Cognitive behaviour

The cognitive models correspond to the reception, perception and processing of information of the human driver. These models represent the human capabilities of predicting and anticipating situations. In particular for the driving task, this can be illustrated as the driver being able to create a preview of the upcoming road curvature and, as a consequence, generating the desired control action.

A.1.1. The Central Nervous System

The Central Nervous System [57] is composed of the brain and spinal cord and its main function is to send control neural signals to the neuromuscular system, NMS. These motoneurone commands (α, γ) are calculated through a certain control strategy based on the states of the closed-loop system, such as vehicle position, velocity, and steering wheel torque, among others. However, how the CNS decides its preferred control strategy, in terms of which costs or states are minimised, has been the subject of significant controversy. The differences in the objective function to be minimised can lead to different control strategies that range in performance and resemblance to the actual human behaviour. In Fig. A.1, the divisions of the CNS in the brain are illustrated.

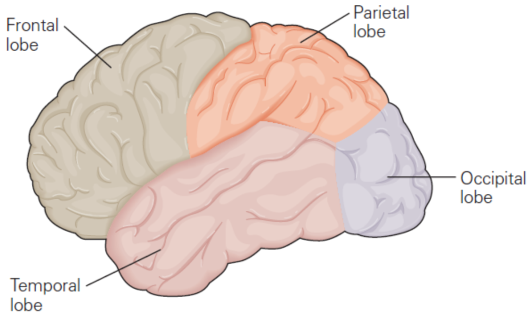

Figure A.1: Divisions of the Central Nervous System [57].

All the signals coming from the CNS, known as efferent signals, are subject to small time delays that are a function of the neurones' firing rates. This rate is variable and has an upper limit. The higher this firing rate is, the lower the transportation delays are, keeping the control stable. The α-motoneurone is also subject to motor noise, which has been found to be signal-dependent.

The cost function of the different strategies consists of different factors, each of which is associated with a weighting parameter, and both the factor as well as the weighting play important roles in determining the performance of the controller. The most common cost functions found in literature include weights on the driver's input command to the system, and path-following performance, based on lateral position and yaw angle error. Nevertheless, indicators such as the steering effort or muscle energy consumption have also been evaluated [47], in which the minimisation of such a cost function represents a trade-off between performance accuracy and energy consumption minimisation.

A.1.2. Cognitive control models

This section contains an overview of the vast amount of research that has been undertaken in the understanding of the human brain and the use of internal mental models. This allows us to determine the preferred driver's control strategy. Moreover, the human learning capabilities and robustness against uncertainty are also acknowledged. More extensive reviews of driver cognitive models can be found in the research of MacAdam [67] and Plöchl and Edelmann [89].

The first type of model introduced in this outline is based on compensatory control and its general structure can be seen in Fig. A.2.

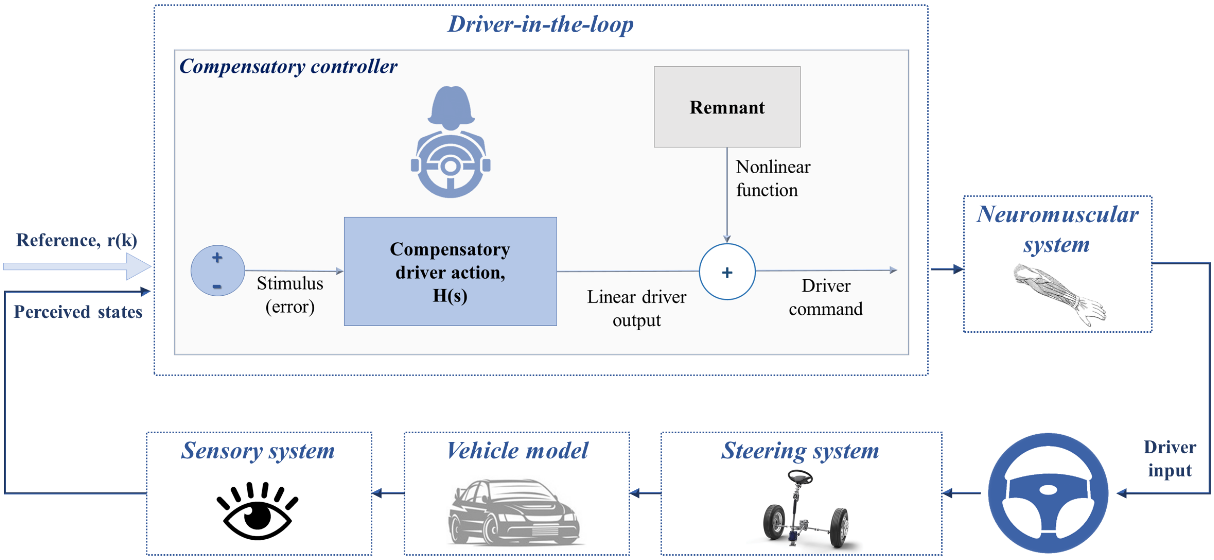

Figure A.2: Schematic representation of a compensatory controller for the steering task.

PID Compensation Model

The first mathematical representation of the steering task was developed by Tustin [103], who approximated the steering human strategy as a linear transfer function. This method relies on a proportional controller minimising the error and rate of the error subject to a time delay in the control action.

Another PID compensation model can be found in early literature, by Iguchi [50]. The general structure of the transfer function is

$$H(s) = K_p + K_d \cdot s + \frac{K_i}{s} \tag{A.1}$$

Such approaches are an oversimplification of the actual cognitive control behaviour. This was already observed by Tustin, who acknowledged that there was an unmodelled control part which could not be defined by a linear transfer function. This nonlinear function was named the *remnant*. Another disadvantage is that, in general, these models do not include any cognitive time delays within the function either, such as Iguchi's model. Lastly, there is an additional difficulty of determining the optimal gains for the controller, which makes this approach less advantageous.

Crossover-Compensatory models

The steering task can be seen as a closed-loop compensatory control strategy, as described by McRuer and Krendel [75, 76]. This strategy defines a closed-loop system representing the driver and vehicle dynamics as a whole, where the driver corrects, or compensates, for the tracking error based on the current states of the system.

The main objective of McRuer was to illustrate how the human-vehicle system can be described in engineering terms when the human is actively participating in the control task. In his research, the human was characterised by a quasi-linear mathematical model. Within the model, he defined a linear transfer function representing the compensatory behaviour and an additional *remnant* [103] to account for human nonlinearities. Further improvements are the introduction of time delays representing the driver response delay and a gain related to the experience of the driver.

This type of models are robust against disturbances at low frequencies. However, human delays in the NMS make this strategy unsuitable for the steering task. Another drawback is that the compensatory models' efficiency is limited to a certain frequency range, below the *crossover frequency* w_c. If the closed-loop system is subject to inputs above this frequency w_c, the dynamics are drastically changed and the system's closed-loop response becomes poor.

Although McRuer did not include a more detailed driver model in his initial research, he pointed out that a more complete cognitive control strategy should also include the predictive-anticipatory human behaviour.

Preview-Anticipatory models

Unlike the above methods, preview-tracking approaches make use of future path information, which results in better tracking accuracy. These models take into account the human anticipatory capabilities and are also known as predictive, closed-loop models. They are based on the current vehicle states, the previewed path to follow over a time horizon, the vehicle dynamics, and the knowledge of their own interaction with the steering wheel interface. This last component can be seen as the internal mental representation that the driver has of the driver-vehicle system.

The human predictive abilities allow them to send control signals to the neuromuscular system even before actual sensory feedback is available [111]. The outcome of such a control strategy results in accurate and fast tracking behaviour.

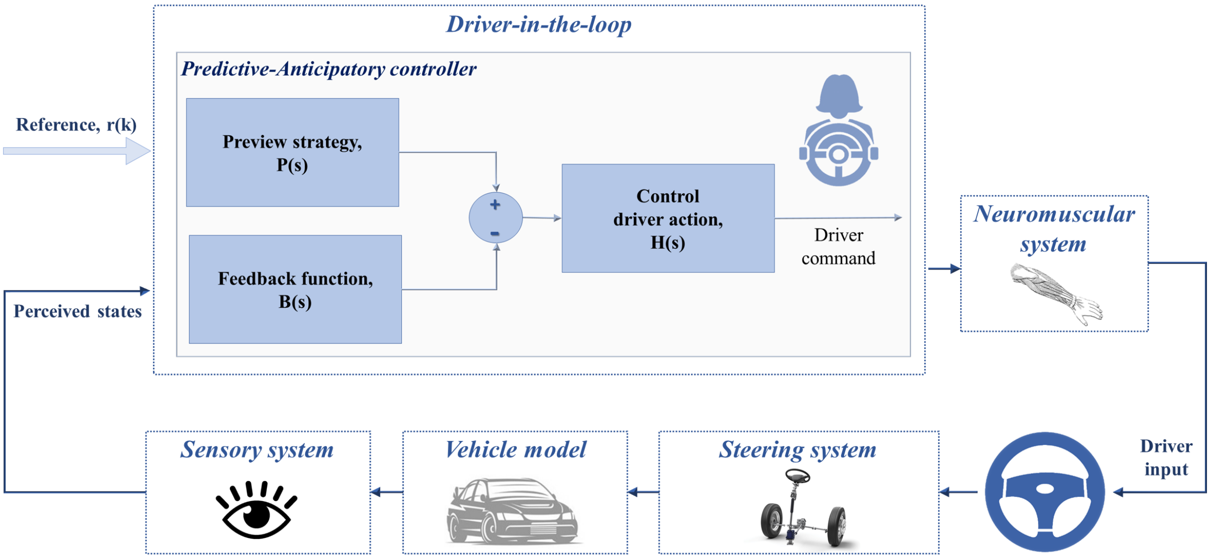

Figure A.3: Schematic representation of a predictive controller for the steering task.

Within the predictive models, which structure can be seen in Fig. A.3, it is possible to differentiate two main subcategories.

- Single-point preview models [23, 39, 64, 90]:

  One of the earliest attempts was made by Kondo and Ajimine [64], in which one single preview point was used to calculate the control strategy. In this first model, the response delay of the driver is ignored, and little background about the system's gain is provided. However, it is considered to add a significant step in the understanding of the cognitive tracking strategies. The general structure of the transfer functions of this model, in agreement with the notation in Fig. A.3, is described by Eqs. A.2, A.3, and A.4. As can be seen, this is based on a linear prediction model, where the inputs to $B(s)$ are the lateral position, y_p, and yaw angle, ψ.

$$P(s) = e^{T_p s} \tag{A.2}$$

$$H(s) = K \tag{A.3}$$

$$B(s) = (1, T_p \cdot V) \tag{A.4}$$

- Multiple-point preview models:

  More complex representations include multiple preview points to represent the upcoming road trajectory information available to the driver, as represented in Fig. A.4.

  This optimal control strategy, initiated by MacAdam [69, 70], has been subject to different modifications, both in the defined cost function, as well as in the control method selected to perform the optimisation of the control input.

  Among the control algorithms, the author highlights the use of *Model Predictive Control* [59, 61, 69, 70, 86] and *Linear-Quadratic-Regulator* [87, 88, 99]. The LQR algorithm can explicitly compute the optimal control input based on linear plant dynamics and a quadratic cost function, but it can't consider the system's constraints. The MPC strategy is discussed in detail in Chapter B. Some of the benefits of using MPC are the suitability to investigate nonlinear systems and the possibility to add constraints to the system, as discussed by Cole et al. [19]. This can represent human limitations and result in more realistic control strategies.

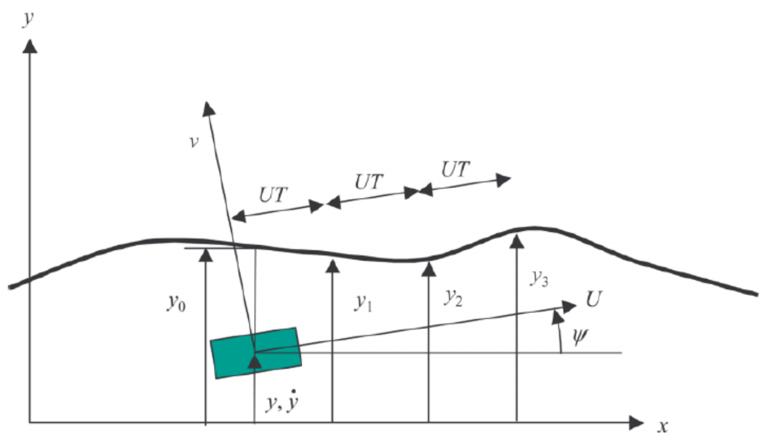

Figure A.4: Top view of the road displacements ahead of the vehicle [19].

The combination of both forward predictive control and feedback control allows for accurate path tracking performance as well as compensate for disturbances and inaccuracies of the driver's internal mental model.

Neural networks and driver's adaptation

The extensive research on drivers' cognitive behaviour emphasises the complexity of the human CNS. Therefore, in order to deal with these highly nonlinear input-output relationships, as well as with the uncertainty of a clear control algorithm method, the use of Neural Networks has also been investigated. In Fig. A.5, a general representation of a Neural Network is presented.

The main benefit of using a NN is being able to mimic the human adaptive control behaviour. Also, it is possible to identify the system's input-output relationships, including nonlinear properties, without predetermining the control strategy. The general structure of a NN includes a varying number of layers, in which each added layer increases the complexity of the system but also its performance or capabilities. For instance, a three-layer system would be comprised of an input layer, an output layer, and a hidden layer. This hidden layer is derived by *training* the network based on examples of multiple different scenarios, also known as back-propagation. In other words, the NN exemplifies the *learning* behaviour.

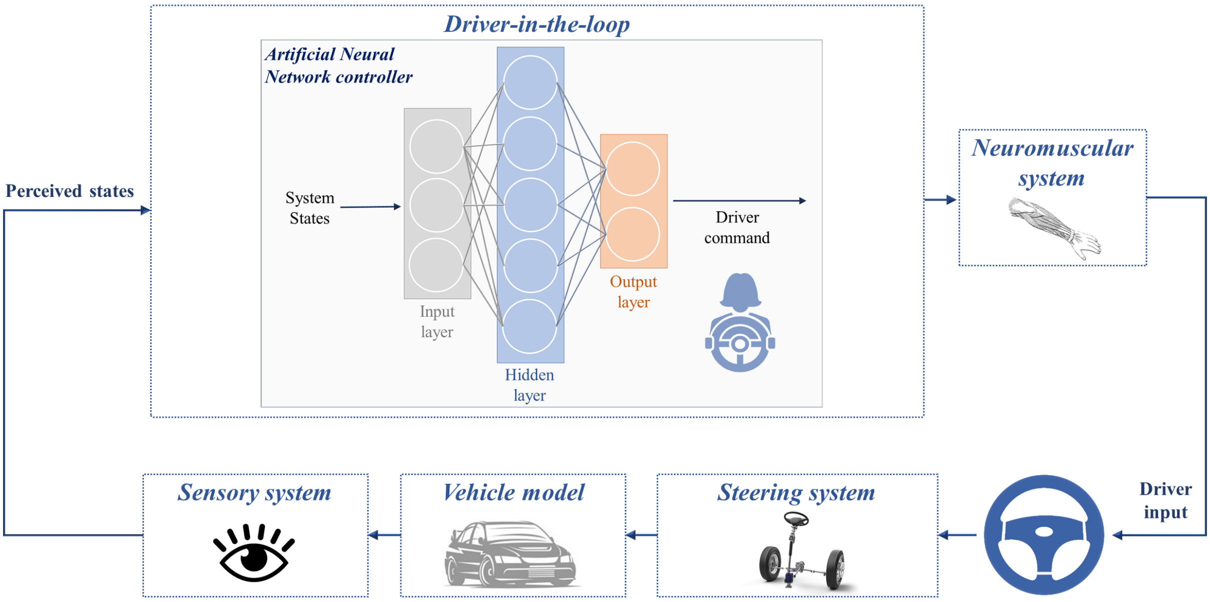

Figure A.5: Schematic representation of a Neural Network controller for the steering task.

The use of neural networks has proven to be effective for certain task scenarios [56, 68] within the Identification Theory framework. One of the key features implemented in both papers is the use of time delayed states information within the input layer, which symbolises the human cognitive delays. However, the need for huge amounts of data and their poor performance when tackling novel tasks, makes them less suitable to model the unpredictable, human behaviour.

Furthermore, from Kageyama et al. [56], it is interesting to highlight that the most significant weighting variables found for the NN to compute the output steering torque were based on the vehicle speed and information about the upcoming road shape. This result is in agreement with the cognitive control strategy based on predictive models. Moreover, it was also found that these weighting parameters can change over time, and that the drivers are able to learn. This learning capabilities can result in less dependency on the environment states, for example, the curvature of the upcoming road.

Modular approaches for learning behaviour

Cognitive models can also include the human adaptability, variability, and learning capabilities when executing a task [43]. For instance, drivers can learn based on previous driving history or adapt their behaviour depending on the criticality of the scenario. Models portraying such qualities display humans' characteristics of learning and their adaptive behaviour [41, 53, 55, 112]. These models are based on a Mixture of Experts architecture, where expert networks are classified and selected through a gating network, as shown in Fig. A.6. However, these models have not been particularised to the driving task.

In the research carried out by Haruno et al. [41], these human capabilities are represented through a modular approach, which was named the modular selection and identification for control model (MOSAIC). In the model, each controller is applicable to a small set of contexts. The model is composed of multiple coexisting pairs of forward and inverse models, which are learnt and appropriately selected based on the environment. The learning architecture has been based both on the gradient-descent method [112] and the expectation-maximization algorithm [41], which resulted in a more robust behaviour against starting conditions and learning parameters. However, the simulations were limited to cases of object manipulation tasks. The selection of the suitable inverse model, the controller, is based on the shape of the object, which has certain associated dynamics. In order to reduce transient periods where no controller is selected, the model combines both feedforward selection based on the accuracy of predictions and feedback of the outcome of the task. For novel situations, the model was able to adapt and correct online for objects of which dynamics lie within the polyhedra of already learnt dynamics.

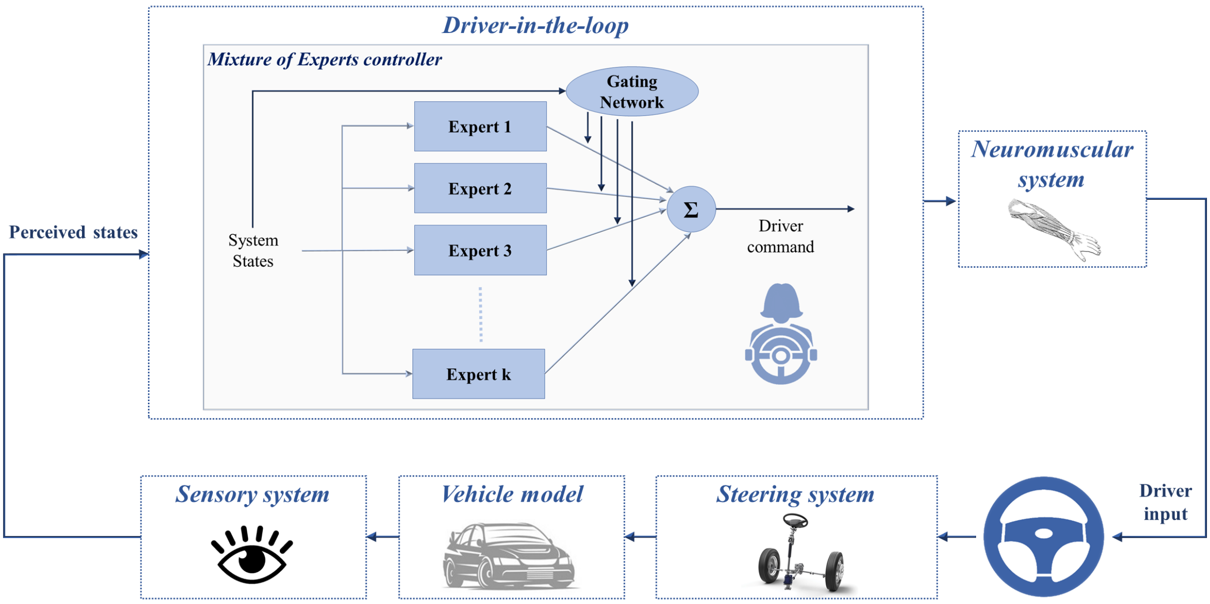

Figure A.6: Schematic representation of a Mixture of Experts controller for the steering task.

A.1.3. Internal mental models

In Section A.1.2, the main driver cognitive modelling strategies have been described. However, these methods alone are not enough to describe the cognitive behaviour of the driver. The aforementioned models rely on the assumption that the driver has access to certain states of the driver-vehicle system. In reality, the states available are subject to neural noise and they are not a perfect copy of the actual states. Therefore, the knowledge about these states can represent the level of experience of the driver [63].

The required states for the control task are assumed to be available to the individuals through an internal mental model, which is a virtual representation of both the internal and external dynamics that compose the system. In particular in the driving case, this can be seen as the *learnt* dynamics that drivers have of their own NMS dynamics coupled with the vehicle through the steering system.

An important function of the mental models is to allow the estimation of feed-forward commands to the system. Therefore, they estimate the α-motoneurone signals that go into the NMS, which can be interpreted as the expected torque command. Another function of the internal mental model is to facilitate the adaptation to new environments. As presented in Section A.1.2, it has been studied that drivers exhibit an adaptive behaviour while driving.

Throughout the years, several attempts to represent this internal mental model have been made, which can be divided into two main categories.

Inverse internal mental models

Inverse internal mental models are a direct transformation of task goals into motor commands [32]. In other words, within the driving framework, they transform the desired steering wheel angle output into the motoneurone command, α, that goes into the NMS. The first attempts to represent internal mental models were often based in inverse dynamics representations [32, 88], but later driver models implemented at TU Delft [23, 58] also made use of this approach.

One significant drawback of these models is that their output is also the ultimate goal of the controller. Moreover, due to the complexity of driver-vehicle systems, the inverse of the model results in a highly improper transfer function, which needs to be filtered in order to remain proper. Another disadvantage, which is a direct consequence of this method, is the high order of the transfer functions of these models. Also, although a simplification can be derived to describe the relationship between the task goals and motor commands, if the order of the inverse internal representation is reduced, the model becomes imperfect by definition. This can influence several outputs of the system. For instance, even with the same plant dynamics as in the internal model, there will always be a certain degree of stretch reflex present in the system due to the mismatch, which is not realistic.

Forward internal mental models

Forward internal mental models allow an estimate of the states to be calculated, which are then used as inputs for the driver's cognitive controller. This controller can be based on one of the previous methods described in Section A.1.2, such as LQR or MPC-based models. Examples of forward models are best found in the investigations of Cambridge University [18, 47, 82].

Furthermore, the perceived states of the system can be transformed into reliable estimates through a variety of methods. These states are subject to measurement noise and acquired through the sensory organs as described later in Section A.3. Among the possible estimation approaches, the most commonly used one is the Kalman Filter. Depending on the requirements of the system, an Extended Kalman Filter can be used to deal with nonlinearities.

A.1.4. Block diagram of the cognitive subsystems

The general subsystems of which the cognitive model of a driver can be composed of can be seen in Fig. A.7. The input of the cognitive model of a driver are the sensed states of the driver-steering-vehicle system, $x_{perceived}$. These perceived states, subject to sensory delays and measurement noise, can be transformed into reliable estimated states and are described in further detail in Section A.3. The estimated states are then used to calculate the desired control command to the NMS. This command is calculated through a control strategy like the ones described in Section A.1.2.

In Fig. A.7, the measurement and process noise are represented by the parameters v and w_α, respectively. As defined in Section A.2, the α-motoneurone signal represents the desired torque input command to the NMS, whereas the γ-motoneurone signal symbolises the expected muscle angle of the arms, both of them key to illustrate the co-activation mechanism of the muscles, described in Section A.2.5.

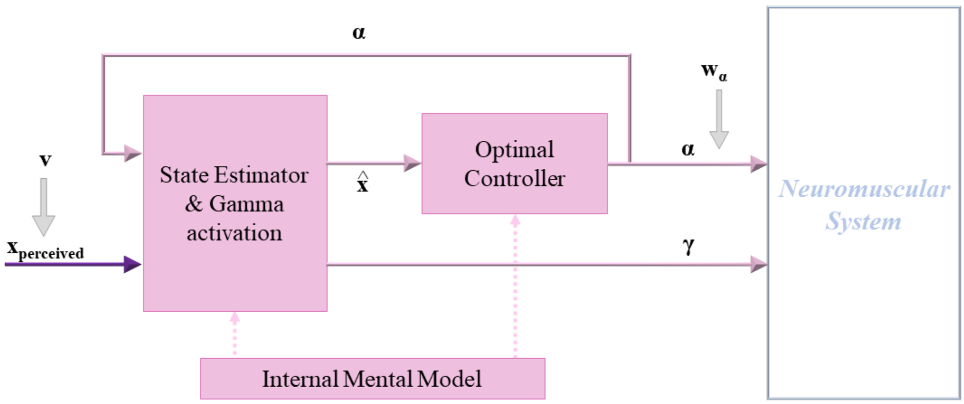

Figure A.7: Block representation of a driver's general cognitive model.

A.2. Neuromuscular dynamics

The central nervous system, described in Section A.1.1, sends different types of efferent signals to the periphery. In the scope of this thesis, special attention is given to the motoneurone signals (α, γ) that stimulate the neuromuscular system with major impact.

The neuromuscular dynamics of the arms are essential to investigate the driver's response to feedback from the vehicle system, such as steering torque feedback or disturbances. Moreover, it makes it possible to understand human discomfort at a neuromuscular level.

This section highlights the main features of the neuromuscular physiology which are relevant to the steering task, along with some state-of-the-art modelling alternatives with their respective advantages and limitations.

A.2.1. Skeletal muscle

There are two main types of motoneurones in the spinal cord, α- and γ-motoneurone signals. On the one hand, α-motoneurones coming from the cortex in the brain directly activate the muscles, or more precisely, they induce the contraction of the extrafusal fibres contained within the skeletal muscle.

The skeletal muscle [6] is an excitable, contractile tissue that connects bones via the tendons. These muscles are arranged in opposing pairs of agonist-antagonist muscles . When the skeletal muscle is activated, the muscles can generate force, or torque, through their contraction. Another function of the skeletal muscle is to generate information about the load encountered.

In the literature, many attempts to model the muscles can be found. A general overview is presented in this section.

Phenomenological models

This type of models are mathematically less complex and in proper agreement with the dynamic behaviour of the muscles, but they provide bad muscle energy consumption predictions. The most used types of models within this category are second-order low-pass filters [110] representing the muscles as a spring-damper system. Generally, they are derived from fitting experimental data into a 2^{nd} order transfer function. They can also be described in terms of the damping ratio and the natural frequency of the model.

These models describe pairs of agonist-antagonist muscles grouped together. The level of co-contraction of the muscles, explained in Section A.2.5, can be modelled by varying the coefficient related to the muscle stiffness.

Physiological models

Physiological muscle representations are extremely complex mathematical models. They provide a good fitting of both the muscle behaviour and metabolic energy consumption of the muscles. The most used models within this category are described below.

- *Fractional order models* [91], which attempt to describe the viscoelastic properties of muscle tissue as a whole.
- *Hill-muscle models* are high-order, nonlinear, lumped-parameter models [110]. They can be defined by two ordinary differential equations representing the excitation-to-activation dynamics and activation-to-force dynamics. The Hill-muscle model is composed of three main elements, as can be seen in Fig. A.8.

  (a) A contractile element (CE) represents active muscle contraction and force generation.

  (b) Nonlinear passive elements, representing the physiological muscle tissue response under compressive and tensile loads. It includes a parallel elastic spring element (PE) describing the passive elastic properties of the muscle fibres. A series elastic elements group (SE), spring and damper, can also be modelled within this second group of elements. However, this second term can be neglected [7] without introducing significant inaccuracy when the short-tendon actuator is not involved in the task.

  (c) In series with the muscle, the tendon can be represented as a spring attached in series, which describes the tendon's elastic properties. This term is often neglected due to the increased complexity, despite the relevant physiological meaning. The tendon's elasticity contribution is particularly important if the tendon stretches an amount approaching the fibre length of the particular muscle [113].

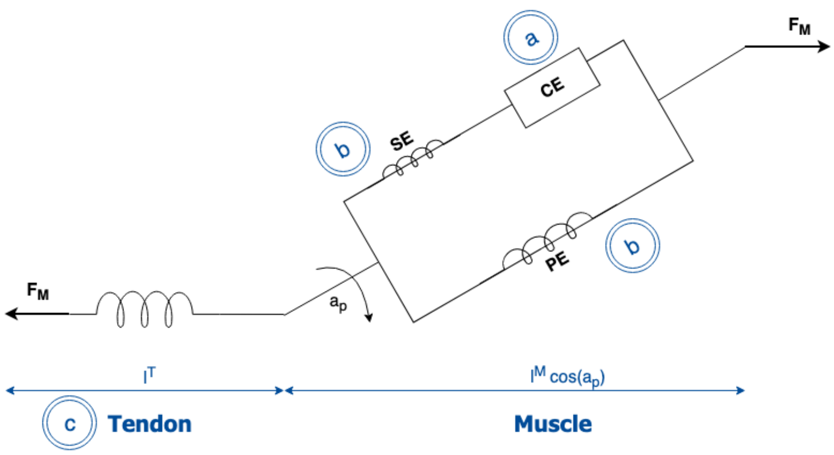

Figure A.8: Hill-muscle model representation.

- *Huxley-based muscle models* [42] are distributed-parameter models which require high computational cost. They provide insignificant advantages with respect to Hill-muscle models unless the study of the muscles in detail is needed, where the description of the muscle contraction mechanism and its accuracy are critical.

In most of the research undertaken in this area, the α-motoneurone has been modelled as actuating on a lumped pair of agonist-antagonist muscles to reduce complexity of the models.

Activation dynamics

The α-motoneurone is transformed into muscle activation force through an internal process known as *activation dynamics*. This mechanism can be simplified into two sub-processes [110].

I. Excitation-to-activation dynamics.

   It can be described by an ordinary differential equation that represents the time delay due to the neural excitation lag time (τ_1).

II. Activation-to-force dynamics.

   It is the activation force, or torque, derived from the muscle-tendon components. This can be described by another time delay (τ_2), known as the neuro-muscular transduction delay. In reality, the time delay corresponding to the activation dynamics is lower than the one associated with the deactivation dynamics. However, this is generally modelled as the same constant value symbolising both processes.

An example of how the simplified muscle activation dynamics can be modelled by a transfer function is shown in Eq. (A.5). Third-order systems can also be found in literature to model the activation dynamics [18], which include an additional time delay representative of the tendons, independent of the activation time delay.

$$H_{act} = \frac{1}{\tau_1 \cdot s + 1} \cdot \frac{1}{\tau_2 \cdot s + 1} \tag{A.5}$$

A.2.2. Muscle spindles

As mentioned in Section A.1.1, the CNS sends efferent signals to the periphery. Apart from α-motoneurones, another relevant type of signals is γ-motoneurones which go into the muscle spindles and cause the stretch reflex activation. The muscle spindles [6] are special fibres in the muscles, also called intrafusal fibres. These fibres are located in parallel to the extrafusal fibres within the skeletal muscles.

Furthermore, the contraction of muscle spindles alone is not enough to generate forces due to the smaller size of the muscle spindle fibres with respect to the extrafusal fibres, along with a lower number of γ-motoneurone signals [47]. Instead, when the muscle spindles are tensed, this triggers the initiation of the stretch reflex loop. Their main function is to reject disturbances and to stabilise the closed-loop performance of the NMS. However, the muscle activation through the stretch reflex loop is subject to a small time delay. Moreover, the muscle spindles have been found to linearise the nonlinear muscle behaviour [66].

The activation of the muscle spindles takes place when there is a difference between the expected muscle angle of the arms, represented by the γ-motoneurone, and the actual muscle arm angle. This can be explicitly manifested, for instance, when the torque command coming from the motor cortex, α, is not accurate due to an imperfect internal representation of the system, or, due to disturbances, which results in an operation mismatch. In these situations, the muscle spindles react in order to correct the error and reject disturbances.

Another relevant function of the stretch reflex loop is to maintain the muscle length and muscle stiffness. This is achieved by sending feedback information to the brain [57]. There are two types of signals travelling to the brain from the muscle spindles, also known as afferent signals. In Fig. A.9, it can be seen how the α-motoneurones activate the extrafusal fibres, also known as skeletal muscle, whereas the intrafusal fibres are innervated by the γ-motoneurones. On the other hand, information signals are also sent from the muscles to the brain through the sensory nerves, described below.

- Ia afferent signals: They send stretch and velocity feedback information about the muscle.
- II afferent signals: They send mainly stretch information about the muscle.

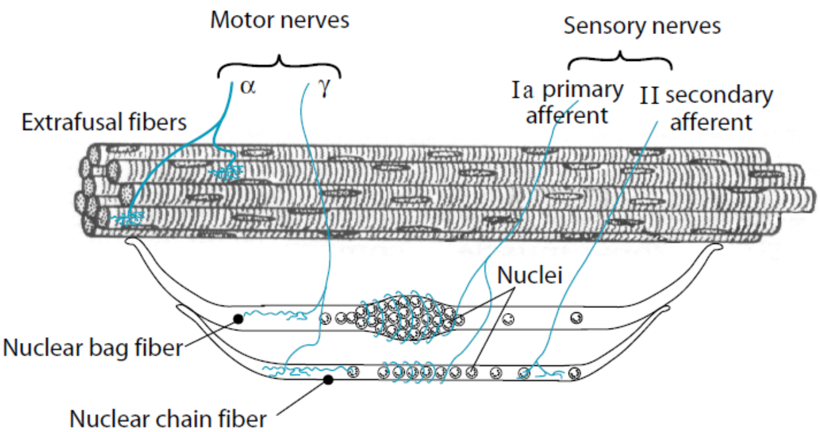

Figure A.9: Muscle model representation of the extrafusal fibres and the intrafusal fibres. The latter is also known as muscle spindles [6].

Modelling alternatives

In particular for the steering task, the muscle spindles compare the actual muscle length of the arm to the γ-signal, representing the expected muscle length. The difference between these signals results in an error signal.

In most of the previous research, such as the investigations carried out at Cambridge University [47, 82] and Delft University of Technology [23, 58], these signals have been modelled as muscle angle instead of muscle length.

The stretch reflex delay, τ_r, represents the finite motoneurone signal transmission rate. This delay depends on the neural conduction velocities, as well as the distance that the signals have to travel, from the muscles to the motor neurons in the spine [57]. It is important to highlight that this delay can lead to instabilities when the reflex gain, k_r, exceeds a certain threshold in relation to the delay.

One relevant modelling alternative is to represent the stretch reflex as a phase compensator [47]. Another one is to model it as a function of the muscle stretch and stretch velocity [58]. Lastly, in discrete-time, as a shift-time register multiplied with the reflex gain.

An example of how the simplified muscle spindle dynamics can be modelled by a transfer function is shown in Eq. (A.6). In this case, the input to the system can be the difference between the expected muscle angle and the actual muscle angle, $\gamma - \theta_a$. Apart from the stretch dependency, more complex examples can also model the velocity dependency of the muscle spindles.

$$H_r = \frac{k_r}{\tau_r \cdot s + 1} \tag{A.6}$$

Mismatch between the real and modelled behaviour

Ideally, given a perfect internal mental model of the driver-vehicle system, the muscle spindle error signal should always be zero if there is no noise present and no disturbances. In other words, there should be no stretch reflex activity during voluntary movements. However, it is not possible to replicate this behaviour when using linear controllers such as the LQR [47]. In this case, given finite weight function costs, the muscle spindles error cannot reach zero.

Moreover, the muscle spindle sensors are subject to a time delay. If high reflex gains are included into the modelling of the stretch reflex dynamics, the model is destabilised [47]. This behaviour is explained in further detail in Hagbarth [40] and Van der Helm et al. [105], and can be summarised by the stretch reflex being most effective at low-frequency inputs. For high reflex gains, the reflex time delay results in a resonance peak at the eigenfrequency of the closed-loop system.

A.2.3. Golgi tendon organs

Golgi Tendon Organs are located in the tendons. The tendon can be modelled as a spring attached in series to the muscle model.

The main function of these tendons is to send force feedback information to the brain via Ib afferent signals. Golgi tendon organs have been found to have a significant contribution for ankle movements [79] and studies on airplane pilots [45], but their influence during the steering task still remains unclear.

Modelling alternatives

An example of how the golgi tendon organs could be modelled is shown in Eq. (A.7), where k_{gto} is the tendon gain and τ_{gto} represents the time lag of the organs.

$$H_{gto} = k_f \cdot e^{-s\tau_{gto}} \tag{A.7}$$

Golgi tendon organs have been found to deliver both excitatory and inhibitory effects [79]. Thus, depending on the task, the sign of the tendon gain can change.

An overview of the aforementioned muscle components can be seen in Fig. A.10.

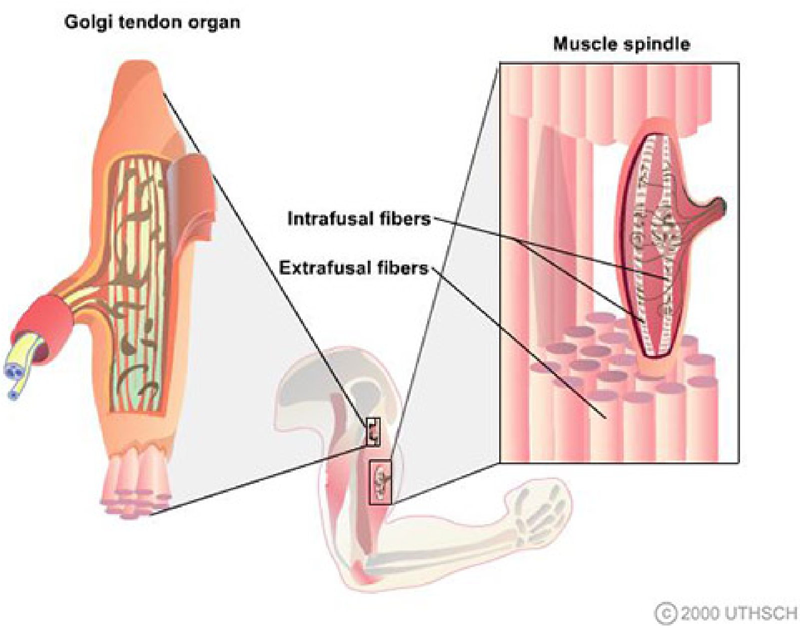

Figure A.10: Representation of the Muscle spindle and Golgi tendon organ [62].

A.2.4. Intrinsic muscle dynamics

The muscle intrinsic properties include passive visco-elastic human properties of the muscle, such as the intrinsic muscle stiffness and damping. These properties can be varied by means of co-contraction, described in Section A.2.5. Unlike the muscle spindle properties, they do not introduce delay, which translates into an instantaneous suppression of disturbances for all frequencies [21]. However, their activation involves a considerable energy cost [96].

Modelling alternatives

The modelling alternatives are generally based on a spring-damper-like behaviour of these properties. Previous studies showed that the behaviour was strongly dependent on the stiffness coefficient, k_p [23, 88]. However, a more recent, muscle-centered driver model highlighted that, at low frequencies, the intrinsic dynamics are dominated by the damping term, c_p [46].

A.2.5. Muscle processes within the NMS

In this section, the main processes that take place within the NMS are described. During the learning phase, the below specific processes can be intensified:

- *Stretch reflex activity:*
  In order to reject disturbances, the stretch reflex activity increases. This activation is also thought to decrease the learning phase duration [32] via feedback error learning. Besides, the stretch activity indirectly contributes to the skeletal muscles' activation through the muscle co-activation process, described below.
- *Muscle co-contraction:*
  Muscle co-contraction can be seen as increased intrinsic muscle properties such as intrinsic muscle stiffness. This helps to stabilise the system and it improves the control performance.

Muscle co-activation

Muscle co-activation [32] is the process by which the skeletal muscles are activated to generate torque. Hence, muscle co-activation results in a certain degree of muscle activity. This mechanism can be activated, mostly, from two sources which are described below.

I. Feedforward commands, α-motoneurones.

   Motoneurones, α-signals, coming from the motor cortex in the brain, directly activate the skeletal muscles to produce a torque. Conceptually, it can be seen as the estimate of the load that the muscle will operate against and can be calculated based on the human cognitive strategies described in Section A.1.2 .

II. Feedback commands, γ-motoneurones.

The main function of the γ-motoneurones in the spine is to activate the muscle spindles. However, these signals do not only activate the reflex loop, but they can also increase the muscle activation level indirectly. The muscles' activation via γ-signals is known to be more energy-efficient, since the stretch reflex is only activated in the presence of disturbances.

The co-activation mechanism occurs to a greater degree during the learning phase of the CNS. For example, an increase in co-activation can be seen when the internal mental model is not perfect due to the novelty in the undergoing task or the exposure to disturbances. The main functions of the co-activation mechanism are:

- High levels of co-activation can effectively reduce the influence of disturbances [21]. However, muscle activation entails high metabolic energy consumption because the muscles need to be continuously activated.
- Adjust the degree of muscle tension in step with voluntary movement and ensure that muscle spindles are not unloaded during voluntary movement [47]. This maintains the spindles' sensitivity.
- Suppressing the reflex loop during voluntary movement [47]. In this situation, ideally, the γ-signal is equal to the actual muscle length.

Muscle co-contraction

As described in Section A.1.2, humans can adapt their dynamics depending on the situation. This can be particularised for the capability of varying their own muscle impedances. For instance, the driver can consciously increase the intrinsic muscle properties, such as stiffness and damping. This is largely exemplified while adapting to novel tasks and this co-contraction is usually maintained until a new, more accurate internal mental representation of the environment is acquired. This mechanism also takes place when the system is subject to disturbances, as well as noise in the motor and sensory systems.

Muscle co-contraction is the stiffening or relaxation of the muscle properties. Higher levels of co-contraction entail a high metabolic energy consumption, since the activation command α-signal needs to be sent continuously to maintain the level of co-contraction.

It is essential to stress that this behaviour is an *instantaneous* mechanism that occurs in response to a mismatch between the driver's expectations and the actual reaction of the closed-loop system to the driver's inputs, as described in Franklin et al. [32]. The fast activation of the process results in a reduced discrepancy during novel scenarios and it also provides additional stability. This co-contraction build-up is possible due to muscle activation [14]. The deactivation process is, on the contrary, slow. Once the new dynamics of the system are learnt, the driver impedance is reduced in order to minimise the metabolic energy consumption, thereby reducing the activation levels of all muscles. However, the impedance level never reaches zero. Despite the metabolic energy consumption, there is always a minimum level of co-contraction present to guarantee the stability of the system.

A.2.6. Block diagram of the neuromuscular subsystems

A complete structure of the different components of the neuromuscular system, as explained in the previous sections, can be seen in Fig. A.11. For the scope of this thesis, some of the elements have been simplified or removed, such as the golgi tendon organs.

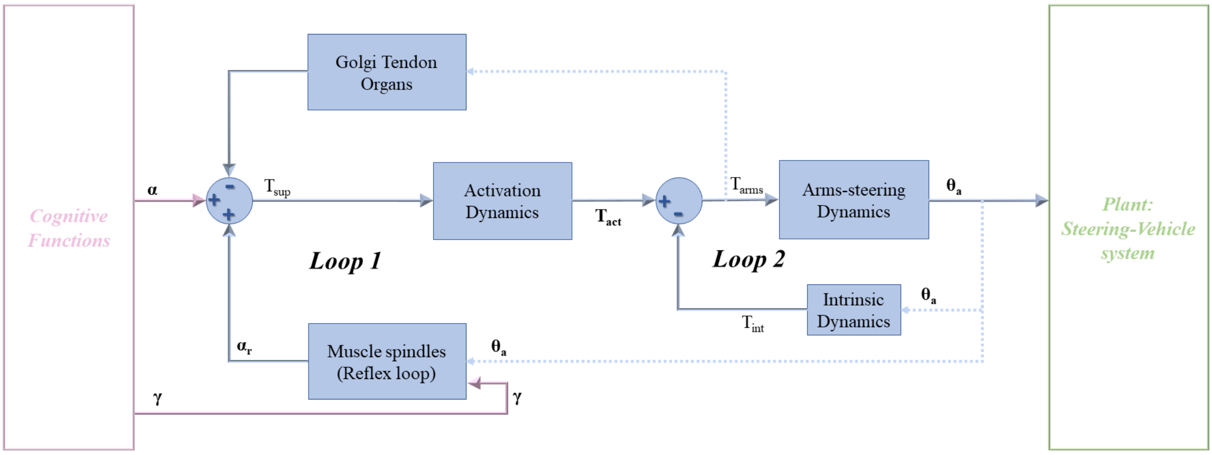

Figure A.11: Block representation of a driver's general neuromuscular system.

The inputs of the NMS are the motoneurone signals coming from the cognitive model, α and γ. On the other hand, the output of the system is the muscle activation torque, T_{act}, that goes into the arms-steering-vehicle system. Moreover, at the steering wheel, the muscle angle of the arms, θ_a, interacts with the steering wheel angle, θ_{sw}.

As can be seen in Fig. A.11, two loops can be defined within the NMS system. The first one corresponds to the reflex loop, which influences the amount of supraspinal torque, T_{sup}, that activates the muscles. This process represents to the co-activation mechanism defined in Section A.2.5. The second loop can be derived from the impact of the muscle intrinsic dynamics.

A.3. Sensory organs

The sensory organs represent the human capabilities to perceive the states of the controlled closed-loop system. Thus, these organs characterise the driver skills to convert noisy sensed signals into accurate estimates of the system states.

However, most of the research described in Section A.1 and A.2 neglects or oversimplifies the importance of these organs. The sensory organs for human perception can be divided into three subcategories [63].

I. *Visual perception organs*

   The driver makes use of vision to sense the lateral deviation (e_y) and heading error (e_ψ) with respect to the desired path.

   This can be translated as the driver being able to sense a preview of the road path ahead.

II. *Proprioception or somatosensory organs*

   Apart from the visual perception, drivers are capable of acquiring information about the applied steering wheel angle (θ_{sw}), steering wheel velocity ($\dot{\theta}_{sw}$), and applied steering wheel torque (T_{sw}) or muscle angle (θ_a).

   This is done via several organs that detect the states of the body, such as contact pressure, temperature, and limb position.

III. *Vestibular perception organs*

   The vestibular organs, together with the vision, allow drivers to sense the lateral velocity (a_y) and yaw rate (r) of the vehicle. In a driving simulator experiment, this can only be integrated if a moving-base simulator is available.

   The organs responsible for the vestibular perception are the otoliths, for the lateral velocity, and the semi-circular canals, for the yaw rate.

The feedback sensed by these organs is then sent to the CNS, subject to measurement noise, which has been found to be signal-dependent [63, 102] but, for simplicity, this characteristic is omitted and additive noise is used instead. An extensive review of human sensory organs, human detection thresholds, and time delays was performed by Nash et al. [81].

A.4. Relevant parameter values found in literature

From the literature, typical values characterising the most relevant human thresholds, time delays, and physical limitations can be seen in the following tables.

In Table A.1, the main human parameters within the cognitive control model can be found.

	Cognitive model parameters		
Block	**Cognitive Controller**		
Variable	T_p	τ_{cog}	T_t
Value range	[0.85-3] s	[0.4-0.5] s	[0.15-0.55] s

Table A.1: Table of cognitive model parameters gathered from literature.

Table A.2 includes the range of neuromuscular parameters relevant for the steering task. The wide range of the values is due to the fact that, as explained in Section A.2, drivers can consciously co-contract their muscles, increasing the stiffness and damping of the different components with respect to the relaxed conditions. The neuro-muscular (de-)activation transduction delay, τ_2, corresponds to the lumped activation and deactivation process and the range of these processes significantly varies. For instance, typical values found in literature for the neuro-muscle activation range between 5 and 15 milliseconds, whereas the deactivation varies between 20 and 60 milliseconds. However, in order to reduce the complexity and number of parameters in the neuromuscular model, these processes are commonly lumped into one single constant, τ_2.

	Neuromuscular parameters											
Block	**Activation Dynamics**		**Reflex Dynamics**			**Golgi Tendon Organs**		**Intrinsic Dynamics**		**Muscle Arms Dynamics**		
Variable	τ_1	τ_2	τ_r	k_r	c_r	τ_{gto}	k_{gto}	k_{int}	c_{int}	I_{arm}	k_a	c_a
Value Range	[20-50] ms	[5-60] ms	[20-50] ms	[0-50] Nm/rad	[0.2-3.4] Nms/rad	[20-48] ms	[-] Nm/rad	[5-100] Nm/rad	[0.7-2] Nms/rad	[0.048-0.16] $kg \cdot m^2$	[3.7-30] Nm/rad	[0.2-3] Nms/rad

Table A.2: Table of neuromuscular human parameters gathered from literature.

Lastly, in Table A.3, the relevant delays related to the sensory organs are listed. The vestibular perception organs are omitted within the scope of this research since the experimental results will be based on computer simulations and a fixed-base driving simulator experiment.

	Sensory organs parameters		
Block	**Visual perception**		**Somatosensory organs**
Variable	$\tau_{vi,y}$	$\tau_{vi,\psi}$	τ_{θ_a}
Value range	[0.1-0.56] s	[0.1-0.56] s	[0.16-0.19] s

Table A.3: Table of sensory organs parameters gathered from literature.

A.5. Adapted driver model

An extensive review of the cognitive behaviour, neuromuscular system, and the sensory organs was presented in Section A.2. The complexity of modelling all the aspects of a driver can rapidly increase. Therefore, there is a trade-off between the realism with which the driver is represented and the possibility to use such a driver model for real-time vehicle control applications. Another factor to consider while modelling the driver behaviour is to take into account how the different human parameters can be identified. A great number of variables can be not realistically possible or result in over-fitting during the parameter identification.

A.5.1. Driver model description

The driver aspects modelled within the scope of the thesis are adapted from the state-of*the-art work carried out at Cambridge University by Niu and Cole [82], because of the suitable LQG control strategy based on a forward internal mental model, as well as an extensive, but adequate representation of the NMS. The model designed by Katzourakis [58] was extensively studied because of the detailed representation of the NMS, but the high-order of the transfer function of the inverse internal mental model, as part of the cognitive controller, was a limiting factor. Fig. A.12 shows a general scheme of the driver-steering-vehicle model.

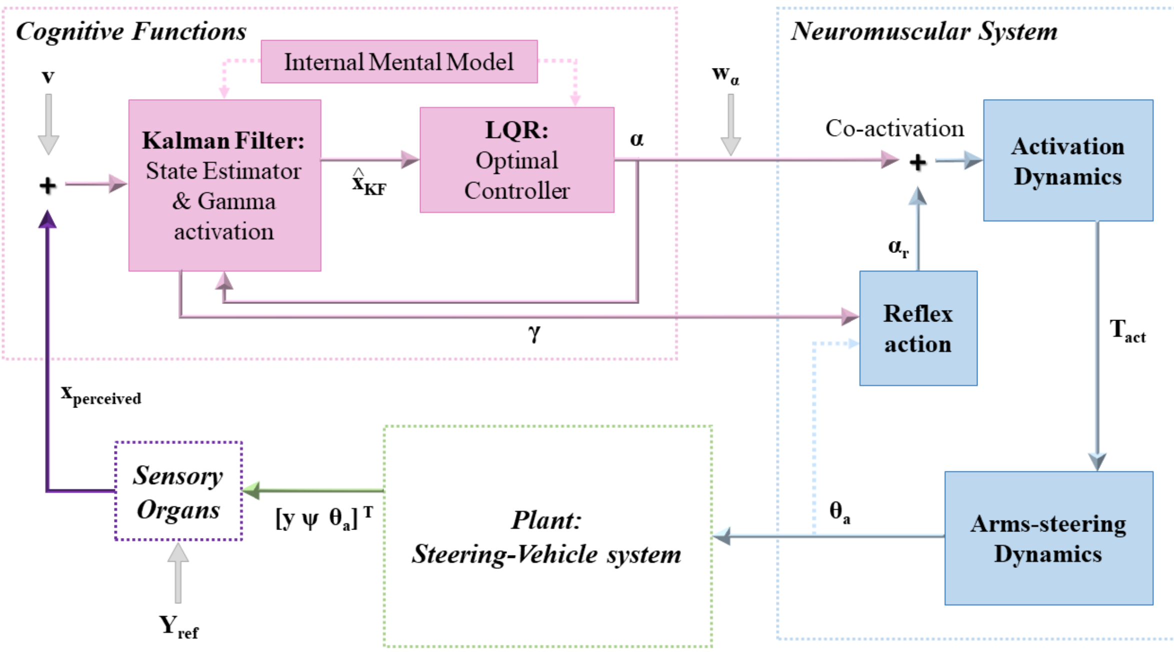

Figure A.12: General scheme of a driver-vehicle model.

Cognitive Behaviour

The controller chosen for the optimisation of the driver's torque input is a predictive strategy based on LQR. Along with the control strategy, the states of the system are estimated through a Kalman Filter to reduce the effect of measurement noise of the sensory organs and process noise of the muscle activation. This combination is also known as the Linear Quadratic Gaussian, LQG. Moreover, the upcoming curvature of the road, illustrated in Fig. A.13, is considered by introducing the human preview capabilities in the model, which is an improvement with respect to the single-preview point model developed by Niu and Cole [82]. Lastly, the internal mental representation that the driver has of the driver-vehicle system is based on a forward mental model, which was found to be more advantageous with respect to inverse internal mental models, as explained in Section A.1.3.

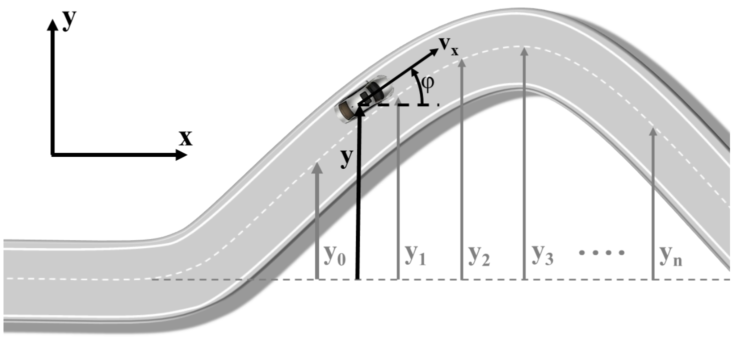

Figure A.13: General scheme of a driver-vehicle model.

The cost function of the LQR, which calculates the expected driver torque input, minimises the lateral deviation of the vehicle with respect to the upcoming reference trajectory of the road with a certain preview time, T_{prev}.

$$J_{LQR} = \sum_{0}^{\infty} \left[\begin{bmatrix} \mathbf{x}_{KF} & \mathbf{y}_p \end{bmatrix} \mathbf{C}^T \mathbf{Q} \mathbf{C} \begin{bmatrix} \mathbf{x}_{KF} \\ \mathbf{y}_p \end{bmatrix} \right] + \alpha R \alpha \tag{A.8}$$

where $\mathbf{C}$ is a matrix that selects the states on the lateral position, heading angle, and the road preview points. In addition, there is a penalty in the amount of torque applied by the driver, R. Finally, the expected driver torque input, α, is calculated as:

$$\alpha = -\mathbf{K}_{LQR} \cdot \begin{bmatrix} \mathbf{x}_{KF} \\ \mathbf{y}_p \end{bmatrix} \tag{A.9}$$

where $\mathbf{K}_{LQR}$ is the LQR gain, $\mathbf{x}_{KF}$ is a vector with the estimated states, and $\mathbf{y}_p$ a vector containing the upcoming preview road points of length $N_p = T_{prev}/T_{s,DM}$.

Neuromuscular Dynamics

The neuromuscular dynamics of the driver are composed of the reflex action of the muscle spindles and a linearised Hill-muscle model including the activation dynamics of the muscles. These elements are necessary for the modelling of the co-activation mechanism of the muscles. Moreover, the muscle dynamics of the arms that are interacting with the steering system are also modelled. In order to reduce the complexity of the model, the intrinsic dynamics are omitted because it is assumed that the passive stiffness and damping properties are dominated by the steering system properties. Besides, based on previous research, it is considered that the effect of the intrinsic properties during the rejection of unexpected events is less significant than the reflex action of the muscle spindles. Lastly, the golgi tendon organs are set to zero because of their unknown impact on the steering task.

The NMS dynamics are modelled as defined below, with the activation dynamics in Eq. A.10 and the reflex dynamics in Eq. A.11.

$$H_{act} = \frac{1}{(\tau_1 \cdot s + 1) \cdot (\tau_2 \cdot s + 1)} \tag{A.10}$$

$$\alpha_r = \frac{k_r}{\tau_r \cdot s + 1} \cdot (\gamma - \theta_a) \tag{A.11}$$

The expected muscle angle, γ, is calculated based on the internal mental model of the driver.

$$\gamma = \begin{bmatrix} \mathbf{0} & 1 & \mathbf{0} \end{bmatrix} \cdot \hat{\mathbf{x}}_{KF} \tag{A.12}$$

Moreover, the arm-steering dynamics are modelled as

$$T_{act} = c_a \dot{\theta}_a + k_a(\theta_a - \theta_{sw}) \tag{A.13}$$

In Eq. (A.12), the vector $\hat{\mathbf{x}}_{KF}$ represents the estimated states via the Kalman Filter. The general formulation of the Kalman Filter can be seen in Eqs. (A.14) – (A.15).

$$\dot{\hat{\mathbf{x}}}_{KF} = \mathbf{A}_{KF} \cdot \hat{\mathbf{x}}_{KF} + \mathbf{B}_{KF} \cdot \begin{bmatrix} \alpha \\ \mathbf{z} + \mathbf{v} \end{bmatrix} \tag{A.14}$$

$$\mathbf{x}_{KF} = \mathbf{C}_{KF} \cdot \hat{\mathbf{x}}_{KF} + \mathbf{D}_{KF} \cdot \begin{bmatrix} \alpha \\ \mathbf{z} + \mathbf{v} \end{bmatrix} \tag{A.15}$$

The Kalman Filter state-space matrices, Eqs. (A.16) – (A.19), are based on the internal mental model that the driver has concerning their own NMS dynamics, coupled in a closed-loop system with the vehicle and steering system dynamics. The internal mental representation is described by the state-space model composed of the matrices $\mathbf{A}_{int}$, $\mathbf{B}_{int}$, $\mathbf{C}_{int}$, $\mathbf{D}_{int}$, where $\mathbf{D}_{int} = \mathbf{0}$.

$$\mathbf{A}_{KF} = \left[\mathbf{A}_{int} - \mathbf{L}_{KF} \cdot \mathbf{C}_{int}\right] \tag{A.16}$$
$$\mathbf{B}_{KF} = \left[\mathbf{B}_{int} \quad \mathbf{L}_{KF}\right] \tag{A.17}$$
$$\mathbf{C}_{KF} = \left[\mathbf{I} - \mathbf{M}_{x} \cdot \mathbf{C}_{int}\right] \tag{A.18}$$
$$\mathbf{D}_{KF} = \left[\mathbf{0} \quad \mathbf{M}_{x} \cdot \mathbf{C}_{int}\right] \tag{A.19}$$
$$\tag{A.20}$$

The gain matrix, L_{KF}, and the innovation gains, M_x and M_y, that are used in the equations above, are shown in Eqs. (A.21) – (A.23).

$$\mathbf{L}_{KF} = \mathbf{A}_{int} \cdot \mathbf{P} \cdot \mathbf{C}_{int}^{T} \cdot (\mathbf{C}_{int} \cdot \mathbf{P} \cdot \mathbf{C}_{int}^{T} + \mathbf{R}_{KF})^{-1} \tag{A.21}$$
$$\mathbf{M}_{x} = \mathbf{P} \cdot \mathbf{C}_{int}^{T} \cdot (\mathbf{C}_{int} \cdot \mathbf{P} \cdot \mathbf{C}_{int}^{T} + \mathbf{R}_{KF})^{-1} \tag{A.22}$$
$$\mathbf{M}_{y} = \mathbf{C}_{int} \cdot \mathbf{P} \cdot \mathbf{C}_{int}^{T} \cdot (\mathbf{C}_{int} \cdot \mathbf{P} \cdot \mathbf{C}_{int}^{T} + \mathbf{R}_{KF})^{-1} \tag{A.23}$$

Finally, the matrix $\mathbf{P}$ is obtained by solving the Riccati equation, Eq. (A.24).

$$\mathbf{A}_{int}^{T}\mathbf{P}\mathbf{A}_{int} - \mathbf{P} - \mathbf{A}_{int}^{T}\mathbf{P}\mathbf{C}_{int}(\mathbf{C}_{int}^{T}\mathbf{P}\mathbf{C}_{int})^{-1}\mathbf{C}_{int}^{T}\mathbf{P}\mathbf{A}_{int} + \mathbf{B}_{int}\mathbf{Q}_{KF}\mathbf{B}_{int}^{T} = \mathbf{0} \tag{A.24}$$

Where the diagonal matrix with the variance of the process noise is represented by $\mathbf{Q}_{KF}$ and the variances of the measurement noise form the noise covariance matrix, $\mathbf{R}_{KF}$. The measurement noise includes the noise over the plant outputs y, ψ, and θ_a. Once the estimated states of the system are obtained, the expected muscle angle can be derived, as shown in Eq. (A.12).

Sensory Organs

The sensory organs modelled are the visual perception organs and the proprioceptors. The modelling of the vestibular organs is considered out of the scope of the thesis because the investigation will be carried out in a fixed-base driving simulator.

Driver model parameters

The parameters of the driver model are listed in table A.4. Most values are extracted from [82], whereas T_{prev} and Q are selected based on the pilot experiment, described in section A.5.2.

Table A.4: Driver model parameters

Parameter	Value	Parameter	Value
T_{prev}	1.4 s	I_{arms}	0.0718 kg m^2
k_a	30 Nmrad	c_a	3 Nms/rad
k_r	21 Nm/rad	τ_r	0.04 s
τ_1	0.03 s	τ_2	0.02 s
τ_{visual}	0.24 s	τ_{muscle}	0.19 s
Q	diag$(3 \cdot 10^3, 1 \cdot 10^2)$	R	1

A.5.2. Driver model validation

The aim of this research is to reduce the conflicts between the driver and controller torque, as well as to understand the driver-vehicle closed-loop interaction. For this purpose, a validated driver model is essential.

The driving scenario designed was a route of 12 km long with straight and sinusoidal segments in order to obtain consistent driving data for analysis. In every trial, the vehicle was driving at a constant vehicle speed of 100 km/h and the test subject's sole task was to control the lateral motion of the vehicle to drive in the centre of the lane, indicated with a white line. The graphics were rendered with rFpro software based on an IPG CarMaker scenario in a 210 projection screen.

Three drivers participated in this pilot driving simulator experiment. In order to test the driver model with different control strategies, drivers with great differences in the level of driving experience and experience in driving simulators were selected.

Offline simulations

The driver torque predictions are simulated using a high fidelity plant on IPG CarMaker, which includes a detailed characterisation of the tyre dynamics and a validated Toyota steering model [16], enabling more realistic simulations. The vehicle parameterisation corresponds to a mass production commercial vehicle.

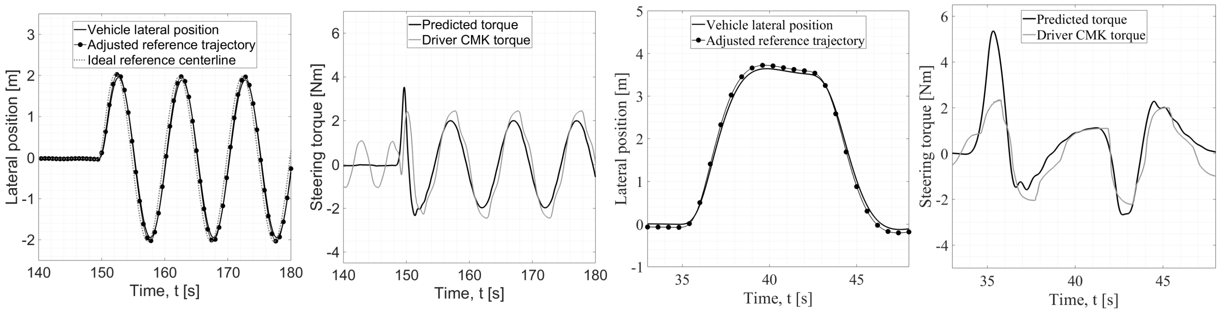

Figure A.14: Driver model prediction based on CarMaker driver with a nonlinear, high-fidelity steering system.

The driver model is initially validated against “robotic” behaviour, using CarMaker’s virtual driver. In Figure A.14, it can be seen that the driver model predictions are accurate both in magnitude and in shape, with the exception of the initial torque peak. This initial mismatch is because the LQR cognitive controller cannot enforce constraints. This could be resolved by introducing a new MPC controller instead. However, the use of two MPC controllers, driver and ADAS, may lead to instabilities due to competing objectives and increase the computational cost. The driver model is also tested with simpler steering models, shown in Figures A.15 to A.16. With decreasing nonlinearities, the accuracy of the torque predictions improves.

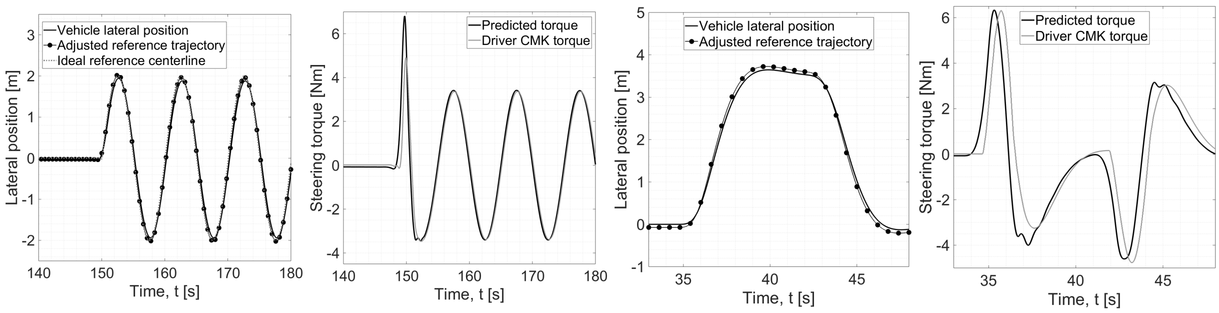

Figure A.15: Driver model prediction based on CarMaker driver with a kinematic steering system.

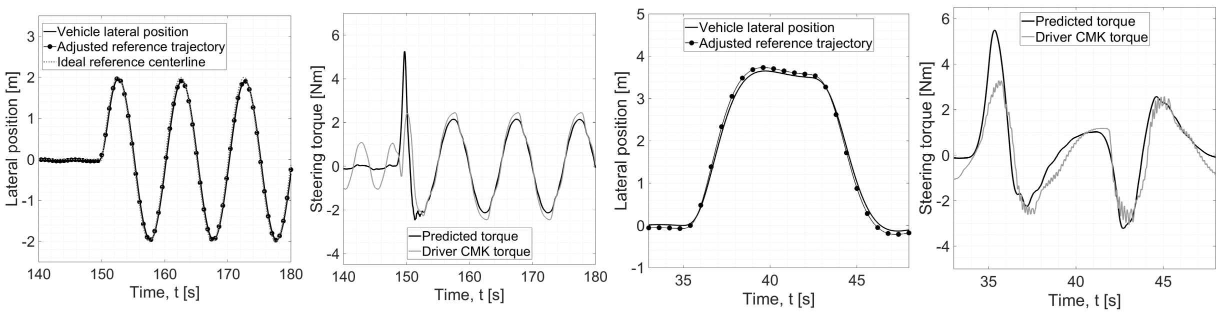

Figure A.16: Driver model prediction based on CarMaker driver with a Pfeffer steering system.

Driving Simulator experiments

In order to test the driver model in a more realistic case, a driving simulator experiment was performed with three different human drivers for the task of following a sinusoidal trajectory. The drivers are listed in ascending order of driving experience, which can be observed in the respective driving styles.

The driver model prediction fits all three drivers' inputs well, even in the presence of high noise, Figures A.17 to A.19, showing a good capability of the model to capture inter-driver variability. The numeric results of the driver model predictions are listed in A.5.

Steering	**Pfeffer**			**TME-TMC**
Driver	Driver 1	Driver 2	Driver 3	CMK Virtual
$T_{\mathbf{RMSE}}$	0.7344	0.6232	0.7355	0.6828
% Accuracy	89.96	90.96	87.30	85.08

Table A.5: Driver prediction accuracy values.

The sensitivity of the driver model parameters was investigated to obtain the best possible fit. The most relevant ones are the driver preview distance of the road and the real reference trajectory employed by each subject, which can significantly differ among drivers. Driver 3 has a longer preview distance, resulting in smooth torque inputs, and it is assumed that the minimal activation of the muscle spindles can be related to the driver's good knowledge of their own closed-loop dynamics (IMM). The perception of the reference trajectory has a major impact on the model's prediction. The reference trajectory was changed from the ideal invariant road centerline to the actual lateral position of the car using road sensors in CarMaker.

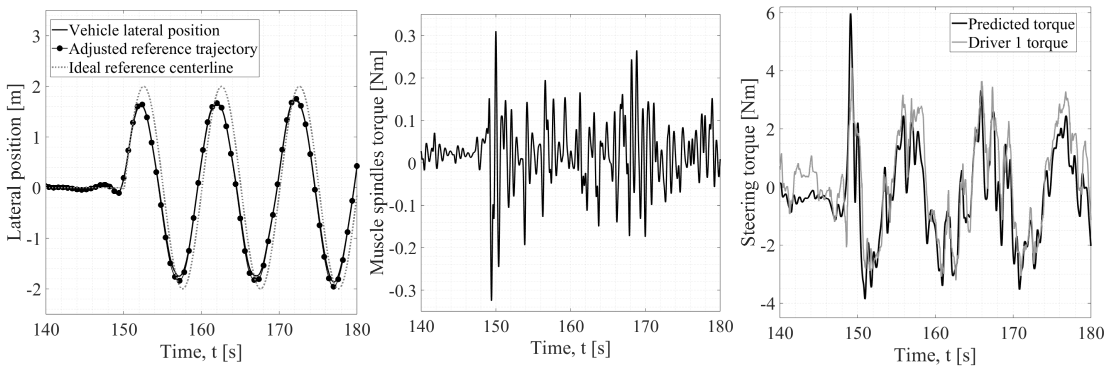

Figure A.17: Driver model validation based on driver 1.

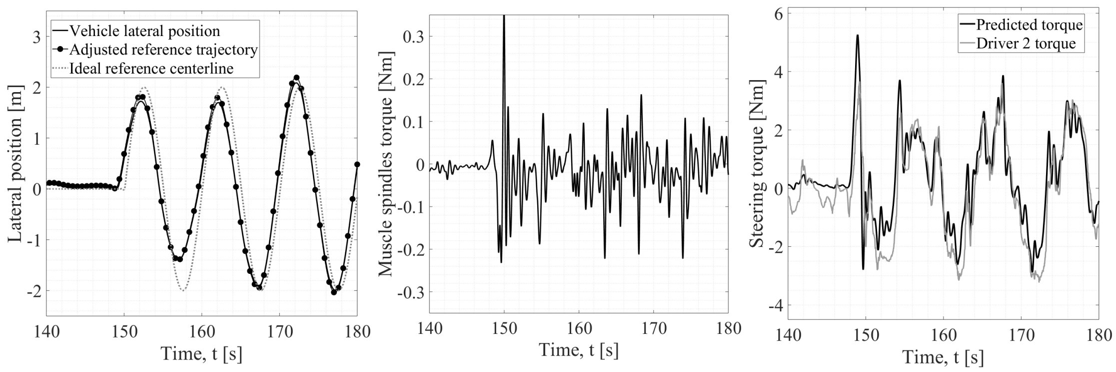

Figure A.18: Driver model validation based on driver 2.

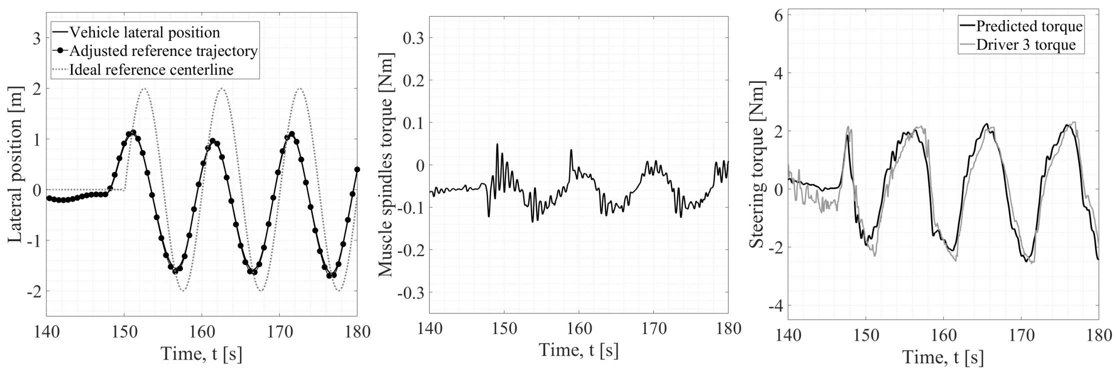

Figure A.19: Driver model validation based on driver 3.

A.6. Conclusions

The integration of a realistic driver model is central to the design of the collaborative shared control strategy. A better accuracy of the torque predictions can directly improve the collaborative behaviour of the proposed driving assist system.

In particular, within the HSC framework, driver models can facilitate the investigation of how the driver reacts in the presence of the haptic feedback guidance. Thus, including the modelling of the human behaviour is beneficial for the study of collaborative driving assist systems.

In the scope of this thesis, a validated mathematical driver model is used in the design of the shared control strategy. The author of this thesis considers the research conducted at Cambridge University [1]. to be the state-of-the-art reference for driver modelling focused on the steering task. Driver models can represent human drivers' behaviour and predict subjective assessment of the steering torque feedback within the haptic control framework. Therefore, they can minimise the need for testing of real vehicles, which is often time-consuming and involves a higher cost than testing in a driving simulator.

One of the most relevant simplifications taken in the following chapters regarding the driver model is the omission of certain parts of the NMS. For instance, due to their unknown impact on the steering task, the modelling of the golgi tendon organs is omitted. The intrinsic dynamics are also excluded in the scope of this thesis because of the less significant effect that they present with respect to the reflex loop. The intrinsic dynamics, being passive properties, have a lower influence during the steering task because these properties are dominated by the steering system properties, k_t and c_t. Moreover, due to the necessity of a moving-base driving simulator to assess the vestibular perception of the drivers, the modelling of these organs is also considered out of the scope of the thesis.

Finally, a comprehensive driver model has been implemented, providing accurate torque predictions when the driver target trajectory is known, as shown by the experiments performed in a fixed-base driving simulator.

B

MPC Background

This section presents a concise introduction to MPC, in Fig. B.1, its mathematical background, and an overview of the software related to its implementation, the ACADO Toolkit. In particular for the steering task, MPC-based systems are suitable due to the need for accurate precision in the path tracking task performance. Also, smooth tracking makes MPC advantageous because input constraints can be easily implemented. Thereby, these constraints avoid that the system behaves abruptly when interacting with the driver, increasing safety and comfort.

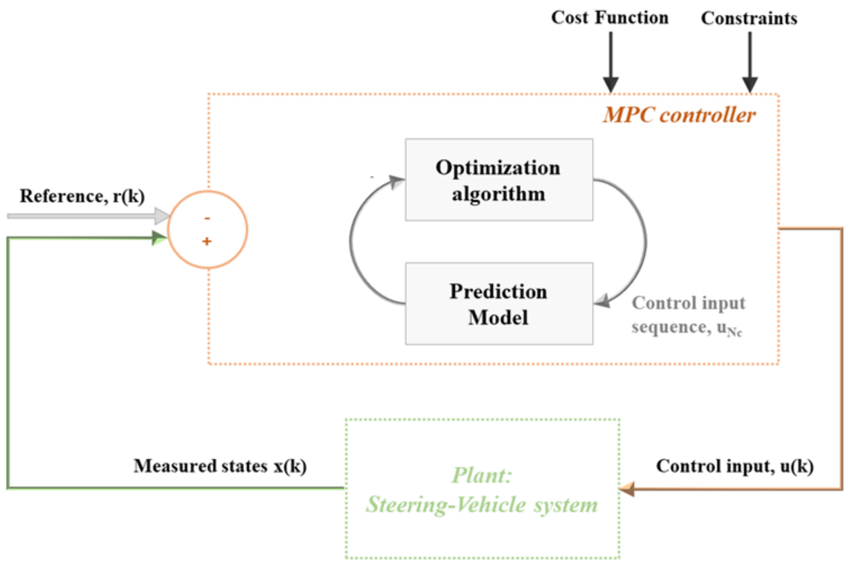

Figure B.1: Schematic representation of the MPC approach for the steering task.

B.1. Model Predictive Control

Model Predictive Control is a control strategy of which the main objective is to calculate the trajectory of a future control input variable $u(k)$ in order to optimise the future behaviour of the plant being controlled. The optimisation is performed within a finite-time window based on the plant states' information at the start of the time window $x(k)$ [108]. The time window is composed of a number of time steps, called the prediction horizon, N_p. The control horizon of the control input sequence is denoted by N_c. This optimal control problem is iteratively performed to minimise a cost function subject to constraints. A diagram of this process can be seen in Fig. B.2, where $N = N_p = N_c$.

Model Predictive Control systems are based on a mathematical model of the plant, which should be as close as possible to the actual plant being controlled. Moreover, the systems can operate in open- or closed-loop and the MPC framework allows the introduction of constraints to the states and / or inputs to incorporate the physical limitations of the vehicle system, as well as being able to handle nonlinearities. This makes the MPC framework very attractive for the real-time dynamic optimisation of controllers for the driving steering task [60].

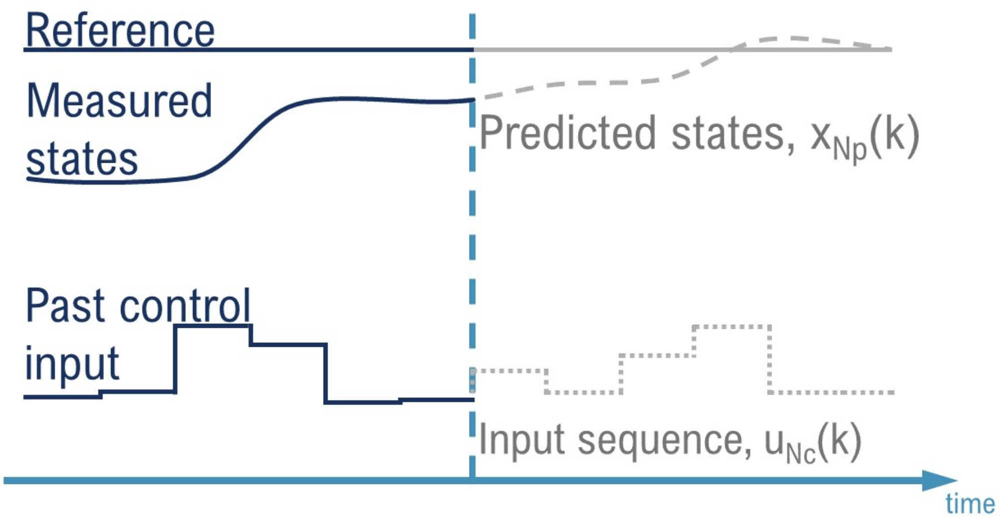

Figure B.2: General representation of the MPC prediction over the horizon.

Feedback control is introduced to the model by applying only the first control input of the calculated optimal control sequence instead of the complete sequence. Applying the complete sequence would result in open-loop control and it would make the system incapable of reacting to external disturbances or uncertainties. In the next time-step, the finite-time window is shifted and the process is repeated, which is also known as Receding Horizon Control, RHC [108]. With this process, MPC can make use of a preview trajectory to calculate the optimal control input, which leads to higher performance.

Therefore, it is clear that the MPC represents a strong control algorithm to tackle the current issues in the path towards fully automated vehicles. An extensive summary of recent developments of MPC and future applications is given by Mayne [74]. In particular to vehicle control systems, MPC strategies have been implemented for lane keeping assist systems [13], active steering control [12, 27], collision avoidance [101], and emergency scenarios [34].

Furthermore, following the increasing trend to acknowledge the importance of the driver and the interaction with the vehicle, there have also been MPC-based approaches that try to include the driver model into the system, such as the lane keeping model of Gray et al. [36], the shared steering system model by Guo et al. [37], and a novel driver assistance steering system that takes into account the human impedances of the arm, implemented by Ercan et al. [25].

B.1.1. Prediction model

As previously mentioned, the MPC exploits a simplified plant model to predict the future plant states' evolution and to calculate the best control input sequence. For nonlinear systems, the Nonlinear Model Predictive Control structure can be used. Therefore, it is fundamental to have a model for the prediction of the plant that is accurate enough to capture the most significant dynamics of the system, without compromising computational efficiency, in order to allow the optimisation problem to be solved in real-time. This model is solved iteratively, resulting in an optimisation based feedback control.

A general representation of the prediction model can be seen in Eq. (B.1),

$$\begin{aligned} \mathbf{x}(k+1) &= f(\mathbf{x}(k), u(k)) \\ \mathbf{x}(0) &= \mathbf{x}_0 \end{aligned} \tag{B.1}$$

where $\mathbf{x}$ is the vector of the differential states of the system, with $\mathbf{x} \in \mathbb{R}^{N_x}$. The variable $\mathbf{x}_0$ denotes the initial states, and f is the function that describes the prediction model dynamic equations, which can be linear or nonlinear. Lastly, the variable $u \in \mathbb{R}^{N_u}$ is the control input. For the scope of this thesis, the dimension of the control input, N_u, is equal to one and it represents the torque that the driving assist system exerts on the steering system.

The state solution is

$$\mathbf{x}(k) = \phi(k; \mathbf{x}_0, \mathbf{u}_k) \tag{B.2}$$

And the control input sequence is

$$\mathbf{u}_k := (u(0), u(1), ..., u(k-1)) \tag{B.3}$$

B.1.2. OCP formulation

Cost function

The general cost function of the MPC to be minimised can be defined as

$$J_{N_c,N_p}(\mathbf{x}(\cdot),u(\cdot)) = \sum_{k=0}^{N_p-1}[(h_x(\mathbf{x}_k)-\mathbf{y}_{ref,k})^T\mathbf{W}_x(h_x(\mathbf{x}_k)-\mathbf{y}_{ref,k})]+ \tag{B.4}$$

$$+\sum_{k=0}^{N_c-1}[h_u(u_k)^T\, W_u\, h_u(u_k)] \;+\; (h_N(\mathbf{x}_{N_p})-\mathbf{y}_{ref,N_p})\mathbf{W}_{x_N}(h_N(\mathbf{x}_{N_p})-\mathbf{y}_{ref,N_p})$$

Where $\mathbf{W}_x$, $\mathbf{W}_{x_N} \geq 0$, are the weighting matrices of the stage and terminal cost for the states, with appropriate matrix dimensions. The parameter $W_u > 0$ corresponds to the stage cost for the input. These matrices can be used as tuning parameters that influence tracking performance. The time-varying state reference vector is denoted $\mathbf{y}_{ref}$.

Constraints of the system

The state constraints are

$$x \in \mathbb{X} \subseteq \mathbb{R}^n \tag{B.5}$$

and input constraints are

$$u \in \mathbb{U} \subseteq \mathbb{R}^m \tag{B.6}$$

where subspaces $\mathbb{X}$ and $\mathbb{U}$ denote the allowed values that the differential states and input variables can have, respectively. In other words, these subspaces denote the bounds of the model.

B.1.3. Constraints and infeasibility

An MPC controller is only defined when the set of possible solutions is non-empty. If there are no possible solutions, the MPC problem is infeasible and the control input might result in arbitrary values. Therefore, the introduction of constraints to the system needs to be carefully considered, both in terms of added complexity and solution feasibility.

The main sources of constraint violations are unrealistic control objectives or a mismatch between the actual plant and the modelled plant dynamics. Moreover, constraints can be defined as hard or soft, where the latter can be slightly violated. In general, input constraints are hard because they are directly considered in the optimisation and can always be satisfied. On the other hand, state constraints arise from the allowed operating plant range or preferred operation limitations.

B.2. ACADO Toolkit

ACADO Toolkit [49] is an open-source software environment for automatic control and dynamic optimisation written in C++. It is suitable for the study of closed-loop MPC applications in real-time and its use is supported in MATLAB [8]. The modularity of the solver makes it possible to combine different specialised algorithms and features.

The controller implemented for this thesis is based on a discrete-time model of the plant and the optimal control input minimises the system's response along a number of discrete time steps, known as the prediction horizon. The predicted response is compared with the actual reference and the difference is penalised with the defined cost function to improve path tracking performance and the collaborative behaviour. The torque input and its rate are also penalised by the cost function in order to obtain a smooth, within the system constraints, control input.

Some of the solution methods available within the ACADO solver are listed in this section [48].

B.2.1. Discretisation method

The discretisation of the prediction model is necessary to solve the optimisation problem. The prediction horizon is divided into N_p sampling periods, which leads to a shooting grid of the form $[t_k,\ t_{k+1},\ \ldots,\ t_{k+N_p}]$. This grid is commonly defined as an equidistant grid. Then, the control input sequence is parametrised for each sub-interval $[t_j,\ t_{j+1}]$ for $j \in [k, k+N_p-1]$, with $j \in \mathbb{Z}$.

Afterwards, the discretised OCP can be solved with either a single-shooting or multiple-shooting approach. The multiple-shooting method handles better highly nonlinear and unstable systems. However, it also increases the number of variables and complexity of the OCP.

B.2.2. Integration method

Dynamic optimisation usually requires integrating differential equations. Hence, numerical algorithms are fundamental. The most common integration algorithms available are the Runge-Kutta and BDF integrators. All the integrators provide first and second order sensitivity generation via internal numerical differentiation.

B.2.3. NLP methods and solvers

MPC is most often formulated using a quadratic cost function and, thus, solved as a Quadratic Programming instance. In order to incorporate the system dynamics into the QP problem, there are two main approaches.

First, a sparse or simultaneous approach, in which both the states and the control inputs form the optimisation variables. The second formulation, named primal dense or sequential, uses recursion of the state transition to express the predicted states as a function of the control input sequence and the initial state.

There are several types of Sequential-Quadratic-Programming, SQP, methods available for the NLP solution with, for instance, Hessian approximations or Gauss-Newton Hessian approximations. These approximations can be in sparse form or dense, reduced form. An overview of the three main methods to solve QP instances is presented below [29].

Active Set Method

This method is based on the possibility that only some of the inequality constraints are active at the constrained optimum. The solution lies within the boundary of the active set, and inactive inequality constraints do not influence the solution. The active set method works in an iterative way until a feasible solution is found. This can lead to a potential drawback when the number of constraints is too big. In order to improve the computational performance, the previous active set can be reused as an initial guess for the next control input calculation.

Barrier Interior Point Method

The barrier interior point method transforms the constrained OCP into an unconstrained nonlinear problem at each iteration. This is approximated by a quadratic function, and Newton's algorithm is applied to solve the problem. For this, the inequality constraints are removed from the problem, and the optimisation performance criterion is modified by a differentiable additive barrier function to prevent constraints violations. Logarithmic functions are often used for this purpose. As a disadvantage, the method is required to start in the interior of the feasible region. On the other hand, it is computationally more efficient and, thus, appealing for real-time applications.

Gradient Projection Method

The gradient projection method makes use of the steepest descent, which is a step in the negative gradient direction at each iteration, projected into the feasible set. Depending on the type of constraints, the projection into the feasible set can become computationally expensive. For ill-conditioned problems, the method can converge slowly because of an uneven scaling of the problem.

Lastly, the above methods are used with different solvers, which can be found in further detail in [29]. Among the great number of solvers, the author highlights the following ones.

`FORCES`

Fast Optimal Real-time Control on Embedded Systems [22] automatically generates code featuring interior point methods coupled with Newton's algorithm, particularly focused on MPC systems. It has a very good computational performance and it scales well with problem size.

`qpDUNES`

The `qpDUNES` solver is specialised for QP [33]. It makes use of the Dual Newton strategy, which combines the benefits of the structure exploitation of the interior point method and the capabilities to introduce an initial guess from the active set methods. Unlike the previous solver, this one is a free software for both academic and commercial use.

`qpOASES`

Lastly, the resulting large, but sparse, QP can be condensed and passed to the dense solver, `qpOASES` [30], that employs an active set method. It makes use of an initial active set guess, known as a warm start, based on the assumption that the active set does not change significantly between consecutive control steps. This allows the system to be computationally very efficient as long as the assumption remains valid. This solver is also free for both academic and industrial use.

For all of the above methods, Linear Time-Varying, LTV, systems are supported.

B.2.4. Controller settings

The MPC and ACADO Toolkit settings for the LKA controller are defined in Tables B.1 and B.2. The values included in the controller settings are the sampling time of the MPC, and the sampling times for the vehicle-steering system simulation and the driver model, respectively. Finally, the prediction horizon, N_p, and control horizon, N_c, are also included. These two last parameters are set to the same value.

	MPC Settings				
Variable	T_s	$T_{s,sim}$	$T_{s,DM}$	N_p	N_c
Value	$1^{-2}\ s$	$1^{-3}\ s$	$2^{-2}\ s$	40	40

Table B.1: MPC settings.

The different sampling times and prediction horizons are appropriately chosen to ensure that the MPC model can be run in real-time without compromising its performance, prediction capabilities, and stability. The nonlinear plant operates at a higher sampling frequency, $T_{s,sim}$, whereas the linear driver model can be accurately run at a lower sampling frequency, $T_{s,DM}$, which reduces the computational requirements. For the MPC, the maximum sampling frequency that allows the model to compute the optimal control input in real-time, $T_{s,cont}$, is selected to ensure stability and a long enough prediction time, $T_{s,cont} \cdot N_p$, which has a direct impact on its performance.

For the ACADO Toolkit settings, there are many algorithm options that can be tuned. Table B.2 shows the most relevant settings that were considered. For the rest of the algorithm possibilities, default settings are used, which can be found in further detail in Houska et al. [48]. An explanation of the main function of the selected settings can also be found in the table below.

ACADO Settings		
Variable	**Value**	**Function**
HESSIAN_APPROXIMATION	GAUSS_NEWTON	Solving algorithm: Gauss-Newton Hessian approximation
DISCRETIZATION_TYPE	MULTIPLE_SHOOTING	Shooting discretisation algorithm
SPARSE_QP_SOLUTION	FULL_CONDENSING_N2	Condensing technique of the sparse QP solution
INTEGRATOR_TYPE	INT_EX_EULER	State integrator: Euler integration method
NUM_INTEGRATOR_STEPS	3*N_prediction	Number of integration steps along the prediction horizon
QP_SOLVER	QP_QPOASES3	Quadratic-Programming solver type
LEVENBERG_MARQUARDT	1^{-4}	Value for Levenberg-Marquardt regularisation
MAX_NUM_QP_ITERATIONS	20	Maximum number of QP iterations
HOTSTART_QP	YES	Hotstart QP from previous solution

Table B.2: ACADO settings.

B.3. Conclusions

An extensive investigation on the MPC's mathematical background presents Model Predictive Control as an attractive framework to implement the shared control objectives between the driver and the driving assist system.

First of all, Model Predictive Control fulfils the requirements needed for real-time implementation of the steering system control, as well as being able to handle nonlinearities and constraints on the system. Moreover, the RHC approach makes it possible to be robust against disturbances and iteratively calculate the optimal torque input of the controller.

Secondly, this approach enables us to respect the driver-vehicle constraint limitations by explicitly introducing bounds to certain states. This is beneficial in terms of safety, as well as driving comfort. For instance, limiting the maximum torque input of the MPC, T_c, allows the driver to overrule the system and remain in control of the task in case of conflict of intention with the assist guidance. Thereby, the range of T_c should be restricted to a value below the maximum torque that a human can apply. Moreover, a maximum torque and torque rate input, coming from the controller, ensures an appropriate level of comfort and safety. In addition, the introduction of constraints in the vehicle states, such as lateral acceleration or yaw rate, also enhances driving comfort.

Furthermore, MPC-based approaches are especially suitable within the vehicle steering control context, where there is a need for accuracy in the path tracking performance, as well as smoothness of the control actions. These characteristics are fundamental to guarantee the development of safe, intelligent ADAS.

Lastly, the chosen solver for real-time implementation is the open-source ACADO Toolkit. As previously mentioned, this software is designed for dynamic optimisation control and it is suitable to predict the behaviour of closed-loop systems online. Therefore, the real-time optimisation facilitates the integration of the driver's behaviour in the loop. As a consequence, the controller can be used to dynamically allocate the control authority between the driver and the driving assist system. This feature further fosters collaboration and reduces potential conflicts while driving, while still improving the path tracking performance.

C

Haptic Shared Control

This appendix presents an overview of the state-of-the-art Haptic Shared Control strategies that are relevant within the scope of this thesis. In Fig. C.1, a schematic representation of a shared steering system control can be seen.

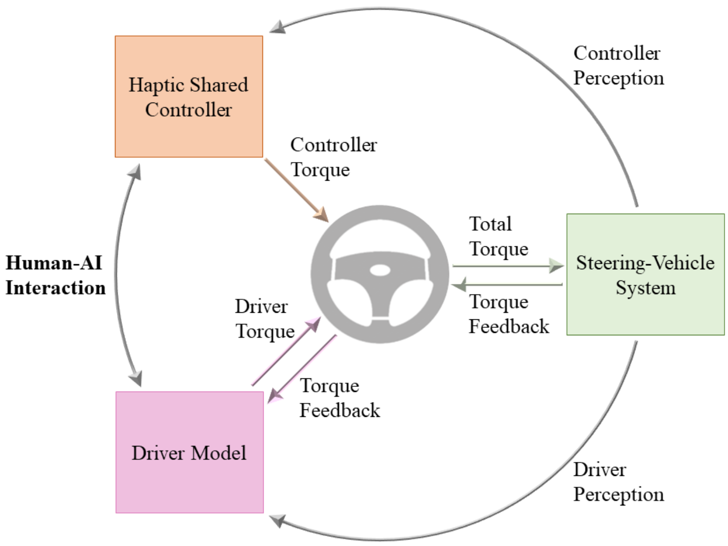

Figure C.1: Representation of shared steering system control.

As highlighted in Chapter 1, it is essential to understand the driver behaviour and their interaction with automation. However, human complexity and unpredictability make it difficult to guarantee collaboration and seamless control between the human and the driving assist systems. A potential control strategy that has gained increased attention throughout the past decade is Haptic Shared Control.

C.1. Automation and the role of the driver

The current exponential technological progress drives the development of new, more capable automated systems. In the driving context, this has become patent from the rising importance of ADAS. However, until fully automated driving vehicles become a reality, it is paramount to take into account the interaction between the driver and the vehicle in the development of more collaborative driving assist systems.

A well-established first approach in the design of driving assist systems lead to the introduction of a new role for the human driver. Initially, the focus of automation was to increase performance by substituting the driver in specific tasks. Hence, this can be translated into assist systems capable of taking over a driving task in a specific Operational Design Domain, ODD. Notwithstanding, this approach imposed the role of supervisor to the driver, having to monitor the automation system for the tasks that designs cannot automate. This new role has been thoroughly investigated, and it is widely acknowledged that humans often perform badly under supervisory control roles, as highlighted by Parasuraman [84] and Wickens and Kessel [109]. This role is remarkably challenging during driving and can be considered a highly demanding task. This context leads to an interesting *irony of automation* [9] where, if there is an automation failure, the driver is expected to detect the errors from the automation system [83] and take over during critical situations that are out of the control of the automation system.

Therefore, it is clear that the human-machine interaction needs to be carefully treated in order to guarantee an increase of performance, safety, and the appropriate use of automated systems [77]. One important aspect to be taken into consideration is clarifying what the driving assist systems are capable of doing and transmitting this to the driver in a suitable manner [15]. Besides, drivers should be capable of maintaining a good level of situation awareness to correctly react in case of an automation failure [92, 97, 98]. Drivers can easily disengage from the driving task when they are not aware of the status of the scenario. This can lead to dangerous situations [83], also known as the ‘out-of-the-loop’ performance problem [11]. In addition, the lack of manual driving activity can result in skill degradation [17] due to automation.

In line with the aforementioned automation issues, Haptic Shared Control is presented as a promising alternative. Through HSC, the authority of the driving task is balanced between the automation system and the driver in order to accomplish a common objective. The goal of this strategy is to keep the driver in the loop, rather than letting the automation exert full control over the vehicle. Additionally, this approach ensures smooth, intuitive authority transitions.

Furthermore, some other potential benefits of HSC are to reduce human control activity, and thus the steering effort, while still enhancing driving performance, safety, and keeping the driver in the loop. Ultimately, this can be seen as the ideal combination between the human intelligence and adaptability with the benefits of automation systems [80].

C.1.1. Design guidelines for shared control

The shared control approach is particularly suitable for the steering task because forces can be exchanged through the common interface. This interconnection at the steering handwheel promotes the interaction of both controllers, the driver and driving assist system. It also facilitates the awareness of each other's actions and intentions. Moreover, it allows drivers to overrule the system by, for instance, increasing the co-contraction level of the muscles, as described in Section A.2.5.

In order to model such an approach, a clear understanding of how shared control is interpreted and its foremost design guidelines are required. The definition of shared control used for this thesis is taken from Abbink et al. [5]:

> "In shared control, human(s) and robot(s) are interacting congruently in a perception-action cycle to perform a dynamic task that either the human or the robot could execute individually under ideal circumstances."

The design guidelines for human-machine interaction towards the development of shared control systems are defined based on Abbink et al. [4], and particularised for the driving steering task.

I. The driver should always remain in control, although subject to different levels of automation authority. To guarantee this principle, the haptic guidance limits should remain within the boundaries of the human limitations.

II. The control should be provided to the driver through continuous feedback and effectively communicating the limits of automation and functionality.

III. Continuous interaction between human and driver assistance system should be provided.

IV. Shared control should result in increased performance and/or reduced driver workload.

C.1.2. Human-machine conflicts

An interesting result found by Mulder et al. [80] is that, although HSC can lead to less steering control activity and increased safety, drivers often resist the assist system's guidance **??**. This can be due to, for example, a difference in the desired vehicle trajectory or different driving control strategies.

One approach to deal with the competing behaviour between human and driving assist systems is to adapt the level of automation [51]. However, most automation systems restrict the shift of authority to binary models.

In order to understand how these conflicts arise, it is necessary to illustrate the different levels of cognition, which were reported by Michon [78]. These levels are present during the accomplishment of any task. Afterwards, a general outline of the influence of different levels of authority on performance is presented.

Levels of Cognition

- Strategic level:

  This level corresponds to the navigation or route planning over a long time window.

- Tactical level:

  In a manoeuvre, shared tactics can be represented by the guidance that influences the direction of the vehicle.

- Operational level:

  The control of the vehicle belongs to this level. The control commands are often the most time critical, and highly influence vehicle stability.

- Execution level:

  This fourth stage has been described by Abbink et al. [5] and comprises the neuromuscular control loops, which execute the operational level control commands.

The above cognitive levels are not independent from each other, but rather interdependent. Consequently, it seems plausible that, in order to enhance the human-machine interaction, all levels should be taken into consideration.

Level of Authority

Another concern in the development of HSC systems is how to appropriately determine the level of automation [100]. This level of authority can be constant [24] or adaptive [51, 94]. The latter can potentially adjust to the time-varying behaviour of the driver. However, most research studies fail to design the adaptive transitions of control authority in a natural way. Instead, binary switches of control authority are often implemented. A more intuitive approach is to smoothly switch the control authority [31], which results in more compliant systems. On the other hand, it has an increased complexity in the dynamic task allocation.

Furthermore, the maximum level of torque guidance provided to the driver should not exceed the human limitations to exert torque. This is because of safety concerns and to allow the driver to remain in control and being capable of overruling the system at any point if desired.

C.1.3. Importance of modeling the driver behaviour

A key element in the design of shared controllers is the accurate modelling of the driver in order to improve the prediction of their behaviour and intentions. As emphasised by Abbink and Mulder [2], a better understanding of the human behaviour is expected to reduce conflicts between humans and automated systems.

In particular, in order to describe the strategic level of cognition of the drivers, it is necessary to model their complex cognitive behaviour. As described in Section A.1, this includes the selection of an appropriate human control strategy to predict their intentions, an estimator of the states of the system, and an accurate internal mental representation of the driver-vehicle dynamics and their interaction. Secondly, the use torques through HSC allows for the exploitation of the NMS, which is highly adaptive and fast. Hence, a detailed representation of the muscle dynamics, as presented in Section A.2, is fundamental. Lastly, it is also important to consider the driver limitations in the perception of the environment. This involves the introduction of the sensory organs described in Section A.3.

Furthermore, on a tactical level, the driver can feel the torque guidance of the controller through the steering handwheel. This continuous feedback facilitates the driver awareness and maintains the driver engaged in the steering task.

Nevertheless, although there is an increase in the research of driver models applicable to the driving task, based on neuro-scientific background and summarised in Chapter A, the study of these models is often independent from the driving assist systems development.

C.2. State-of-the-art research

Nowadays, there is a significant increase in the amount of research found in literature for driver modelling, both in the field of neuroscience, as well as particularised to the driving task. Likewise, HSC has received an increased amount of attention in the path towards automation, appearing as a promising control strategy that keeps the driver in the loop, while improving driving performance and safety.

In agreement with the recent directions of research, the need to blend driver modelling and vehicle controller systems has been widely acknowledged [2]. However, there has been limited implementation of detailed driver models in haptic shared controllers, with a haptic gas pedal by Abbink [3] and, for the steering task, [73]. In his research, Abbink modelled the haptic driver-vehicle interaction with a high emphasis on the development and investigation of an extensive NMS.

In particular to the steering task, the most relevant representations found in literature are highlighted and briefly described in this section. The main focus of the models below is to predict the driver behaviour better in order to develop more collaborative ADAS. Some of these approaches consider the driver as an external disturbance. Hence, global stability, collaboration, and robustness cannot be guaranteed [93].

Psycho-physiology-based driver model

A psycho-physiology-based driver model is implemented by Mars and Chevrel [72] for the design of a lane keeping assist system. The model is then embedded into an HSC system, blending the driver's sensorimotor control and a continuous assist support.

The cognitive behaviour of the driver is based on a two-point predictive model including visual anticipation of the road curvature and compensation of the lateral error. The NMS includes a transfer function transforming motor commands to the steering wheel torque, as well as the reflex loop. The identified driver parameters were validated, resulting in only a 70% steering fit for an average driver, which can be considered not accurate enough with respect to high-fidelity driver models. On the controller's side, an H2-Preview optimisation approach is used [93].

One of the main drawbacks of the proposed model is the limitation of the human representation, which is not particularised for the driving context. Apart from that, the stability of the system is highly sensitive to the cognitive processing delay. Besides, the results of the experiment were only validated with one single participant in a fixed-base driving simulator. The results show less steering effort in most of the simulation. However, there are clear conflicts during many parts of the curve negotiation path, even though the experiments were restricted to a lane keeping scenario. Lastly, another key disadvantage is the impossibility to exploit the information about the driver's intentions in real-time.

An interesting finding of this research was the creation of different indicators for collaborative behaviour, which are scarce in literature. Examples of such criteria are the consistency rate, resistance rate, and contradiction rate. These indicators are based on the direction of the assist torque and the driver torques, as well as their respective magnitudes.

Hierarchical cooperative control architecture using MPC

An MPC shared control strategy was proposed by Guo et al. [38]. The novelty of the approach originates from the introduction of two competing costs to minimise, the driver torque and assist torque. Through a varying weighting parameter, ρ, the cost weight between these two objectives can be modified, representing the shift in the level of control authority.

One limiting factor is that the driver presence was oversimplified to a stiffness and damping parameter representing the arms, coupled with the steering system dynamics. Another major concern that can be highlighted from this implementation is the binary parametrisation of ρ. Therefore, the system is set to zero when the driver exerts more than a certain torque value. On the other hand, when the value is set to one, there are two scenarios that can take place. One scenario is full automation if the driver has their hands off the steering wheel. Alternatively, the shared driving scenario can be represented, where the MPC minimises the two competing objectives. However, the reduction of conflicts between driver and the assist system is not directly addressed and a detailed driver model is not present either. This becomes clear by analysing the large variance of steering wheel reversals when the assist system exerted torque guidance, which suggests that drivers tend to correct the suggested trajectory by the automation system.

MPC-based driver steering assistance system

The research carried out by Ercan et al. [25] presents an MPC-based driver steering assistance system providing corrective torque guidance to the driver for a lane-keeping scenario. A similar model, applied for highway scenarios [26], was also developed by the authors based on the same principles.

Again, using an oversimplified approach, the interaction between the driver and steering system are considered. The neuromuscular dynamics are included by modelling the arms as a spring-damper system coupled with the steering system dynamics.

An interesting novelty of the approach was the online estimation of the driver parameters through a nonlinear recursive least squares algorithm. Although the controller's ability to adapt to changes in the time-varying NMS properties was demonstrated, the estimated impedances of the arms were not consistent due to lack of robustness in the estimation method for the applied signals.

Haptic shared controller to reduce steering conflicts

The model developed by Scholtens et al. [95] takes special care in tackling the human-machine conflicts in terms of the difference in the applied torque sign. It is based on the Four-Design-Choice-Architecture [106], where a human-compatible reference is introduced as the input reference for the haptic shared controller. Moreover, the controller corrections are based on both anticipatory and compensatory control. The added contribution of both types of corrections is then weighted within a Level of Haptic Authority specification. A complete schematic representation of the described architecture can be seen in Fig. C.2.

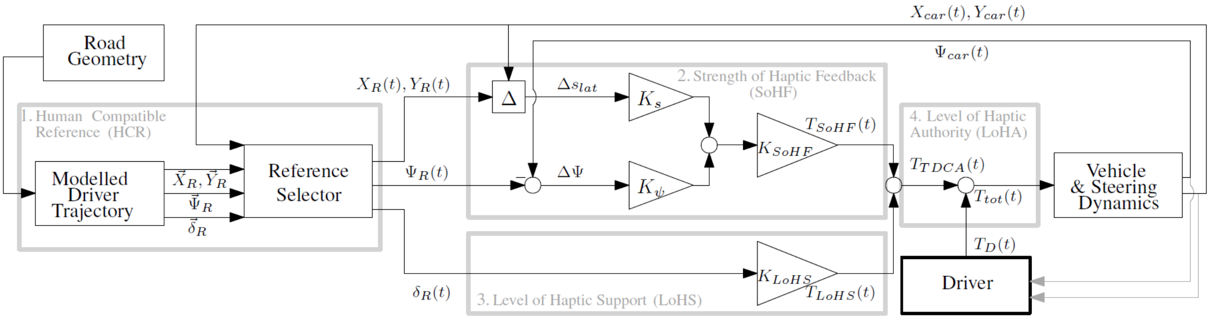

Figure C.2: The implemented Four-Design-Choice Haptic Shared Controller from [95].

A major limitation of the model is that the human-compatible reference trajectory is calculated offline based on a two-point control strategy, the far and near point. Thus, the model is constrained to predefined trajectories and no modification during online simulations is possible. Furthermore, the LOHA was set to a value of one, which can be translated as no adaptation to a particular optimal steering angle. Lastly, no neuromuscular behaviour is modelled.

Game-Theoretic Approach

In this paper, the shared steering torque control problem is tackled by an affine-Linear-Quadratic method and makes use of a new trend to model driver-vehicle interaction, the game theory models [54]. The controller is used to optimise path tracking performance during lane changes, using only computer simulations.

A sixth-order driver–vehicle system is presented and the model includes the uncertainty of the system. The stochastic Nash and Stackelberg equilibrium solutions were derived using stochastic dynamic programming. This is considered a potential research direction in the understanding of the driver-controller interaction.

C.3. Conclusions

Haptic Shared Control increases driving performance with respect to manual driving, while keeping the driver in the loop, which positively influences the situation awareness of the drivers.

One of the main advantages of this control strategy is the possibility to model the interaction between the driver and the driving assist system and provide haptic guidance. However, the driver can react differently to this external torque input. For instance, drivers can be compliant with the driving assist system, amplifying the forces provided by the assist. On the other hand, the driver can also resist these forces. The resisting behaviour can come both from a mismatch between the driver's cognitive intentions and the automation, or from a neuromuscular level, such as the reflex action of the muscle spindles.

Consequently, the understanding of the human-machine interaction needs to be carefully analysed in order to avoid steering torque conflicts and keep the driver in control, while still guiding their behaviour to improve path tracking performance.

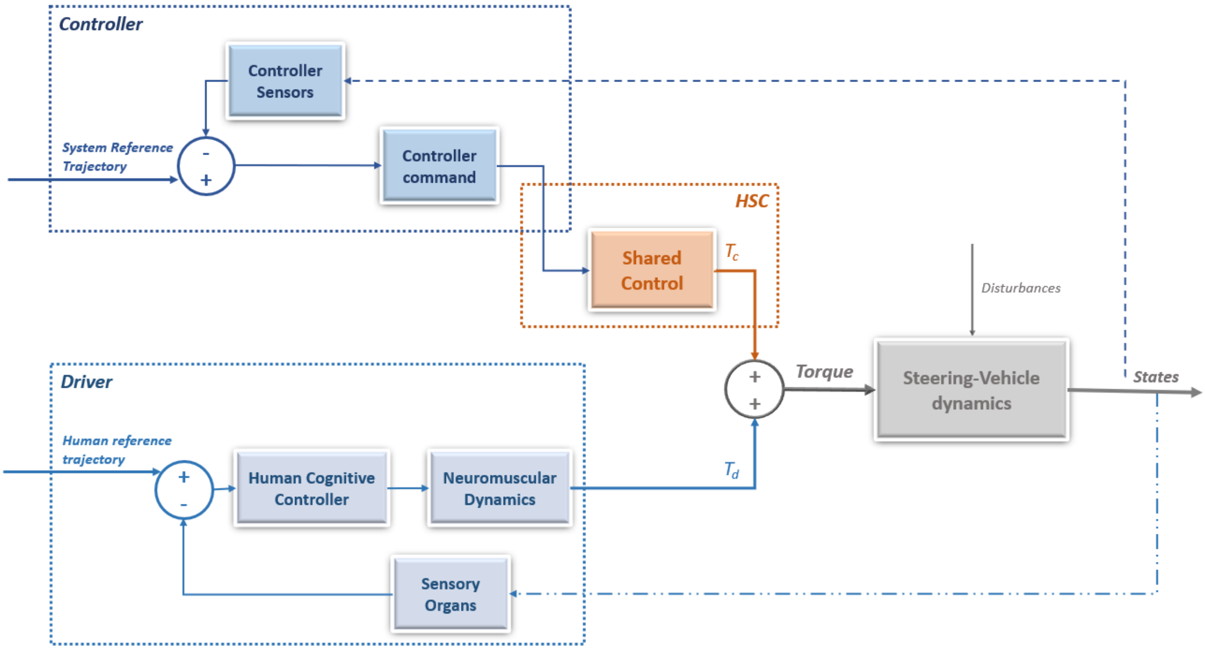

Figure C.3: General scheme of the Haptic Shared Control strategy.

In short, a potential benefit of HSC is that it provides an effective, fast, and intuitive communication between the driver and driving assist system. The exchange of torques through the steering handwheel interface can be exploited to take advantage of the human neuromuscular behaviour. Therefore, the drivers can interact with the driving assist system both at a cognitive or strategic level, as well as in a more operational-execution level.

However, current HSC approaches do not try to reduce driver-vehicle conflicts, or, when they do, this is tackled in a reactive manner. Therefore, a promising course of action to reduce conflicts and increase user acceptance is to focus on the development of reliable driver models. By integrating them in the controller, we can predict better the driver's behaviour and foster a more collaborative guidance. However, there is no clear consensus on how these driver models should be implemented, the amount of detail required, or how to make the interaction between the human and automation system possible.

Lastly, other key features in the development of collaborative ADAS can be the model's adaptability to human behaviour and / or a dynamic shift of the control authority depending on the scenario. These feature can be introduced with a mindful selection of the most appropriate cost function. This human adaptability can be observed when, for example, the driver consciously decides to increase their level of muscle co-contraction or instantaneously reacts through reflex action of the muscle spindles.

D

Results and Discussion

The purpose of the driving assist system is to allow the controller to provide a more intuitive torque guidance to the driver through the steering wheel, also known as haptic guidance. The system can predict the behaviour of the vehicle plant being controlled, as well as the driver-in-the-loop action.

The contents of this Appendix include the initial computer simulation results, as well as the outcome of a fixed-base driving simulator experiment. In the latter, the proposed MPC controller is evaluated against a state-of-the-art commercial benchmark. The results include the subjective evaluations of 19 drivers, as well as 13 objective Key Performance Indicators calculated from the experiment of each participant.

D.1. Computer simulation results

The simulations of the initial linear MPC-based Haptic Shared Control strategies are included here, along with a discussion of the benefits of using this novel approach.

The MPC assist system is assessed for different scenarios, such as a lane change subject to an external force disturbance and a sine test. Initially, both were assessed in a bicycle model plant. To further validate its applicability, the sine test was chosen to be performed in a high-fidelity environment using CarMaker. The nonlinear vehicle dynamics and steering system [16] are based on a validated mass production vehicle model.

D.1.1. Lane change scenario

The MPC controller is investigated for a lane change manoeuvre to test its robustness:

- Case 1. Baseline scenario. Manual driving.
- Case 2. Manual driving with a disturbance of 800 N at 12 s.
- Case 3. Shared driving.
- Case 4. Shared driving with a disturbance of 800 N at 12 s.

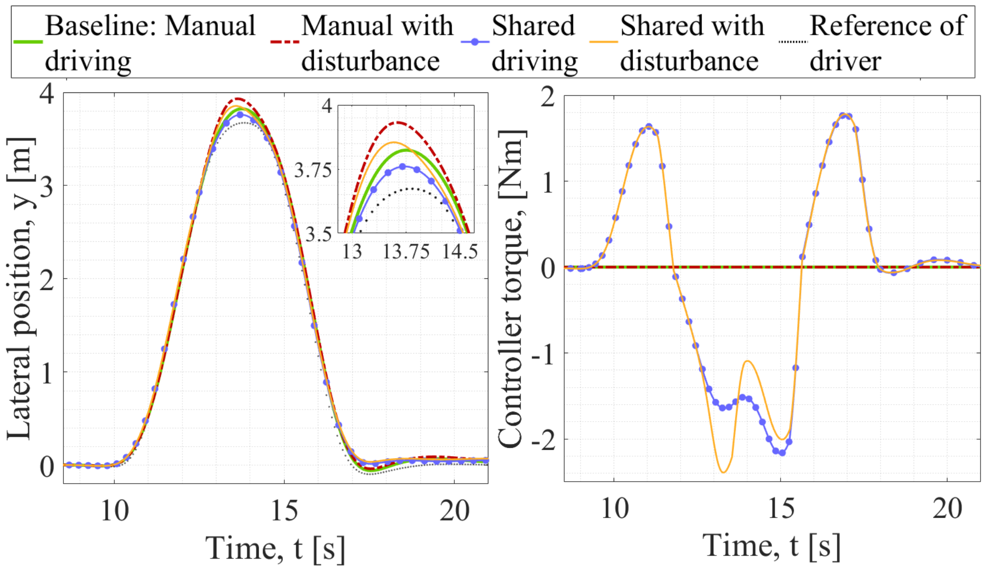

Figure D.1: Lane change scenario: Path tracking performance and MPC-controller torque.

The controller adapts to the different situations, improving the path tracking performance while minimising the muscle spindle torque and the overall driver effort. In Figure D.1, it can be seen that the RMSE is lower for the shared case ($y_{rms} = 0.054\ m$) compared to manual driving ($y_{rms} = 0.055\ m$). The same applies for the case with a disturbance with shared control ($y_{rms} = 0.073\ m$) and manual driving ($y_{rms} = 0.076\ m$). Moreover, in cases 2 and 4, the MPC helps the driver to reject the disturbance, thus, minimising the reflex action by 25.27 %, as displayed in Figure D.2.

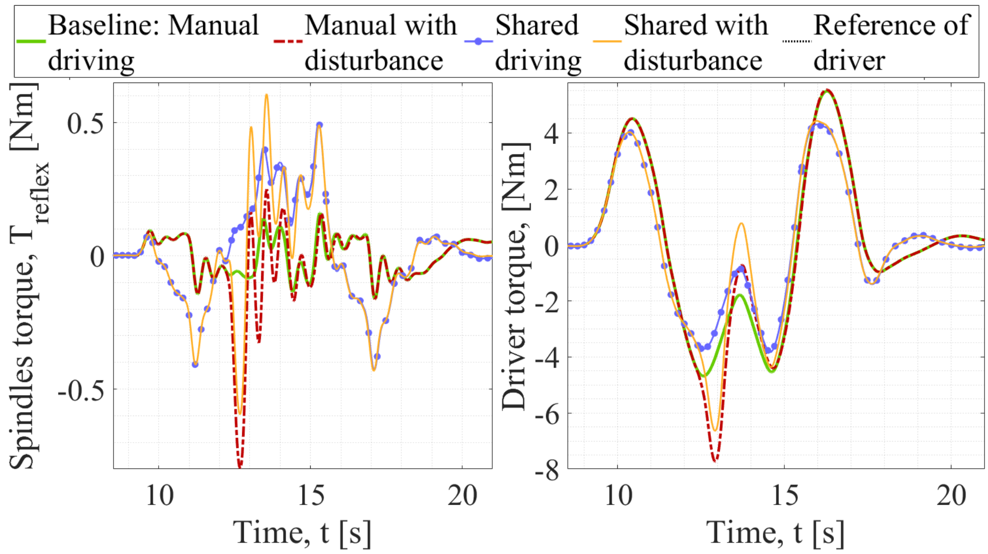

Figure D.2: Lane change scenario: Driver torques.

D.1.2. Sine test manoeuvre

The controller can be tuned to portray different behaviours and the competing objectives of driver comfort and path tracking performance are investigated in Figures D.3 to D.4.

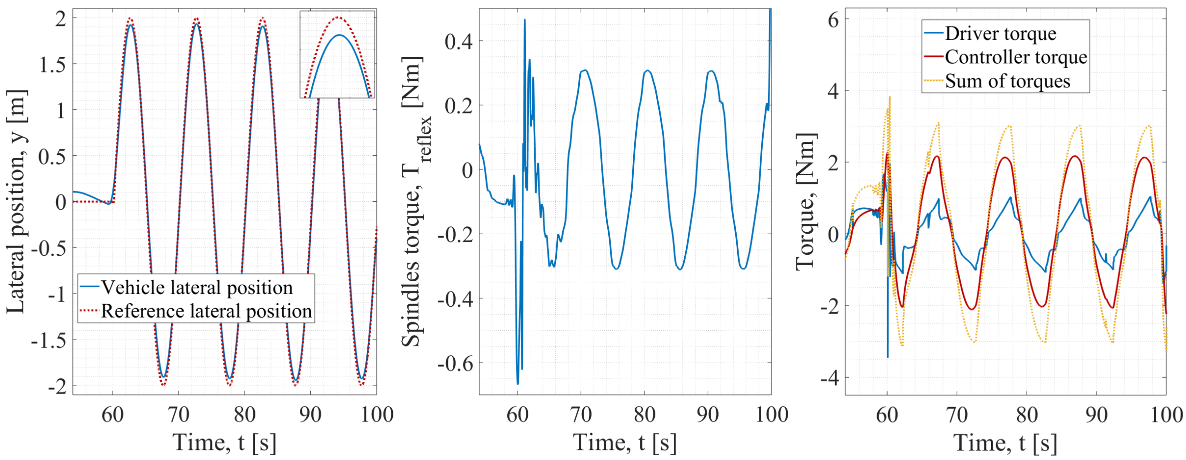

Figure D.3: Mode 1: Performance optimisation.

A strong torque guidance of the assist system is presented in Figure D.3. The optimisation algorithm makes use of the prediction of the driver behaviour to provide a human-like guidance and release the driver of most of the steering effort, which results in a more accurate path tracking performance. This controller could potentially be helpful to more inexperienced drivers or compliant users.

In Figure D.4, on the other hand, the aim is to reduce the conflicts with the driver before they arise. The controller exploits the adaptive nature of the MPC cost function and it uses the driver model to enhance driver comfort. Here, reduction of conflict is more relevant than maximum performance, although the latter is also improved with respect to manual driving. In this case, the assist system guidance is less strong, allowing the driver to easily overrule the system if desired. This behaviour is achieved by modifying the settings of this second controller to have a higher cost on the reflex torque of the driver, which is related to driver discomfort and the rejection of disturbances. This makes the MPC to be less intrusive than in the previous case.

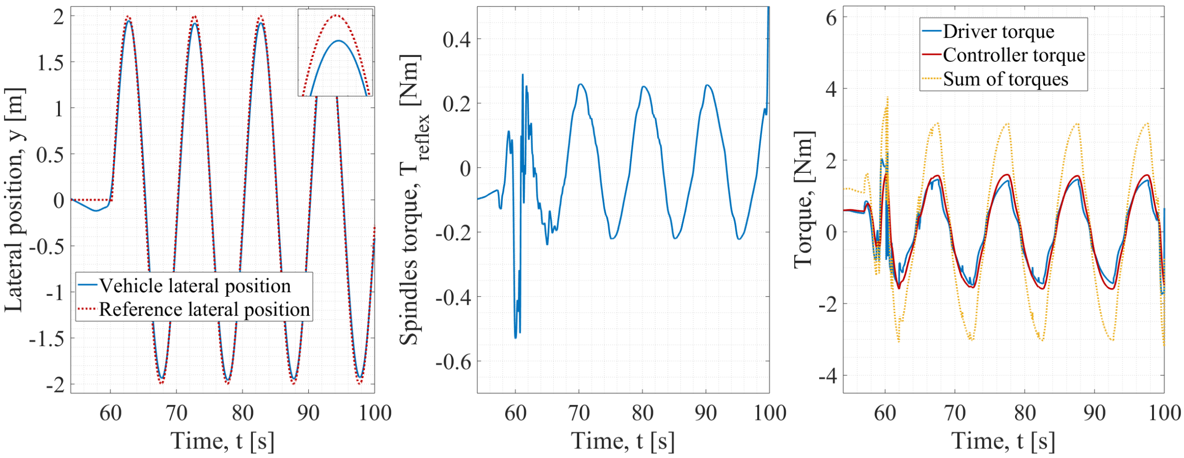

Figure D.4: Mode 2: Conflict minimisation.

In short, the collaborative behaviour of the MPC assist system allows for a better balance between performance and comfort due to the introduction of an advanced driver model within the prediction model.

The MPC computes the optimisation depending on the cost function parameters without compromising driver comfort and its behaviour is enhanced through adaptive costs. Moreover, even though the behaviour of the CarMaker virtual driver is rather constant, the possibility to customise both the driver parametrisation and the MPC assist system makes it possible to tackle the individual needs of each user.

D.2. Driving simulator experiment

The aim of this experiment is to assess the performance and collaborative behaviour of the proposed MPC controller with two different cost-function settings, as well as to compare them against the commercial LKA used as benchmark, both objectively and subjectively. All three controllers provide the drivers with a haptic torque guidance to track the centre of the path. In Fig. D.5, an overview of the driving simulator set-up is presented, with the human driver in the loop interacting with the controllers.

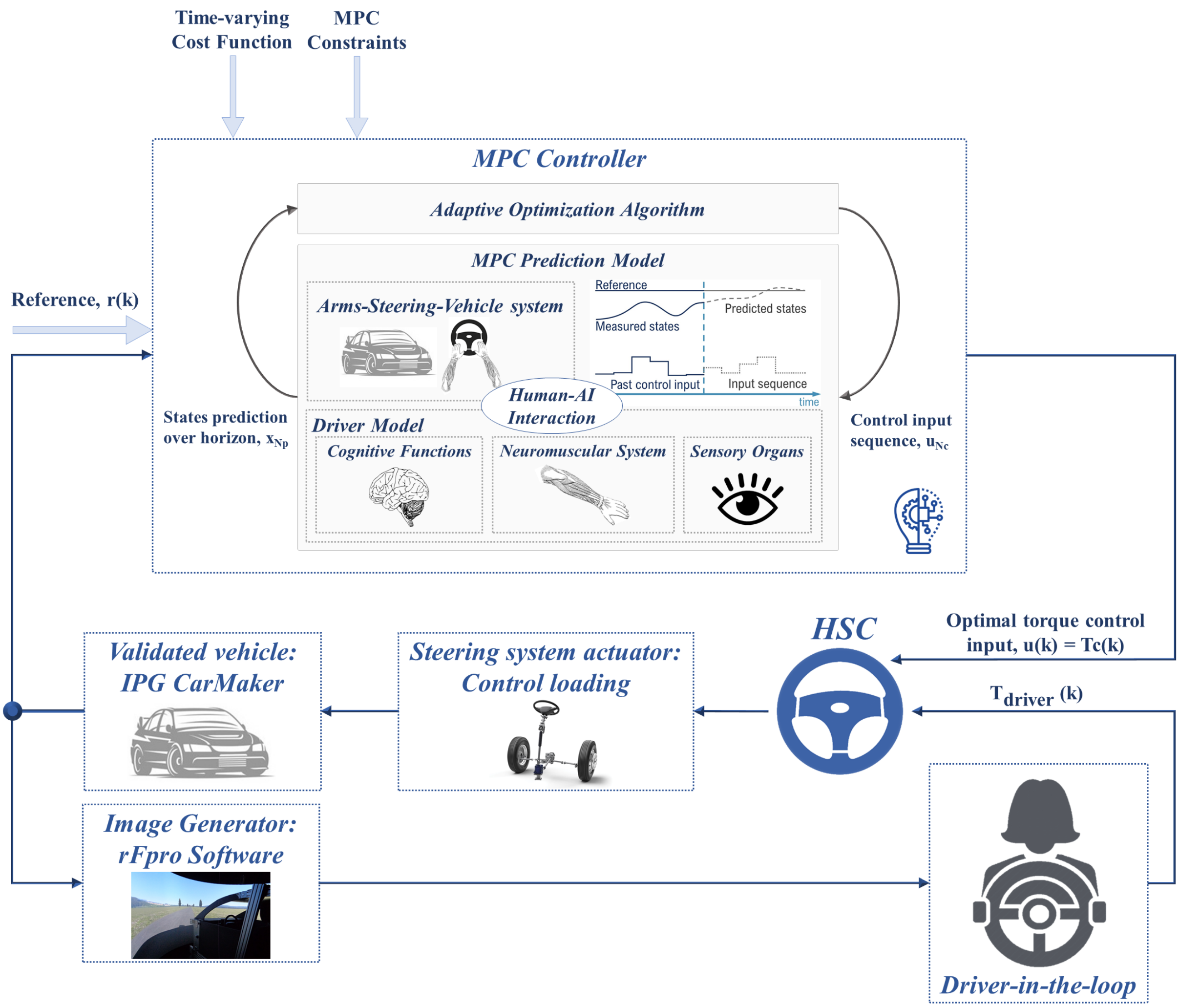

Figure D.5: Driving simulator experiment.

D.2.1. Subjective Evaluations

The box-plots results of the subjective evaluations are presented in Fig. D.6, along with the statistical results in Table D.1. The results are based on the responses of 19 participants, with five qualities per controller in a 7-point scale, with the ideal range in green.

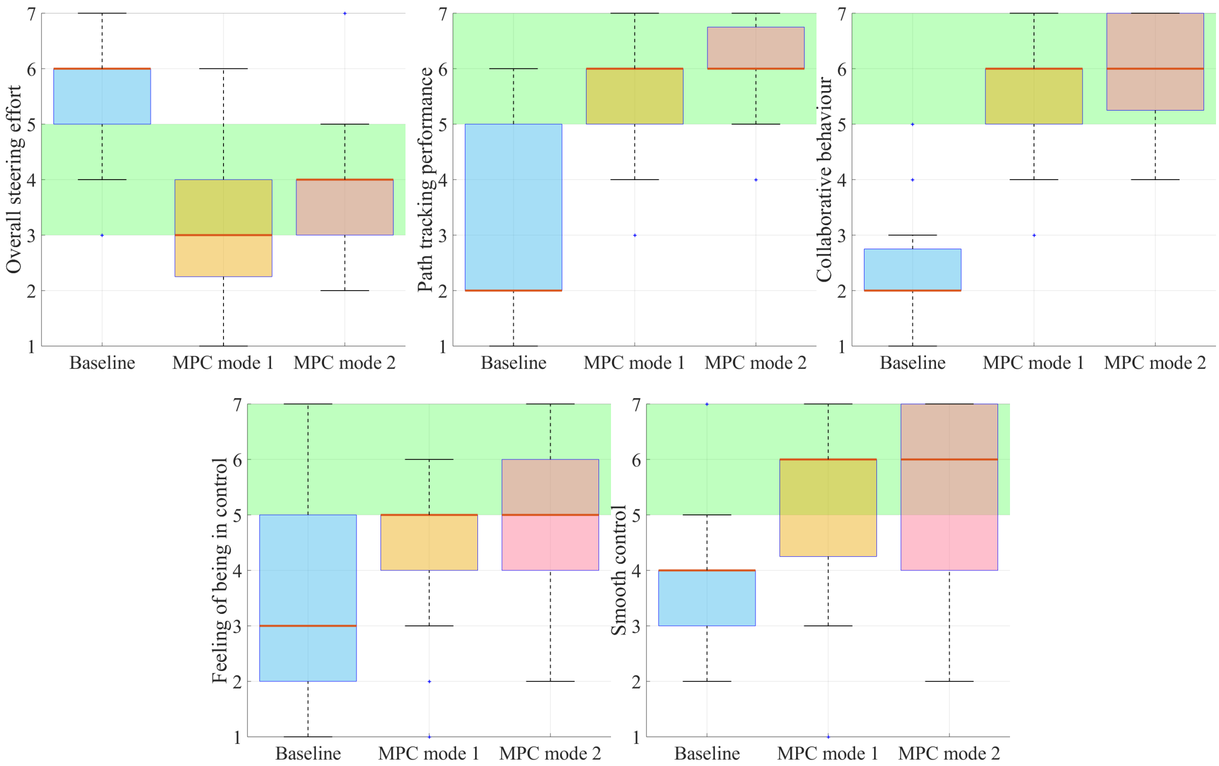

Figure D.6: Boxplot of the subjective evaluations of 19 participants, with the ideal range in green.

Criteria	Baseline	MPC 1	MPC 2	F	p
Overall effort	5.58 (0.90)	3.32 (1.25)	3.79 (1.18)	21.53	<0.001
Tracking performance	3.11 (1.73)	5.68 (1.11)	5.95 (0.91)	**27.86**	<0.001
Collaborative behaviour	2.42 (1.35)	5.32 (1.00)	5.95 (1.08)	50.60	<0.001
Feeling of control	3.42 (1.74)	4.37 (1.34)	4.84 (1.50)	4.21	0.02
Smooth control	3.84 (1.34)	5.16 (1.57)	5.37 (1.67)	5.51	0.007

Table D.1: Analysed data of the subjective evaluations with mean(SD) and ANOVA results.

D.2.2. Objective evaluations

In general, the presence of driver-assist conflicts creates the perception of the baseline controller being heavier than desired, as well as having a lower collaborative behaviour.

In Fig. D.7, we can see from recorded simulator data that the MPC is in phase with the driver inputs. In other words, the MPC actively cooperates with the driver and minimises conflict, which results in improved path tracking performance.

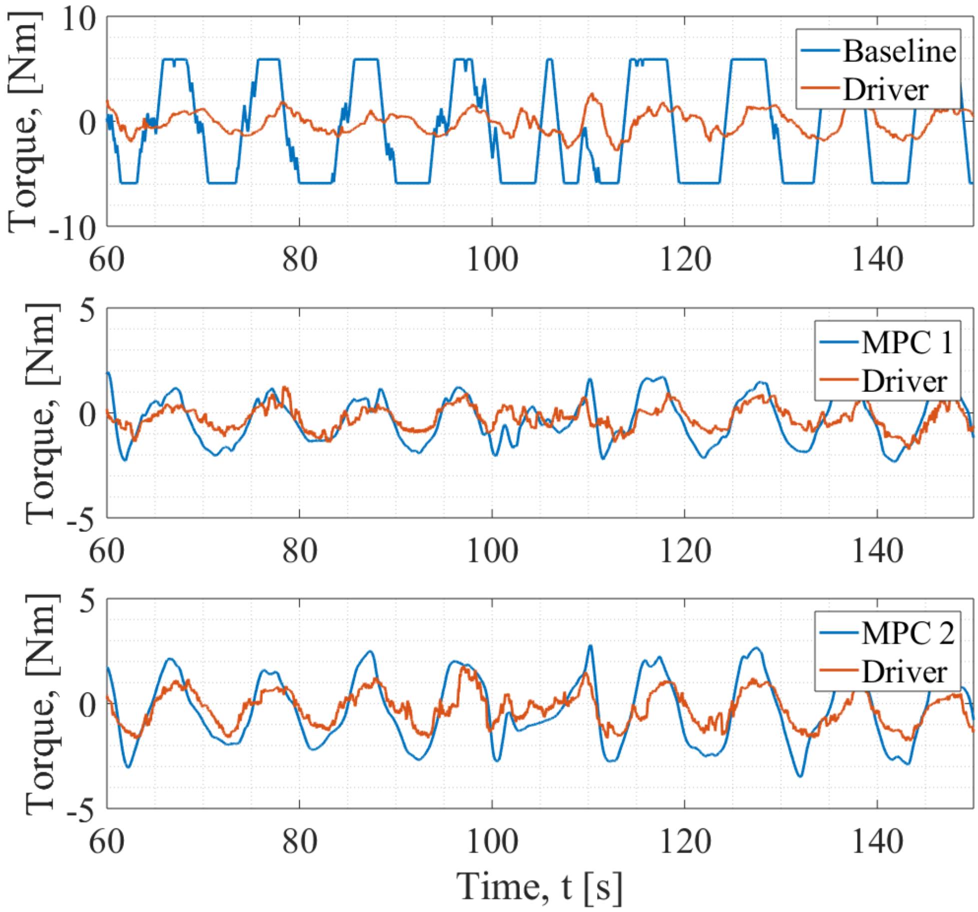

Figure D.7: Torque versus time of the driver and the driving assist system.

Moreover, several Key Performance Indicators were also defined and selected to verify the results impartially and to create a link between subjective and objective evaluations. For this, extensive research was performed, and the KPIs are grouped according to the subjective questions. The formulas of these metrics are defined in Chapter 2.

The steering effort is objectively quantified based on the steering torque effort over the total duration of the manoeuvre for both the driver and assist system, of which the box plots are displayed in Fig. D.8.

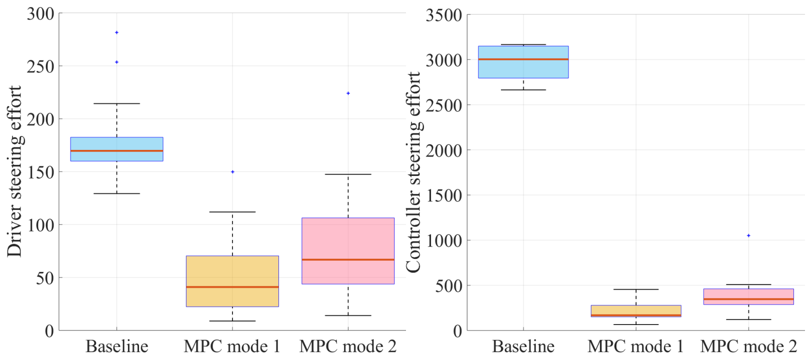

Figure D.8: Boxplot of the objective evaluation of 19 participants for steering effort.

Moreover, the main indicator for the path tracking performance can be defined as the root-mean-square lateral error. Other metrics used to assess the tracking performance are the mean lateral error, the maximum lateral error, and the standard deviation of the lateral error, presented in Fig. D.9.

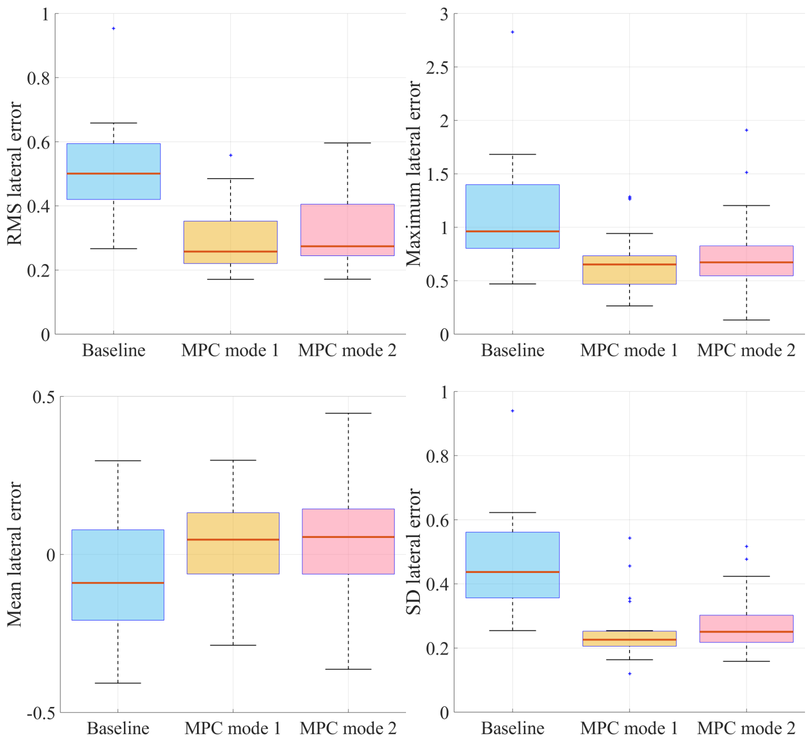

Figure D.9: Boxplot of the objective evaluation of 19 participants for path tracking performance.

For the collaborative behaviour, four different ratios are calculated, where each depends on the signs of the driver's torque and the driving assist's torque. When the signs are the same, the collaborative ratio increases. On the other hand, when there are torque conflicts, the intrusiveness ratio increases, which is subdivided into resistance and contradiction ratio. In addition, the coherence metric indicates when the simulated manoeuvre is collaborative overall.

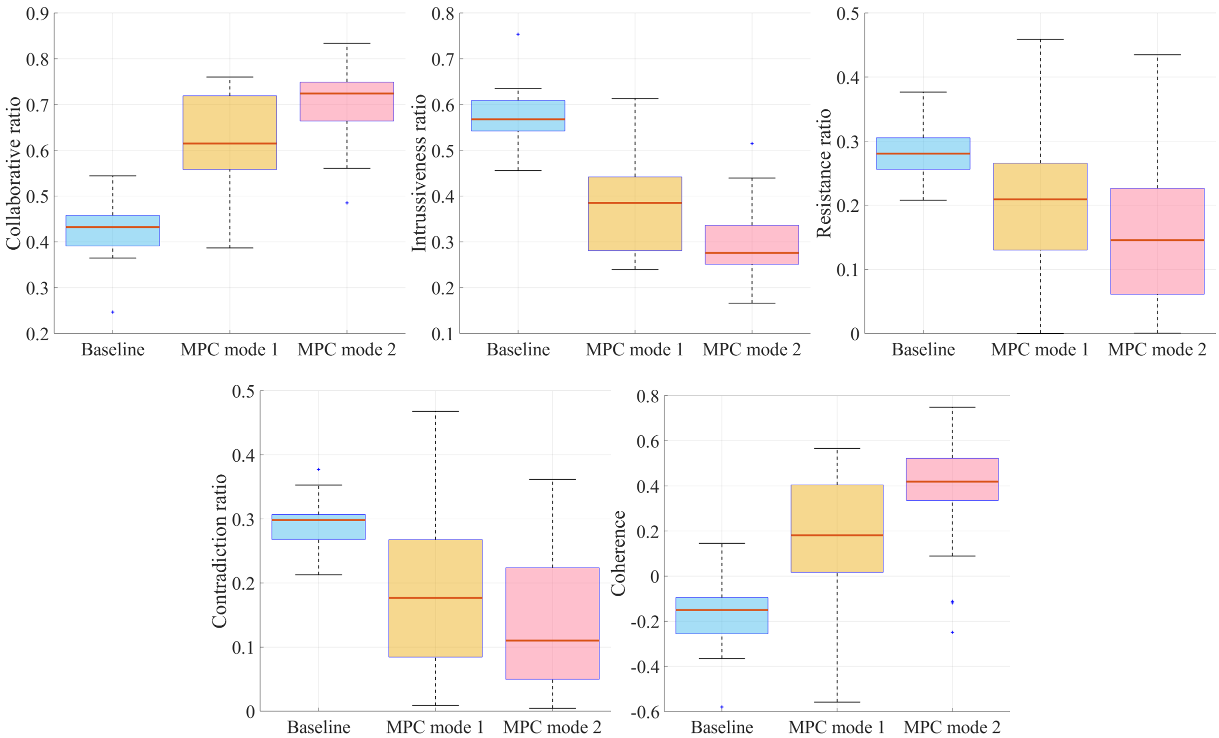

Figure D.10: Boxplot of the objective evaluation of 19 participants for collaborative behaviour.

Lastly, the level of control authority can be determined with the ratio of the driver and controller steering torque effort, whereas the steering reversal rate is calculated according to [71].

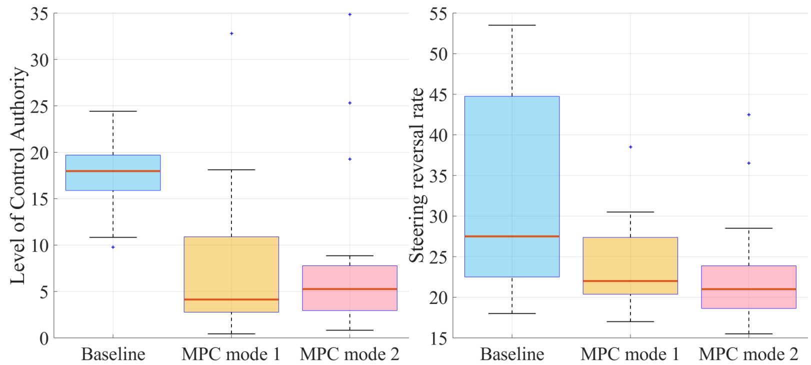

Figure D.11: Boxplot of the objective evaluation of 19 participants for the level of control authority and smoothness.

For all 13 objective metrics, the proposed MPC controllers outperform the commercial system. In Table D.2, the mean and standard deviation values for each KPI are summarised, as well as their statistical results. From these values, we can conclude that, except for the mean error, all differences in the controllers are statistically significant. In other words, the proposed MPC controllers significantly increase the performance of the haptic shared controller. Table D.2 shows the p- and F-values calculated using the statistical test ANOVA. First of all, a Bartlett's test for equal variances between the three groups of controllers was executed. Then, for the metrics where it was not appropriate to use ANOVA, the non-parametric Kruskal-Wallis test was performed. The F-values in bold correspond to the ones calculated through Kruskal-Wallis.

Criteria	Baseline	MPC 1	MPC 2	F	p
Driver effort	177.01 (37.74)	51.32 (37.38)	78.83 (50.31)	46.49	< 0.001
Controller effort	2982.77 (170.05)	209.83 (92.90)	390.08 (193.23)	**43.17**	<0.001
Lateral RMSE	0.51 (0.15)	0.29 (0.11)	0.33 (0.12)	15.38	<0.001
Maximum e_y	1.14 (0.54)	0.66 (0.33)	0.75 (0.43)	6.17	0.004
Mean e_y	-0.06 (0.19)	0.03 (0.15)	0.03 (0.18)	1.81	**0.173**
SD e_y	0.47 (0.16)	0.25 (0.10)	0.28 (0.10)	17.53	<0.001
Collaborative ratio	0.43 (0.06)	0.62 (0.11)	0.70 (0.09)	45.70	<0.001
Intrusiveness ratio	0.57 (0.06)	0.38 (0.11)	0.30 (0.09)	45.70	<0.001
Resistance ratio	0.28 (0.04)	0.20 (0.13)	0.16 (0.11)	**16.10**	<0.001
Contradiction ratio	0.29 (0.04)	0.18 (0.13)	0.14 (0.11)	**18.50**	<0.001
Coherence	-0.17 (0.17)	0.15 (0.29)	0.36 (0.27)	21.88	<0.001
Level of control authority	17.56 (3.68)	7.73 (8.03)	8.22 (8.79)	**20.91**	<0.001
Steering reversal rate	31.84 (12.84)	23.76 (5.27)	22.68 (6.75)	**8.38**	0.015

Table D.2: Analysed data of the objective metrics, with mean(SD) and ANOVA results.

E

Conference paper

This paper has been submitted and accepted to the FISITA 2020 World Congress, Prague. The paper will be presented online on the 24^{th} November 2020.

2020-XXX-NNN

MPC-BASED SHARED STEERING SYSTEM USING TORQUE CONTROL AND DRIVER MODELLING FOR COLLABORATIVE DRIVING

Andrea Michelle Rios Lazcano[1,2], Barys Shyrokau[2], Tenghao Niu[3], David Cole[3], and Xabier Carrera Akutain[1]

[1] *Toyota Motor Europe NV/SA*
Hoge Wei 33B, 1930 Zaventem, Belgium (E-mail: andrea.lazcano@toyota-europe.com)
[2] *Delft University of Technology*
Mekelweg 2, 2628 CD Delft, The Netherlands
[3] *Cambridge University Engineering Department*
Trumpington Street, Cambridge. CB2 1PZ. United Kingdom

ABSTRACT: Driving assist systems aim to increase comfort and safety while driving. However, if the assist system overrules the driver action, user acceptance and comfort become a challenge. Therefore, until fully Automated Driving (AD) vehicles become a reality, it is paramount to take into account the interaction between the driver and the vehicle in the development of more collaborative driving assist systems. In line with the aforementioned requirement, this work describes an optimal torque control law to foster haptic guidance and continuous cooperation with the driver during the steering task. This strategy is implemented within the Model Predictive Control (MPC) framework. Moreover, the driving assist system considers both the behaviour of the vehicle-environment being controlled and the driver's action in the presence of torque input. For this purpose, the closed-loop dynamics of the driver-vehicle interaction are thoroughly investigated. A novel concept of the proposed controller is based on a detailed driver-in-the-loop model generating an estimation of the expected driver torque. In particular, high emphasis is given to the modelling of the driver's cognitive behaviour based on a Linear-Quadratic-Gaussian (LQG) strategy, the sensory organs, and neuromuscular dynamics of the arms, which include the muscle activation dynamics and reflex action of the muscle spindles. Lastly, another key element of the model is the introduction of an adaptive cost function algorithm that fosters the collaborative behaviour and driver comfort. The validity of the driver model is successfully determined based on a driving simulator study in a high-fidelity nonlinear vehicle-steering system with different human drivers. The MPC controller, on the other hand, is assessed via offline computer simulations for several scenarios using a high-fidelity nonlinear plant using CarMaker. It is concluded that this model captures better the driver's intention and is suitable for the investigation of cooperation during the shared driving task. The proposed system predicts the driver's response accurately, enhances the human-vehicle closed-loop interaction, and reduces driver-controller conflicts.

KEY WORDS: Driving assist systems, haptic guidance, driver modelling, driver-in-the-loop, symbiotic driving

1. Introduction

Advanced Driver Assistance Systems (ADAS) are frequently introduced to increase safety and reduce mental workload while driving. However, current intelligent systems often lead to a lack of driver awareness while driving and to decreased user acceptance. The latter is particularly affected when the driver's intention is overruled by the assist systems in non-critical scenarios.

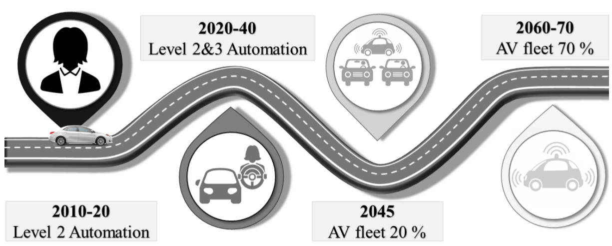

Figure 1. Timeline of the deployment of autonomous vehicles on the road

On the other hand, the different projections concerning Automated Vehicles indicate that their deployment is still decades away from becoming widespread [1]. A prospective timeline of the mobility sector is presented in Figure 1. From these projections, it is clear that vehicles equipped with SAE AD Level 2 and 3 [2] are valuable milestones to be reached in the near future.

One of the key challenges of these levels of automation is how to take into account the driver-vehicle interaction [3]. Therefore, the focus of this research is to design a collaborative shared control strategy that assists users during demanding scenarios while still providing a pleasant driving experience, with the potential to adapt to the ample spectrum of users' needs. In particular, the aim of this study is to reduce the conflicts between the driver's intention and the driving assist torque input, as well as to understand the driver-vehicle closed-loop interaction that occurs through the exchange of torques at the steering handwheel. For this purpose, the use of Haptic Shared Control is considered to be the appropriate strategy for semi-automated vehicles.

In line with these requirements, research concerning control strategies present Model Predictive Control as an attractive framework to implement the shared control objectives between the driver and the driving assist system. The MPC approach can compute the optimal control law online, making it possible to integrate the driver's real behaviour in the loop. As a result, dynamic allocation of the control authority is possible. All these elements are essential for minimising the user-assist conflict and the introduction of the driver model is best handled by MPC.

Finally, an important element to reduce the aforementioned driver-assist conflicts is the integration of a detailed driver model into the controller's logic, as well as a mindful selection of the most appropriate adaptive cost function for the MPC controller.

The contribution of this paper is to introduce a novel approach for the design of shared control strategies using an advanced driver model within the prediction model of the MPC controller. The following sections present an overview of the different elements employed, as well as the main results achieved. Section [2] establishes the steering-vehicle dynamics. Section [3] describes the driver model integrated within the MPC prediction model, and the results of the driving simulator experiments performed to validate its use can be found in Section [4]. Afterwards, in Section [5], an overview of the MPC strategy is presented. In Section [6], the different collaborative behaviours portrayed by the assist system are introduced, along with the results of its application in the presence of external disturbances. Lastly, the main conclusions and the recommendations for future work are outlined in Section [7] and Section [8], respectively.

2. Steering-Vehicle Model

2.1. Vehicle dynamics

In this section, the vehicle-steering dynamics model is presented. The vehicle dynamics are represented in Figure 2 based on the linear bicycle model. This simplified model can adequately capture the path tracking performance and vehicle handling characteristics in the range of lateral acceleration up to 4 m/s^2 for passenger cars. It assumes a constant longitudinal velocity, linear tyre dynamics, small angle approximations, and other assumptions.

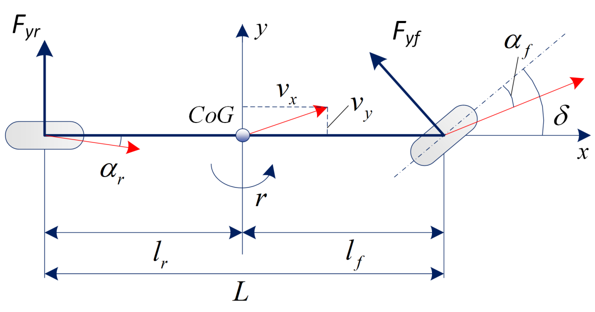

Figure 2. A linear bicycle model

The Newton-Euler equations of the linearised vehicle motion can be found in equations (1)–(2). The notation denotes the mass of the vehicle, m, and inertia with respect to the center of mass, I_{zz}. The vehicle parameters related to the front and rear distance from the center of gravity are l_f and l_r, respectively.

$$ma_y = F_{y,f} + F_{y,r} \tag{1}$$

$$I_{zz}\ddot{\psi} = l_f F_{y,f} - l_r F_{y,r} \tag{2}$$

Moreover, the states of the vehicle are lateral acceleration, a_y, longitudinal vehicle velocity, V_x, lateral vehicle velocity, V_y, yaw rate, r, and heading angle, ψ.

The front and rear lateral axle forces, $F_{y,f}$ and $F_{y,r}$, are assumed to have a linear relation with respect to the slip angles through the cornering stiffness per axle, and are calculated as:

$$F_{y,f} = -C_{\alpha_f,f} \cdot \alpha_f \tag{3}$$

$$F_{y,r} = -C_{\alpha_r,r} \cdot \alpha_r \tag{4}$$

Lastly, the front and rear axle slip angles, derived from the bicycle model, are:

$$\alpha_f = -\delta + \frac{V_y + l_f r}{V_x} \tag{5}$$

$$\alpha_r = \frac{V_y - l_r r}{V_x} \tag{6}$$

2.2. Steering system dynamics

In order to study the interaction between the driver and the vehicle at the steering handwheel interface, it is essential to model the steering dynamics.

In this section, the steering dynamics [4] are represented by two degrees of freedom, the steering wheel angle, θ_{sw}, and steering column angle, θ_c. In equations (7)–(8), the linear dynamics of the steering system are described. It can be seen how the interaction of the driver is already taken into account, through the introduction of the muscle angle of the arms, θ_a, which also interacts with the steering wheel. For readability, the difference of the angles at the steering column is defined as $\Delta\theta_{sc} = (\theta_{sw} - \theta_c)$, and the same notation can be derived for the derivatives with respect to time, $\Delta\dot{\theta_{sc}} = (\dot{\theta}_{sw} - \dot{\theta}_c)$.

$$(I_{sw} + I_{arms})\ddot{\theta}_{sw} = k_a(\theta_a - \theta_{sw}) - c_t\Delta\dot{\theta_{sc}} - k_t\Delta\theta_{sc} \tag{7}$$

$$I_c\ddot{\theta}_c + c_{sw}\dot{\theta}_c + k_{sw}\theta_c = c_t\Delta\dot{\theta_{sc}} + k_t\Delta\theta_{sc} - \frac{T_w}{G} + T_c \tag{8}$$

The inertia of the rack and the front wheels with respect to the pinion is represented by the term I_c, whereas the steering column stiffness and the torsion bar damping are defined by k_t and c_t, respectively. Lastly, the steering system also includes the damping and self-centering stiffness terms with respect to the steering wheel axle, c_{sw} and k_{sw}, respectively. Concerning other torques exchanged at the steering wheel, the model includes the self-aligning moment, T_w, and the torque input from the driving assist system, calculated through the MPC controller. The self-aligning moment is calculated based on the torque generated about the king-pin axes by the lateral axle force, as can be seen in equation (9), where the pneumatic trail is denoted by the parameter d.

$$T_w = dF_{y,f} \tag{9}$$

Finally, the steering gear ratio, G, transforms the steering angle column into the road wheel angle based on equation (10).

$$\delta = \frac{\theta_c}{G} \tag{10}$$

Moreover, the steering dynamics are rigidly coupled to the arms dynamics in contact with the steering handwheel. Thereby resulting in a total inertia that is the summation of the inertia of the arms, I_{arms}, and the inertia of the steering wheel, I_{sw}. Further details concerning the neuromuscular dynamics of the arms, coupled to the steering system, are described in equation (13) of Section [3.2].

3. Driver Model

The integration of a realistic driver model is central to the design of this collaborative shared control strategy. A better accuracy of the torque predictions can directly improve the collaborative behaviour of the proposed driving assist system. For this reason, an extensive driver model is desirable, with each of its elements serving a unique purpose.

The driver model, as presented in Figure 3, was developed by Niu and Cole [4], building upon earlier work by Nash and Cole [5]. The model is implemented in Simulink and adapted to enhance its validity in real-life scenarios and real-time capability. It aims to represent the significant cognitive and physiological mechanisms of the human driver, and includes an internal model, neuromuscular dynamics, sensory dynamics, sensorimotor noise, state estimation, and cognitive and reflex control. In particular, the inclusion of neuromuscular dynamics makes the model appropriate for the development of a new driving assist system with torque feedback.

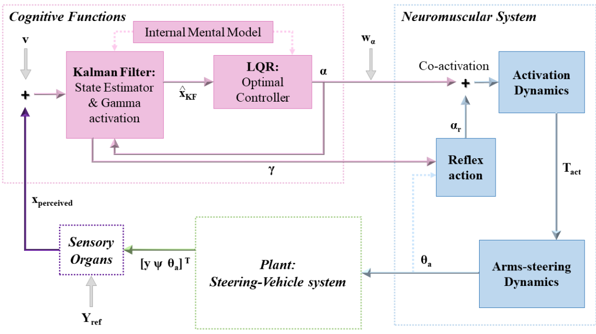

Figure 3. Schematic representation of the driver model

3.1. Cognitive behaviour

The cognitive model is used to predict the driver's steering intentions. For the cognitive control, a predictive approach based on a Linear-Quadratic Regulator (LQR) is chosen. Moreover, the states of the system are estimated with a Kalman Filter to reduce the effect of measurement noise of the sensory organs and process noise of the brain. This combination of approaches is also known as the Linear-Quadratic-Gaussian and it requires an accurate internal mental representation of the environment in order to achieve optimal state estimation. In this regard, a forward internal mental model is assumed to be acquired a priori by the driver.

The cost function of the LQR, which calculates the expected driver torque input, is derived based on previous work [5, 6] and can be seen in equations (11)–(12). This function minimises the lateral deviation of the vehicle with respect to the upcoming reference trajectory of the road with a certain preview time, T_{prev}.

$$J_{LQR} = \sum_{0}^{\infty} \left[\begin{bmatrix} x_{KF} & y_p \end{bmatrix} C^T Q C \begin{bmatrix} x_{KF} \\ y_p \end{bmatrix} \right] + \alpha R \alpha \tag{11}$$

where C is a matrix that selects the states on the lateral position, heading angle, and the road preview points. An illustration of the upcoming road trajectory can be seen in Figure 4. Finally, the expected driver torque input, α, is calculated as:

$$\alpha = -K_{LQR} \cdot \begin{bmatrix} x_{KF} \\ y_p \end{bmatrix} \tag{12}$$

where K_{LQR} is the Kalman Filter gain, x_{KF} is a vector with the estimated states, and y_p a vector containing the upcoming preview road points of length $N_p = T_{prev}/T_{s,DM}$. The rest of the cost function parameters can be found in Table 1.

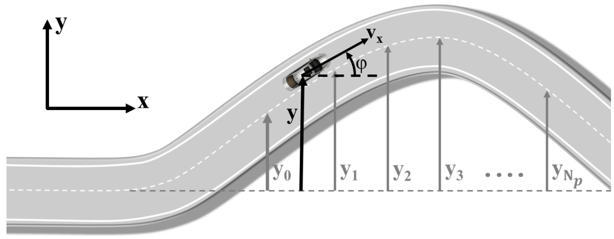

Figure 4. Schematic representation of the road preview points

3.2. Neuromuscular dynamics

The muscle dynamics are described by a linearised Hill-muscle model [7]. The elasticity of the tendons is represented by the stiffness term, k_a. The contractile element, on the other hand, is described by the damping term, c_a, and the neural activation torque, T_{act}, which is a function of the desired driver torque and the reflex action.

The neuromuscular dynamics of the driver are thus composed of the reflex action of the muscle spindles, a linearised Hill-muscle model including the activation dynamics of the muscles, and the muscle dynamics of the arms, which are interacting with the steering system. These elements are necessary for the modelling of the co-activation mechanism of the muscles.

$$T_{act} = c_a \dot{\theta}_a + k_a(\theta_a - \theta_{sw}) \tag{13}$$

The NMS dynamics are modelled as defined in equations (14)–(15) and shown in with Figure 3. The activation dynamics, denoted by H_{act}, are subject to a lag time constant of the motor neurons excitation, τ_1, and a lumped neuro-muscular transduction delay, τ_2. The latter time constant represents the muscle activation and deactivation lag.

$$H_{act} = \frac{1}{(\tau_1 \cdot s + 1) \cdot (\tau_2 \cdot s + 1)} \tag{14}$$

The reflex loop, an essential element of the co-activation mechanism, is subject to a delay time constant, τ_r, and a gain factor, k_r. The expected muscle angle, γ, is calculated based on the internal mental model of the driver and the estimated states by the Kalman Filter.

$$\alpha_r = \frac{k_r}{\tau_r \cdot s + 1} \cdot (\gamma - \theta_a) \tag{15}$$

3.3. Sensory organs

The sensory organs modelled are the visual perception organs and the proprioceptors with the purpose of representing the human limitations in the perception. The modelling of the vestibular organs is considered out of the scope of this research because the validation is carried out in a fixed-base driving simulator. The states perceived by the driver are the vehicle lateral deviation with respect to the desired path, e_y, the heading angle, ψ, and the muscle angle of the driver, θ_a. These states are subject to a visual delay, τ_{visual}, and a muscle sensory delay, τ_{muscle}.

The feedback sensed by these organs is then sent to the Central Nervous System, subject to measurement noise. These noisy signals are used to estimate the states of the plant with the Kalman Filter model, based on the assumption that the driver has a good internal mental representation of the vehicle and their own neuromuscular dynamics. The parameters that the driver model uses can be seen in Table 1.

Parameter	Value
T_{prev}	1.4 s
I_{arms}	0.0718 kg m^2
k_a	30 Nmrad
c_a	3 Nms/rad
k_r	21 Nm/rad
τ_r	0.04 s
τ_1	0.03 s
τ_2	0.02 s
τ_{visual}	0.24 s
τ_{muscle}	0.19 s
Q	$\mathrm{diag}([3 \cdot 10^3, 1 \cdot 10^2])$
R	1

Table 1. Driver model parameters

4. Driver Model validation

4.1. High-fidelity offline simulations

As a first step in the validation process of the driver model, the predictions of the torque are simulated offline in CarMaker, an advanced software for model-based design. Here, the driver model is compared to the CarMaker virtual driver. To represent the plant, nonlinear vehicle dynamics and a TME-TMC nonlinear steering system are used [8] with a Toyota production vehicle parametrisation. This allows for a high-fidelity simulation of real-world scenarios.

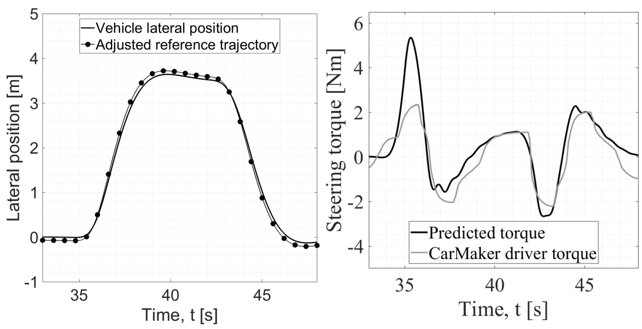

Figure 5. Driver model prediction based on CarMaker virtual driver and high-fidelity steering-vehicle plant

The driver model is initially validated against a rather robotic human behaviour. In Figure 5, it can be seen that the driver model predictions are accurate both in magnitude and in shape, with the exception of the initial peak of the manoeuvre. This initial mismatch is due to the impossibility to introduce constraints in the driver model when using an LQR cognitive controller. This could be resolved by introducing an MPC controller instead, which would have the additional capability of modelling a nonlinear driver. However, the introduction of two MPC controllers, related to driver and driving assist system, can lead to instabilities due to competing objectives as well as rapidly increase the computational requirements.

The model was also tested with simpler steering models, and with the consequent reduction of steering friction nonlinearities. As expected, the precision of the torque predictions is higher for these simplified models, namely a Pfeffer steering and a kinematic ratio steering model [9], both based on the parametrisation of the aforementioned vehicle. For these validations, the internal mental model of the driver was adjusted mainly by introducing a linear assist torque gain depending on the steering system and selecting different preview times for each driver. The nonlinear CarMaker vehicle provided the signals fed to the driver sensory organs.

4.2. Pilot experiments with driving simulator

A pilot study was performed at Toyota Motor Europe, using the fixed-base driving simulator of Figure 6. Three different drivers, listed in Table 2 and Figures 7–9 in ascending order of driving experience, participated in the experiment to further validate the accuracy of the driver model. In order to test the driver model performance for different driving styles and behaviour, there is significant variability in the drivers' experience. Namely, the participants are a novice driver, a driver with 12-years of experience, and a driver with over 20 years of driving experience and expert knowledge in driving simulators.

Figure 6. Driving simulator at Toyota Motor Europe, Belgium

The driver model fits all three drivers well, as objectively shown in Table 2, which further reassures the capabilities of the model to capture driver inter- and intra-variability.

The driver model parametrisation is found to match slightly better the novice and intermediate driver, which could be because the linear internal mental model captures better users with limited driving experience, whereas the mismatch between the linear model and the knowledge of expert drivers is more significant.

Driver	RMSE [Nm]	% Accuracy
Driver 1: Novice	0.7344	89.96
Driver 2: Intermediate	0.6232	90.96
Driver 3: Expert	0.7355	87.30

Table 2. Torque prediction accuracy of the driver model

The sensitivity of the different driver model parameters was preliminary studied in order to obtain the best possible fit. From this analysis, the driver preview time of the road is highlighted. This can be linked to the different cognitive strategies that each driver has in order to follow the road path. The novice driver tends to have a shorter preview time, as well as a noisier torque input. On the other hand, for driver three, even though the perception of the ideal road trajectory was not correct, the torque input is smooth and the muscle spindles are calculated to be barely activated. This can also be associated to the fact that the muscle spindles are active both when rejecting disturbances and when they have a wrong internal mental model.

Another relevant factor is that using a human-like road preview is key for the model to give an accurate torque prediction. This reference trajectory was changed from the ideal invariant road centerline to a lateral position of the vehicle using road sensors in CarMaker. A good fitting of the prediction was obtained for the three drivers under the assumption that the vehicle position corresponds to the desired vehicle trajectory. This assumption would not be valid in the presence of, for instance, external disturbances, in which case the muscle spindles torque would be activated. This element is further analysed in Section [6].

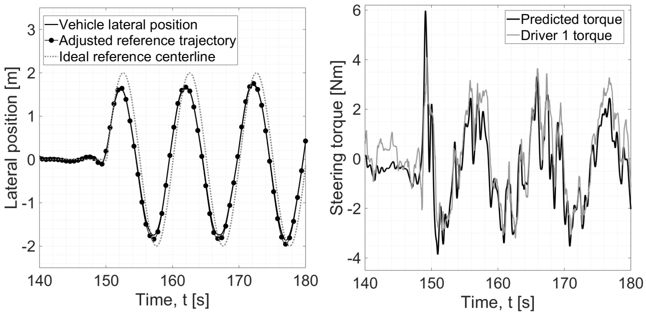

Figure 7. Driver model predictions based on driver 1, novice

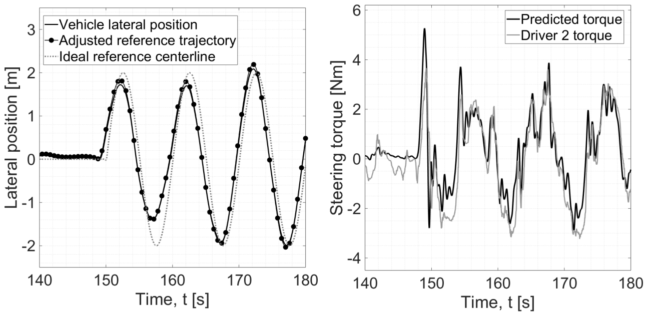

Figure 8. Driver model predictions based on driver 2, intermediate expertise

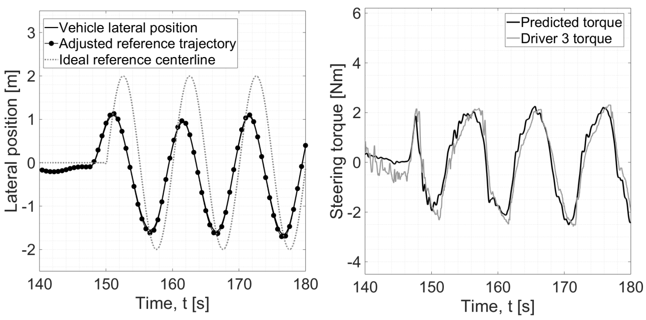

Figure 9. Driver model predictions based on driver 3, expert level

5. MPC framework

Model Predictive Control is an approach of which the main objective is to calculate the trajectory of a future control input variable, $u(k)$, in order to optimise the future behaviour of the plant being controlled. The optimisation is performed within a finite-time window based on the plant states' information at the start of the time window $x(k)$ [10]. The time window is composed of a number of time steps, called the prediction horizon, N_p. The control horizon of the control input sequence is denoted by N_c. This optimal control problem is iteratively performed to minimise a cost function subject to constraints.

5.1. General structure of the MPC

MPC-based systems are particularly suitable for the steering task due to the need for accurate precision in the path tracking task performance. Moreover, it is possible to introduce input and state constraints to guarantee safety and comfort. This makes the MPC particularly advantageous for the shared driving task, where smooth control inputs can foster a more pleasant interaction with the driver.

The general representation of the prediction model can be seen in equation (16).

$$\mathbf{x}(k+1) = f(\mathbf{x}(k), u(k)), \quad \text{with} \quad \mathbf{x}(0) = \mathbf{x}_0 \tag{16}$$

where $\mathbf{x}$ is the vector of the system states, with $\mathbf{x} \in \mathbb{R}^{N_x}$. The variable $\mathbf{x}_0$ denotes the initial states, and f is the function that describes the prediction model dynamic equations, which can be linear or nonlinear. Lastly, the variable $u \in \mathbb{R}^{N_u}$ is the control input. For the scope of this research, the dimension of the control input, N_u is equal to one and it represents the torque rate input that the driving assist system exerts on the steering system.

The state solution is

$$\mathbf{x}(k) = \phi(k; \mathbf{x}_0, \mathbf{u}_k) \tag{17}$$

And the control input sequence is

$$\mathbf{u}_k := (u(0), u(1), ..., u(k-1)) \tag{18}$$

5.2. Cost function and system constraints

In particular for this research, the purpose of the driving assist system is to allow the controller to provide a more intuitive torque guidance to the driver through the steering interface, also known as haptic guidance. Therefore, the cost function of the MPC-based steering controller improves path tracking performance, ensures driving comfort, and reduces the conflicts between the driver and driving assist system.

$$\begin{aligned} J(\mathbf{x}, u) = &\sum_{k=0}^{N_p-1} \|(h_x(\mathbf{x}_k) - \mathbf{y}_{r,k})\|^2_{\mathbf{W}_x} + \\ &+ \sum_{k=0}^{N_c-1} \|h_u(u_k)\|^2_{W_u} + \|h_N(\mathbf{x}_{N_p}) - \mathbf{y}_{r,N_p}\|^2_{\mathbf{W}_{x_N}} \end{aligned} \tag{19}$$

where $\mathbf{W}_x$, $\mathbf{W}_{x_N} \geq 0$, are the weighting matrices of the stage and terminal cost for the states, with appropriate matrix dimensions. The parameter $W_u > 0$ corresponds to the stage cost for the input. These matrices can be used as tuning parameters that influence tracking performance. The time-varying state reference vector is denoted $\mathbf{y}_r$.

First of all, the tracking performance objective is implemented to minimise the lateral deviation with respect to the reference path, subject to a look-ahead distance factor depending on the vehicle velocity and the heading angle, ψ. The relation between the costs for the MPC system can be seen in Table 3.

Moreover, driving comfort can be enhance by applying a weight parameter to the lateral velocity, V_y, and the yaw rate, r. Additional costs on the driver's effort or discomfort indicators can also be added to, for example, reduce the activation of the muscle spindles' torque or the total driver steering torque, as described in Table 3.

Furthermore, the MPC model is subject to constraints that represent the vehicle handling limits. These constraints are imposed on the lateral velocity and the yaw rate. Moreover, in order to guarantee a smooth assist guidance, constraints on the steering wheel angle, θ_{sw}, and assist torque input, T_c, as well as their respective rates are also introduced. The allowed maximum absolute value of the constrained states can be found in Table 3. Hard constraints on the driver model states are avoided for stability and, instead, weights to penalise their magnitude are included.

Variable	Value
$T_{s,cont}$	$1 \cdot 10^{-2}$ s
$T_{s,DM}$	$2 \cdot 10^{-2}$ s
$T_{s,sim}$	$1 \cdot 10^{-3}$ s
N_p	40
N_c	40
W_y	$1 \cdot 10^6$
W_{y_N}	$1 \cdot 10^2$
W_ψ	$V_x \cdot W_y$
W_{T_c}	600
$W_{T_{input}}$	40
W_{V_y}	$1 \cdot 10^2$
W_r	$1 \cdot 10^2$
$W_{spindles}$	$1 \cdot 10^2$
W_{driver}	$6 \cdot 10^2$
$V_{y,max}$	4 m/s
r_{max}	50 deg/s
$\theta_{sw,max}$	360 deg
$\dot{\theta}_{sw,max}$	800 deg
$T_{c,max}$	10 Nm
$\dot{T}_{c,max}$	20 Nm/s

Table 3. MPC Settings and weights

The different sampling times and prediction horizons, as specified in Table 3, are appropriately chosen to ensure that the MPC model can be run in real-time without compromising its performance, prediction capabilities, and stability. The nonlinear plant operates at a higher sampling frequency, $T_{s,sim}$, whereas the linear driver model can be accurately run at a lower sampling frequency, $T_{s,DM}$, which reduces the computational requirements. For the MPC, the maximum sampling frequency that allows the model to compute the optimal control input in real-time, $T_{s,cont}$, is selected to ensure stability and a long enough prediction time, $T_{s,cont} \cdot N_p$, which has a direct impact on its performance.

5.3. Adaptive MPC for conflict minimisation

The software used for the implementation of this MPC system is the ACADO Toolbox [11]. This is an open-source software environment for automatic control and dynamic optimisation written in C++. It is suitable for the study of closed-loop MPC applications in real-time and its use is supported in MATLAB [12]. Moreover, it has the additional advantage to implement adaptive weights of the cost function. These time-varying weights are based both on the difference between the applied driver torque and the driving assist system torque to minimise torque conflicts, and on the MPC controller torque and its rate.

The cost function is designed to be adaptive in order to dynamically share the control authority depending on the driver input and promote smooth control inputs. The adaptive behaviour is applied to the cost on the MPC assist torque and its rate with a factor of 1.5. In other words, when certain criteria are met, the cost on the state and input increases from their baseline to up to 1.5 times more in a parabola-shape. An example of this behaviour is displayed in Figure 10 for one of the weights. Such criteria are, for instance, when the assist torque rate exceeds a threshold or when the driver torque´s direction is opposite to that of the driving assist system torque. The MPC settings for the controller are defined in Table 3.

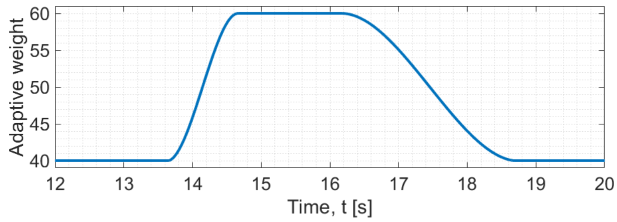

Figure 10. Adaptive behaviour of the cost on the MPC input

The values include the sampling time of the MPC, and the sampling times for the driver model and vehicle-steering system simulation, respectively. Finally, the prediction horizon, N_p, and control horizon, N_c are set to the same value. The different possibilities for the ACADO Toolkit settings can be found in further detail in [13]. In this research, a Quadratic-Programming solver is used, with a Gauss-Newton Hessian approximation and a multiple shooting discretisation algorithm. The integration type used is an implicit Runge-Kutta integrator with a maximum of $3N_p$ integration steps.

6. MPC application

The MPC assist system is assessed for different scenarios, such as a lane change subject to an external force disturbance and a sine test. Initially, the lane change was assessed in a bicycle model plant. To further validate its applicability, the sine test was performed in a high-fidelity environment using CarMaker. The nonlinear vehicle dynamics and steering system parametrisation are the same as described in Section [4].

6.1. Lane change scenario

The MPC controller is investigated for a lane change manoeuvre to test the robustness of the controller:

- Case 1. Baseline scenario. Manual driving.
- Case 2. Manual driving with a disturbance of 800 N at 12 s.
- Case 3. Shared driving.
- Case 4. Shared driving with a disturbance of 800 N at 12 s.

The controller adapts to the different situations, improving the path tracking performance while minimising the muscle spindle torque and the overall driver effort. In Figure 11, it can be seen that the RMSE is lower for the shared case ($y_{rms} = 0.054\ m$) compared to manual driving ($y_{rms} = 0.055\ m$). The same applies for the case with a disturbance with shared control ($y_{rms} = 0.073\ m$) and manual driving ($y_{rms} = 0.076\ m$). Moreover, in cases 2 and 4, the MPC helps the driver to reject the disturbance, thus, minimising the reflex action by $25.27\ \%$.

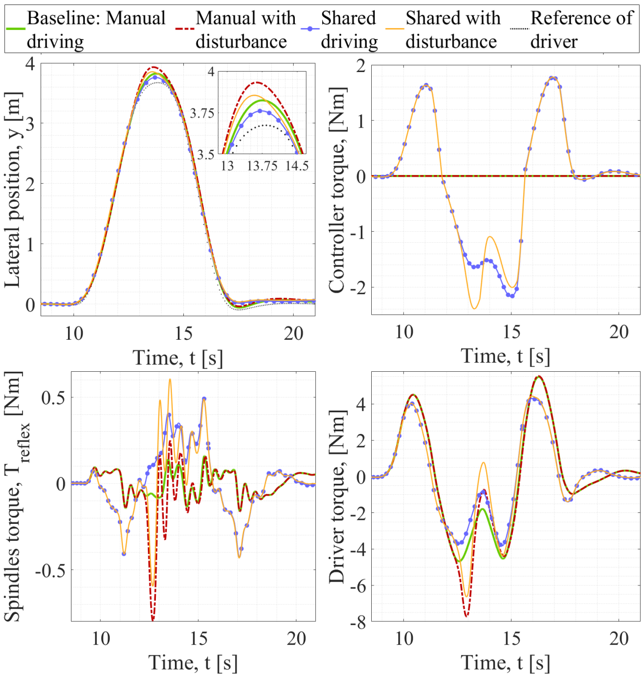

Figure 11. Lane change results of the MPC and driver model

6.2. Sine test manoeuvre

The controller can be tuned to portray different behaviours and the competing objectives of driver comfort and path tracking performance are investigated in Figures 12–13.

A strong torque guidance of the assist system is presented in Figure 12. The optimisation algorithm makes use of the prediction of the driver behaviour to provide a human-like guidance and release the driver of most of the steering effort, which results in a more accurate path tracking performance. This controller could potentially be helpful to more inexperienced drivers or compliant users.

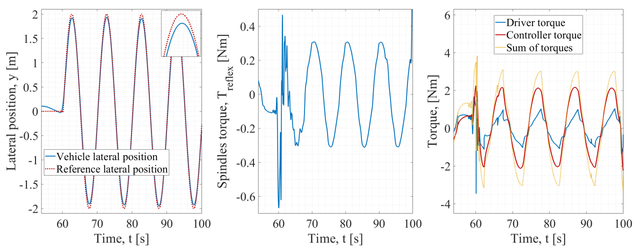

Figure 12. Mode 1: Performance optimisation

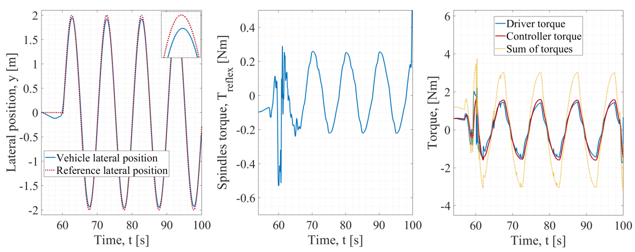

Figure 13. Mode 2: Conflict minimisation

In Figure 13, on the other hand, the aim is to reduce the conflicts with the driver before they arise. The controller exploits the adaptive nature of the MPC cost function and it uses the driver model to enhance driver comfort. Here, reduction of conflict is more relevant than maximum performance, although the latter is also improved with respect to manual driving. In this case, the assist system guidance is less strong, allowing the driver to easily overrule the system if desired. This behaviour is achieved by modifying the settings of this second controller to have a higher cost on the reflex torque of the driver, which is related to driver discomfort and the rejection of disturbances. This makes the MPC to be less intrusive than in the previous case.

In short, the collaborative behaviour of the MPC assist system allows for a better balance between performance and comfort due to the introduction of an advanced driver model within the prediction model. The MPC computes the optimisation depending on the cost function parameters without compromising driver comfort and its behaviour is enhanced through adaptive costs. Moreover, even though the behaviour of the CarMaker virtual driver is rather constant, the possibility to customise both the driver parametrisation and the MPC assist system makes it possible to tackle the individual needs of each user.

7. Conclusion

This study tackles the need to blend driver modelling and driving assist systems in a shared control strategy. The use of a linear yet extensive and complex driver model perfectly matches the requirements of the controller. In other words, an accurate prediction of the driver in the loop is integrated without compromising the real-time capabilities of the controller.

The results show that modelling the driver behaviour is a key feature in order to develop collaborative assist systems that can minimise conflicts with the driver. Driver models can represent the human behaviour and predict the driver's intentions while driving. Therefore, accurate driver models can minimise the need of testing in real vehicles when developing user-accepted AD systems. Besides, they can also be used to predict subjective assessments of the steering feel. In particular, within the Haptic Shared Control framework, driver models can facilitate the investigation of how the driver reacts in the presence of the haptic feedback guidance.

On the other hand, the complexity, adaptability, and unpredictability of the human behaviour makes the use of driver models challenging. Moreover, how to introduce the driver within the loop and how to model the human-machine interaction is often unclear. However, with the increasing research on driver models, the added complexity is worth the potential benefits of taking into account the driver-in-the-loop dynamics, as demonstrated in this work.

On the controller's side, the designed Model Predictive Controller fulfils the requirements needed for real-time implementation of the shared steering task, as well as being able to handle constraints on the system and the nonlinearities of the plant. The constraints are essential to consider the driver-vehicle limitations, as well as guaranteeing smooth control inputs for driver comfort. Finally, the novel cost function allows dynamic allocation of the control authority between driver and driving assist system, which fosters symbiotic driving and reduces potential steering conflicts.

8. Future work

Due to the vast amount of behaviours that can be portrayed by the MPC controller, an intensive fixed-base driving simulator study is required to further assess the subjective acceptance of the different modes of collaboration. This also enables us to test the controller with human dispersion and more variability.

The proposed control strategy should be able to predict the human behaviour and, at the same time, be sufficiently smooth and intuitive so that the driver can perceive it as expected and cooperative. For this purpose, the adaptability of the driver model will be further investigated. Current work focuses on a benchmark comparison between an industry standard Toyota Lane Trace Assist and the proposed MPC driving assist system.

References

[1] Todd Alexander Litman. "Autonomous Vehicle Implementation Predictions: Implications for Transport Planning". In: *Transportation Research Board 94th Annual Meeting* (2015).

[2] "SAE On-Road Automated Vehicle Standards Committee. Taxonomy and definitions for terms related to driving automation systems for on-road motor vehicles". In: *SAE International: Warrendale, PA, USA* (2018).

[3] D. A. Abbink and M. Mulder. "Neuromuscular Analysis as a Guideline in designing Shared Control". In: *Advances in Haptics*. (2010).

[4] *Driver-Vehicle Dynamics Research Group*. Cambridge University Engineering Department. URL: www . vehicledynamics.org (visited on 01/16/2020).

[5] C. J. Nash and D. J. Cole. "Identification and validation of a driver steering control model incorporating human sensory dynamics". In: *Vehicle System Dynamics* 58.4 (2020), pp. 495–517.

[6] R.S. Sharp and V. Valtetsiotis. "Optimal preview car steering control". In: 35 (Jan. 2001), pp. 101–117.

[7] J.M. Winters and L. Stark. "Muscle models: what is gained and what is lost by varying model complexity". In: *Biological Cybernetics* 55 (6) (1987), pp. 403–420.

[8] M. Damian, B. Shyrokau, A. Ocariz, and X. Carrera Akutain. "Torque control for more realistic hand-wheel haptics in a driving simulator". In: *Driving Simulation Conference Europe, Strasbourg, France*. 2019.

[9] *Reference Manual Version 8.0*. http://www.ipg-automotive.com. IPG-Automotive Group. 2018.

[10] Liuping Wang. *Model Predictive Control System Design and Implementation Using MATLAB* ®. Springer, London, 2009.

[11] B. Houska, H.J. Ferreau, and M. Diehl. "ACADO toolkit—An open-source framework for automatic control and dynamic optimization". In: *Optimal Control Applications and Methods* 32.3 (2011), pp. 298–312.

[12] D. Ariens, B. Houska, and H.J. Ferreau. *ACADO for Matlab User's Manual*. http://www.acadotoolkit.org. 2010–2011.

[13] B. Houska, H.J. Ferreau, M. Vukov, and R. Quirynen. *ACADO Toolkit User's Manual*. http://www.acadotoolkit.org. 2009–2013.

Bibliography

[1] Driver-vehicle dynamics research group. URL www.vehicledynamics.org. Cambridge University Engineering Department.

[2] Abbink, D. A. and Mulder, M. *Neuromuscular Analysis as a Guideline in designing Shared Control*, chapter 27. Advances in Haptics, IntechOpen, 2010. Published: April 1st 2010.

[3] Abbink, D. A. Neuromuscular analysis of haptic gas pedal feedback during car following. Doctoral dissertation, Delft University of Technology, Mekelweg 2, 2628 CD Delft, the Netherlands, 2006.

[4] Abbink, D. A., Mulder, M., and Boer, E. R. Haptic shared control: smoothly shifting control authority? *Cognition, Technology & Work*, 14:19–28, 2012.

[5] Abbink, D. A., Carlson, T., , Mulder, M., de Winter, J. C. F., Aminravan, F., Gibo, T. L., and Boer, E. R. A topology of shared control systems — finding common ground in diversity. *IEEE Transactions on human-machine systems*, 48(5):509–525, 2018.

[6] Ackermann, U. *PDQ physiology*. Hamilton : BC Decker Inc., 2002.

[7] Ambrósio, J. A. C. and Kecskeméthy, A. *Multibody Dynamics of Biomechanical Models for Human Motion via Optimization*, volume 4, pages 245–272. García Orden J.C., Goicolea J.M., Cuadrado J. (ed.) Multibody Dynamics. Computational Methods in Applied Sciences. Springer, 2007.

[8] Ariens, D., Houska, B., and Ferreau, H. ACADO for matlab user's manual. http://www.acadotoolkit.org, 2010–2011.

[9] Bainbridge, L. Ironies of automation. *Automatica*, 19(6):775–779, 1983.

[10] Bartels, A., Rohlfs, M., Hamel, S., Saust, F., and Klauske, L. *Lateral Guidance Assistance*, pages 1207–1233. Springer, Cham, 2016.

[11] Berberian, B., Bertille, Sahaï, S. A., and Gouraud, J. The out-of-the-loop brain: A neuroergonomic approach of the human automation interaction. *Annual Reviews in Control*, 44:303–315, 2017.

[12] Borrelli, F., Falcone, P., Keviczky, T., Asgari, J., and Hrovat, D. MPC-based approach to active steering for autonomous vehicle systems. *International Journal of Vehicle Autonomous Systems*, 3(2-4):265–265, 2005.

[13] Bujarbaruah, M., Zhang, X., Tseng, E., and Borrelli, F. Adaptive MPC for autonomous lane keeping. *14th International Symposium on Advanced Vehicle Control (AVEC)*, 2018.

[14] Burdet, E., Osu, R., Franklin, D., Milner, T., and Kawato, M. The central nervous system stabilizes unstable dynamics by learning optimal impedance. *Nature*, 414:446–449, 2001.

[15] Campbell, J. L., Brown, J., Graving, J. S., Richard, C. M., Lichty, M. G., Sanquist, T., and Morgan, J. L. Human factors design guidance for driver-vehicle interfaces. *National Highway Traffic Safety Administration*, 2016.

[16] Carrera Akutain, X., Ono, K., Ocariz, A., Tsitouridis, G., and Iwamatsu, S. Development of a steering characteristics optimization process and its implementation on vehicle projects. *Proceedings of the 9th International Munich Chassis Symposium*, pages 573–596, 2018.

[17] Casner, S. M., Geven, R. W., Recker, M. P., and Schooler, J. W. The retention of manual flying skills in the automated cockpit. *Human Factors*, 56(8):1506–1516, 2014.

[18] Cole, D. J. Influence of steering torque feedback and neuromuscular dynamics on driver vehicle response to lateral force disturbance. Technical report, Department of Engineering, University of Cambridge, 2010.

[19] Cole, D. J., Pick, A., and Odhams, A. Predictive and linear quadratic methods for potential application to modelling driver steering control. *Vehicle System Dynamics*, 44(3):259–284, 2006.

[20] Damian, M., Shyrokau, B., Ocariz, A., and Akutain, X. C. Torque control for more realistic hand-wheel haptics in a driving simulator. In *Driving Simulation Conference Europe, Strasbourg, France*, 2019.

[21] de Vlugt, E., van der Helm, F. C., Schouten, A., and G., B. G. Analysis of the reflexive feedback control loop during posture maintenance. *Biological Cybernetics*, 84 (2):133–141, 2001.

[22] Domahidi, A. Forces pro: Fast optimization for real-time control on embedded systems. https://www.embotech.com/FORCES-Pro, 2012.

[23] Droogendijk, C. A new neuromuscular driver model for steering system development. Master thesis, Delft University of Technology, Mekelweg 2, 2628 CD Delft, the Netherlands, 2010.

[24] Endsley, M. R. and Kiris, E. O. The out-of-the-loop performance problem and level of control in automation. *Human Factors: The Journal of the Human Factors and Ergonomics Society*, 37(2):381–394, 1995.

[25] Ercan, Z., Carvalho, A., Gokasan, M., and Borrelli, F. Modeling, identification, and predictive control of a driver steering assistance system. *IEEE Transactions on human-machine systems*, 47(5):1–11, 2017.

[26] Ercan, Z., Carvalho, A., Tseng, H. E., and Borrelli, F. A predictive control framework for torque-based steering assistance to improve safety in highway driving. *Vehicle System Dynamics*, 56(5):810–831, 2018.

[27] Falcone, P., Borrelli, F., Asgari, J., Tseng, H., and Hrovat, D. Predictive active steering control for autonomous vehicle systems. *IEEE Transactions on Control Systems Technology*, 15(3):566–580, 2007.

[28] Farah, H., Bhusari, S., van Gent, P., Mullakkal-Babu, F., Morsink, P., Happee, R., and van Arem, B. An empirical analysis to assess the operational design domain of lane keeping system equipped vehicles combining objective and subjective risk measures. *IEEE Transactions on Intelligent Transportation Systems*, 2020.

[29] Ferreau, H. J., Almér, S., Verschueren, R., Diehl, M., Frick, D., Domahidi, A., Jerez, J. L., Stathopoulos, G., and Jones, C. Embedded optimization methods for industrial automatic control. *IFAC World Congress*, 50:13194 – 13209, 2017.

[30] Ferreau, H., Kirches, C., Potschka, A., Bock, H., and Diehl, M. qpOASES: A parametric active-set algorithm for quadratic programming. *Mathematical Programming Computation*, 6(4):327–363, 2014.

[31] Flemisch, F., Kelsch, J., Loper, C., Schieben, A., and Schindler, J. Automation spectrum, inner/outer compatibility and other potentially useful human factors concepts for assistance and automation. *Human Factors for assistance and automation*, pages 1–16, 2008.

[32] Franklin, D., Osu, R., Burdet, E., Kawato, M., and Milner, T. Adaptation to stable and unstable dynamics achieved by combined impedance control and inverse dynamics model. *Journal of Neurophysiology*, 90(5):3270–3282, 2003.

[33] Frasch, J. V. qpDUNES, a dual newton strategy for convex quadratic programming. http://mathopt.de/qpDUNES, 2013.

[34] Funke, J., Brown, M., Erlien, S., and Gerdes, J. Collision avoidance and stabilization for autonomous vehicles in emergency scenarios. *IEEE Transactions on Control Systems Technology*, 25(4):1204–1216, 2017.

[35] Goodrich, M. and Boer, E. Model-based human-centered task automation: A case study in acc system design. *IEEE Transactions on Systems, Man, and Cybernetics - Part A: Systems and Humans*, 33(3):325–336, 2003.

[36] Gray, A., Gao, Y., Hedrick, J., Borrelli, F., and Ali, M. A unified approach to threat assessment and control for automotive active safety. *IEEE Transactions on Intelligent Transportation Systems*, 14(3):1490–1499, 2013.

[37] Guo, C., Sentouh, C., Popieul, J.-C., and Haué, J.-B. MPC-based shared steering control for automated driving systems. *IEEE International Conference on Systems, Man, and Cybernetics (SMC)*, 2017.

[38] Guo, C., Sentouh, C., Haué, J.-B., and Popieul, J.-C. Driver–vehicle cooperation: A hierarchical cooperative control architecture for automated driving systems. *Cognition, Technology & Work*, 21(4):657–670, 2019.

[39] Guo, K. and Guan, H. Modelling of driver/vehicle directional control system. *Vehicle System Dynamics*, 22(3-4):141–184, 1993.

[40] Hagbarth, K. Microneurography and applications to issues of motor control: Fifth annual stuart reiner memorial lecture. *Muscle & Nerve*, 16 (7):693–705, 1993.

[41] Haruno, M., Wolpert, D. M., and Kawato, M. Mosaic model for sensorimotor learning and control. *Neural Computation*, 13:2201–2220, 2001.

[42] Hatze, H. A myocybernetic control model of skeletal muscle. *Biological Cybernetics*, 25(2):103–119, 1977.

[43] He, J., Maltenfort, M. G., Wang, Q., and Hamm, T. M. Learning from biological systems: modelling neural control. *IEEE Control Systems Magazine*, pages 55–69, 2001.

[44] Horiuchi, S. and Yuhara, N. An analytical approach to the prediction of handling qualities of vehicles with advanced steering control system using multi-input driver model. *Journal of Dynamic Systems, Measurement, and Control*, 122(3):490–497, 2000.

[45] Hosman, R. J. and Abbink, D. A. The neuromuscular system. Toronto, Ontario, Canada, 2010. AIAA Modeling and Simulation Technologies Conference.

[46] Hoult, W. A neuromuscular model for simulating driver steering torque. Doctoral dissertation, Cambridge University Engineering Department, Queens' College, 2008.

[47] Hoult, W. and Cole, D. J. A neuromuscular model featuring co-activation for use in driver simulation. *Vehicle System Dynamics*, 46(sup1):175–189, 2008.

[48] Houska, B., Ferreau, H., Vukov, M., and Quirynen, R. ACADO Toolkit User's Manual. http://www.acadotoolkit.org, 2009–2013.

[49] Houska, B., Ferreau, H., and Diehl, M. ACADO toolkit—An open-source framework for automatic control and dynamic optimization. *Optimal Control Applications and Methods*, 32(3):298–312, 2011.

[50] Iguchi, M. A study of manual control. *Journal of mechanic Society of Japan*, 62(481), 1959.

[51] Inagaki, T. Adaptive automation: Sharing and trading of control. *Handbook of cognitive task design*, page 147–169, 2003.

[52] IPG. Reference manual version 8.0. http://www.ipg-automotive.com, 2018. IPG-Automotive Group.

[53] Jacobs, R., Jordan, M., and Barto, A. Task decomposition through competition in a modular connectionist architecture: The what and where vision tasks. *Cognitive Science*, 15(2): 219–250, 1991.

[54] Ji, X., Yang, K., Na, X., Lv, C., and Liu, Y. Shared steering torque control for lane change assistance: A stochastic game-theoretic approach. *IEEE Transactions on Industrial Electronics*, 66:3093–3105, 2018.

[55] Jordan, M. and Jacobs, R. Hierarchies of adaptive experts. *Advances in neural information processing systems*, 4:985–993, 1992.

[56] Kageyama, I., Arai, A., and Nomura, T. An analysis of driver's control algorithm using neural network modeling. *Vehicle System Dynamics*, 33:sup1:122–130, 1999.

[57] Kandel, E. R., Schwartz, J. H., Jessell, T. M., Siegelbaum, S. A., and Hudspeth, A. J. *Principles of Neural Science*. The McGraw-Hill Companies, Inc., 2013.

[58] Katzourakis, D. Driver steering support interfaces near the vehicle's handling limits. Doctoral dissertation, Delft University of Technology, Mekelweg 2, 2628 CD Delft, the Netherlands, 2012.

[59] Keen, S. D. and Cole, D. J. Avec '06 steering control using model predictive control and multiple internal models, 2006.

[60] Kim, E., Kim, J., and Sunwoo, M. Model predictive control strategy for smooth path tracking of autonomous vehicles with steering actuator dynamics. *International Journal of Automotive Technology*, 15(7):1155−1164, 2014.

[61] Kim, N. and Cole, D. J. A model of driver steering control incorporating the driver's sensing of steering torque. *Vehicle System Dynamics, International Journal of Vehicle Mechanics and Mobility*, 49(10):1575–1596, 2011.

[62] Knierim, J. Chapter 1: Motor units and muscle receptors. *McGovern Medical School at UTHealth. Department of Neurobiology and Anatomy*. URL https://nba.uth.tmc.edu/neuroscience/m/s3/chapter01.html. [Online; accessed January 7, 2020].

[63] Kolekar, S. A human-like steering model based on sensorimotor control theories. Master thesis, Delft University of Technology, Mekelweg 2, 2628 CD Delft, the Netherlands, 2016.

[64] Kondo, M. and Ajimine, A. Driver's sight point and dynamics of the driver-vehicle-system related to it. *SAE Technical Paper*, 680104, 1968.

[65] Lee, J. Fifty years of driving safety research. *Human Factors*, 50(3):521–528, 2008.

[66] Lin, D. C. and Rymer, W. Z. Damping actions of the neuromuscular system with inertial loads: Soleus muscle of the decerebrate cat. *Neurophysiology*, 83:652–658, 2000.

[67] MacAdam, C. Understanding and modeling the human driver. *Vehicle System Dynamics*, 40(1-3):101–134, 2003.

[68] MacAdam, C. and Johnson, G. Application of elementary neural networks and preview sensors for representing driver steering control behaviour. *Vehicle System Dynamics*, 25(1):3–30, 1996.

[69] MacAdam, C. An optimal preview control for linear systems. *Journal of Dynamic Systems, Measurement and Control, ASME*, 102, 1980.

[70] MacAdam, C. Application of an optimal preview control for simulation of closed-loop automobile driving. *IEEE Transactions on Systems, Man, and Cybernetics*, SMC- 11(6), 1981.

[71] Markkula, G. and Engström, J. A steering wheel reversal rate metric for assessing effects of visual and cognitive secondary task load. *13th ITS World Congress*, 2006.

[72] Mars, F. and Chevrel, P. Chapter 46 - a psychophysiology-based driver model for the design of driving assistance systems. *Neuroergonomics*, page 223, 2018.

[73] Mars, F., Saleh, L., Chevrel, P., Claveau, F., and Lafay, J. Modeling the visual and motor control of steering with an eye to shared-control automation. In *Proceedings of the Human Factors and Ergonomics Society Annual Meeting*, volume 55, 2011.

[74] Mayne, D. Model predictive control: Recent developments and future promise. *Automatica*, 50(12):2967–2986, 2014.

[75] McRuer, D. and Krendel, E. The human operator as a servo system element. *Journal of the Franklin Institute*, 267(5):381–403, 1959.

[76] McRuer, D. and Krendel, E. The man-machine system concept. *Proceedings of the Ire*, 50(5), 1962.

[77] Merat, N., Jamson, A. H., Lai, F. C., Daly, M., and Carsten, O. M. Transition to manual: Driver behaviour when resuming control from a highly automated vehicle. *Transportation Research Part F: Traffic Psychology and Behaviour*, 27:274 – 282, 2014.

[78] Michon, J. A critical view of driver behavior models: What do we know, what should we do? *Human Behavior and Traffic Safety*, page 485–520, 1985.

[79] Mugge, W., Abbink, D. A., Schouten, A., Dewald, J., and Van der Helm, F. A rigorous model of reflex function indicates that position and force feedback are flexibly tuned to position and force tasks. *Experimental Brain Research*, 200(3-4):325–340, 2010.

[80] Mulder, M., Abbink, D. A., and Boer, E. Sharing control with haptics: Seamless driver support from manual to automatic control. *Human Factors*, 54(5):786–798, 2012.

[81] Nash, C., Cole, D. J., and Bigler, R. A review of human sensory dynamics for application to models of driver steering and speed control. *Biological Cybernetics : Advances in Computational Neuroscience*, 110(2-3):91–116, 2016.

[82] Niu, T. and Cole, D. A model of driver steering control incorporating steering torque feedback and state estimation. Technical report, Department of Engineering, University of Cambridge, 2020. (in preparation).

[83] Parasuraman, R. and Wickens, C. D. Humans: Still vital after all these years of automation. *Human Factors: The Journal of the Human Factors and Ergonomics Society*, 50(3): 511–520, 2008.

[84] Parasuraman, R. Human-computer monitoring. *Human Factors: The Journal of the Human Factors and Ergonomics Society*, 29(6):695–706, 1987.

[85] Parasuraman, R. and Riley, V. Humans and automation: Use, misuse, disuse, abuse. *Human Factors*, 39(2):230–253, 1997.

[86] Peng, H. Evaluation of driver assistance systems—a human centered approach. 2002.

[87] Pick, A. J. Neuromuscular dynamics and the vehicle steering task. Doctoral dissertation, Cambridge University Engineering Department, St Catharine's College, 2004.

[88] Pick, A. J. and Cole, D. J. A mathematical model of driver steering control including neuromuscular dynamics. *Journal of Dynamic Systems, Measurement and Control*, 130 (3):031004 (9 pages), 2008.

[89] Plöchl, M. and Edelmann, J. Driver models in automobile dynamics application. *Vehicle System Dynamics*, 45:7-8:699–741, 2007.

[90] Reński, A. Identification of driver model parameters. *International journal of occupational safety and ergonomics: JOSE*, 7:79–90, 2001.

[91] Romero, F. and Alonso, F. J. A comparison among different hill-type contraction dynamics formulations for muscle force estimation. *Mechanical Sciences*, 7 (1):19–29, 2016.

[92] Saffarian, M., de Winter, J. C. F., and Happee, R. Automated driving: Human-factors issues and design solutions. *Proceedings of the Human Factors and Ergonomics Society Annual Meeting*, 56(1):2296–2300, 2012.

[93] Saleh, L., Chevrel, P., Claveau, F., Lafay, J.-F., and Mars, F. Shared steering control between a driver and an automation: Stability in the presence of driver behavior uncertainty. *IEEE Transactions on Intelligent Transportation Systems*, 14(2):974–983, 2013.

[94] Scerbo, M. Adaptive automation. *International encyclopedia of ergonomics and human factors*, page 1077–1079, 2001.

[95] Scholtens, W., Barendswaard, S., Pool, D. M., van Paassen, M., and Abbink, D. A new haptic shared controller reducing steering conflicts. *IEEE International Conference on Systems, Man, and Cybernetics*, pages 2705–2710, 2018.

[96] Schouten, A., de Vlugt, E., and van der Helm, F. C. Optimal posture control of a musculo-skeletal arm model. *Biological Cybernetics*, 84 (2):143–152, 2001.

[97] Seppelt, B. and Victor, T. Potential solutions to human factors challenges in road vehicle automation. *National Highway Traffic Safety Administration*, page 131–148, 2016.

[98] Seppelt, B. D. and Lee, J. D. Making adaptive cruise control (acc) limits visible. *International Journal of Human-Computer Studies*, 65(3):192–205, 2007.

[99] Sharp, R. and Valtetsiotis, V. Optimal preview car steering control. *Vehicle System Dynamics*, 35:101–118, 2001.

[100] Sheridan, T. B. *Telerobotics, Automation and Human Supervisory Control*. MIT Press, 1992.

[101] Taehyun Shim, G. A. and Yuan, H. Autonomous vehicle collision avoidance system using path planning and model-predictive-control-based active front steering and wheel torque control. *Proceedings of the Institution of Mechanical Engineers, Part D: Journal of Automobile Engineering*, 226(6):767–778, 2012.

[102] Todorov, E. Stochastic optimal control and estimation methods adapted to the noise characteristics of the sensorimotor system. neural computation. *Experimental Brain Research*, 17(5):1084–1108, 2005.

[103] Tustin, A. The nature of the operator's response in manual control, and its implications for controller design. *Journal of the Institution of Electrical Engineers - Part I: General*, 94(83):532–533, 1947.

[104] Utriainen, R., Pollanen, M., and Liimatainen, H. The safety potential of lane keeping assistance and possible actions to improve the potential. *IEEE Transactions on Intelligent Vehicles*, 2020.

[105] Van der Helm, F. C., Schouten, A. C., de Vlugt, E., and Brouwn, G. G. Identification of intrinsic and reflexive components of human arm dynamics during postural control. *Journal of Neuroscience Methods*, 119 (1):1–14, 2002.

[106] Van Paassen, M. M., Boink, R., Abbink, D. A., and M., M. Four design choices for haptic shared control. *Advances in Aviation Psychology*, 2:237–254, 2017.

[107] Walker, G., Stanton, N., and Young, M. Where is computing driving cars? *International Journal of Human-Computer Interaction*, 13(2):203–229, 2001.

[108] Wang, L. *Model Predictive Control System Design and Implementation Using MATLAB ®*. Springer, London, 2009.

[109] Wickens, C. D. and Kessel, C. The effects of participatory mode and task workload on the detection of dynamic system failures. *IEEE Transactions on Systems Man and Cybernetics*, 9(1):24–34, 1979.

[110] Winters, J. and Stark, L. Muscle models: what is gained and what is lost by varying model complexity. *Biological Cybernetics*, 55 (6):403–420, 1987.

[111] Wolpert, D. M., Ghahramani, Z., and Jordan, M. I. Forward dynamic models in human motor control: Psychophysical evidence. *Advan. Neural Info. Processing Syst., MIT Press*, pages 43–50, 1995.

[112] Wolpert, M. and Kawato, M. Multiple paired forward and inverse models for motor control. *Neural Networks*, 11:1317–1329, 1998.

[113] Yamaguchi, G. T. *Dynamic modeling of musculoskeletal motion: A Vectorized Approach for Biomechanical Analysis in Three Dimensions*. Springer, Boston, MA, 2001.